UNIVERSITY OF CAPE TOWN

IYUNIVESITHI YASEKAPA • UNIVERSITEIT VAN KAAPSTAD

Potential impact of Stratospheric Aerosol Geoengineering on projected temperature and precipitation extremes in South Africa

Faculty of Science

Department of Environmental and Geographical Sciences

AFRICAN CLIMATE AND DEVELOPMENT INITIATIVE (ACDI)

Dissertation

Submitted in partial fulfilment of the requirements for the degree of

Master of Science

Climate Change and Sustainable Development

Trisha Patel (PTLTRI002)

Supervisor: Dr Romaric C. Odoulami

02 August 2021

ACKNOWLEDGEMENTS

A very special thanks to my sister, Jaynisha, for your unwavering support. Your daily encouragement pushed me to remain resilient and determined during the hardest moments during this process. Outside of research, thank you for encouraging stimulating discussions and productive distractions, which helped rest my mind.

Thank you to my mother and father for always supporting me and believing in me. Both of you inspire me daily to do no less than my absolute best. You are both greatly appreciated.

To my supervisor, Dr Romaric C. Odoulami – thank you for the guidance and words of encouragement. Your feedback taught me to refine my thinking and sharpen my writing skill. You have made this journey a pleasant one through which we worked together to overcome the obstacles brought about by Covid-19.

Thank you to the African Climate and Development Initiative (ACDI) for equipping me with the skills and resources that assisted me in writing this dissertation. Lastly, to my course convener, Dr Marieke Norton, thank you for your support and kindness throughout 2020 and for creating a conducive learning environment despite Covid-19.

DECLARATION

1. I understand what plagiarism entails and I am aware of the University's policy in this regard.
2. I declare that this assignment is my own, original work and that all sources used or quoted have been indicated and acknowledged by means of a complete reference system.
3. I did not copy and paste any information directly from an electronic source (e.g., a web page, electronic journal article or CD ROM) into this document.
4. I did not make use of another student's previous work and submitted it as my own.
5. This dissertation was not previously submitted for a degree at another university.

Signed by candidate

Signature

01 August 2021

Date

TABLE OF CONTENTS

LIST OF TABLES

LIST OF FIGURES

LIST OF ABBREVIATIONS

ABBREVIATION	MEANING
AAO	Antarctic Oscillation
AOD	Aerosol Optical Depth
BECCS	Biomass Energy with Carbon Capture and Storage
CCT	Cirrus Cloud Thinning
CESM1	Community Earth System Model
CG	Climate Geoengineering
CHIRPS	Climate Hazards Group Infrared Precipitation with Stations
CRU	Climate Research Unit
DACCS	Direct Air Carbon Capture and Storage
ENSO	El Niño Southern Oscillation
ETCCDI	Expert Team on Climate Change Detection and Indices
GGR	Greenhouse Gas Removal
GHG	Greenhouse Gases
GLENS	Geoengineering Large Ensemble
IOD	Indian Ocean Dipole
IPCC	Intergovernmental Panel on Climate Change
LTAS	Long-Term Adaptation Scenario
MCB	Marine Cloud Brightening
MJO	Madden-Julian Oscillation
NCAR	National Centre for Atmospheric Research
ND-GAIN	Notre Dame Global Adaptation Initiative
OIF	Ocean Iron Fertilisation
RCP8.5	Representative Concentration Pathway 8.5
RSA	Republic of South Africa
SAA	South Atlantic Anticyclone
SADC	Southern Africa Development Community
SAF	South Africa
SAI	Stratospheric Aerosol Injection
SAM	Southern Annular Mode
SARVA	Risk and Vulnerability Atlas
SIA	South Indian Ocean Anticyclone
SRM	Solar Radiation Management
SST	Sea Surface Temperatures
USA	United States of America
WACCM	Whole Atmosphere Climate Community Model
WMO	World Meteorological Organisation

ABSTRACT

Climate geoengineering technologies are being increasingly investigated by Earth system science researchers to mitigate climate change. Stratospheric Aerosol Injection (SAI) is one such option that is popularly debated as a potential measure to offset anthropogenic warming, while signatories of the Paris Agreement make efforts to reduce emissions and limit warming to 1.5°C. Most modelling studies to date have assessed the projected impact of SAI on global and regional scales, while a little has been done at country scale. Similarly, research into the effectiveness of varying injection characteristics is limited especially in a developing world. As a developing country rife with inequality, poverty, and disease burden, South Africa is highly susceptible to the increasing frequency and magnitude of temperature and precipitation extremes due to anthropogenic warming. The aim of this study is to investigate how SAI deployment would influence temperature and precipitation extremes over South Africa's climatic zones in the future (2075–2095). Climate model simulations from the Geoengineering Large Ensemble (GLENS) project are used to conduct a comparative analysis of what a future with and without SAI (under Representative Concentration Pathway 8.5 (RCP8.5) would look like in South Africa. Using a selection of extreme temperature and precipitation indices from the "Expert Team on Climate Change Detection and Indices" (ETCCDI), the impact of three SAI feedback experiments (GLENS, Equatorial SAI and Lower SAI) is investigated to provide insight into the effectiveness of different injection characteristics. The results indicate that in a future without SAI, the frequency of hot nights (TN90P: +45-60%) and hot days (TX90P: +15-50%) would increase, with north-east SAF projected to become the most vulnerable to extreme warming. Heavy precipitation days (R10MM) and total precipitation (PRCPTOT) are projected to decrease across most SAF's climatic zones (–0.5-2 days/year and –20-70 mm/year, respectively). The KwaZulu-Natal coast is the only region with projected increases in the number of heavy precipitation days and total precipitation (up to +2.5 days/year and +70 mm/year, respectively), and subsequent flood conditions. Overall, all three SAI feedback experiments (to varying degrees) are projected to reduce temperature and precipitation anomalies over SAF. SAI is projected to trigger a nationwide cooling effect with increased frequency of cool nights (TN10P: +1-4%) and cool days (TX10P: up to +3%). This could alleviate heat-induced strain on human health, agricultural production, and the harsh effects of climate extremes on South Africa's most vulnerable communities. The projected general reductions in PRCPTOT (–10-60%) and R10MM (–1-4 days/year) could have negative implications for water security and agricultural production for the country.

Injecting sulfate aerosols into the Equatorial and Lower stratosphere could cause larger decreases in precipitation extremes than in the feedback experiment. These findings should be read with caution as they are specific to the types of SAI deployed in the GLENS project.

1 CHAPTER 1 – INTRODUCTION AND RESEARCH RATIONALE

Southern Africa is very vulnerable to numerous weather and climate extremes, with the four primary categories of weather and climate hazards being droughts, wildfires, floods, and storm surges (Davis-Reddy and Vincent, 2017). The IPCC Special Report on the Impact of Global Warming of 1.5°C (IPCC SR1.5) suggests that Southern Africa will undergo a general decrease in precipitation in addition to severe heating and consequent heat stress (IPCC, 2018). The region's projected drying trend would exacerbate the exposure to desertification and subsequently exacerbate drought occurrence, duration, and magnitude. The anticipated increase in water stress and subsequent decrease in food availability is expected to be the most hard-hitting outcome of the projected changes in climate extremes, subsequently increasing the vulnerability of the people living in the region.

The region's population majorly resides in rural areas and are the most exposed to climate change, which is intensified by existing socioeconomic conditions such as extreme poverty, high pre-existing disease burden, local conflict, poor governance, restrained access to services and resources, technological exclusion, food and water insecurity, education barriers and gender inequality (UNECA, 2010). Rural economies in Southern Africa rely heavily on natural resources for livelihood maintenance which leaves them predominantly sensitive to the direct shocks of climate change; thus, leaving the economies of SADC countries increasingly susceptible to climate change (UNECA, 2010).

The economic consequences of climate extremes are interlinked with social factors, as rapid population growth and urbanisation in SADC countries are intensifying the region's vulnerability to climate extremes. Projected changes in temperature and precipitation extremes are anticipated to negatively affect the region's infrastructure, human well-being, access to water, and food security (Davis-Reddy and Vincent, 2017). The negative socioeconomic impact of weather and climate-related extremes in Southern Africa and South Africa, have evidently increased and will only worsen as global warming intensifies climate extremes (Davis-Reddy and Vincent, 2017).

The observed climate trends in South Africa between 1960–2010 suggest, primarily, a significant overall rise in the frequency of annual hot extremes and drop in the frequency of annual cold extremes, especially over the country's western and northern interior (DEA, 2013). The greatest

warming has been observed in western South Africa (Western and Northern Cape Provinces) and in north-east South Africa (Limpopo and Mpumalanga), as well as over the coastal parts of KwaZulu-Natal (DEA, 2017). There has been a general decrease in rainfall across all of South Africa's identified hydrological zones during autumn, and a significant decrease in annual rainfall and the annual number of rainy days (DEA, 2013). This suggests increased vulnerability to longer dry spells (DEA, 2013). These observed trends in South Africa's climate extremes are projected to continue moving forward. South Africa's 3rd Climate Change Report (DEA, 2017) states that a drastic +4°C warming is projected across Southern Africa over the next six decades, with the northern, central and western regions of South Africa being vulnerable to warming that exceeds +6°C.

Projections under the "Representative Concentration Pathway" (RCP) 8.5 scenario reveal that minimum and maximum temperatures could increase by about 1°C along South Africa coastal areas, and by 1–2°C across the country's interior by 2015–2035 (DEA, 2013). The projected average change for South Africa is below 2.5°C for 2040–2060, whilst it exceeds 4°C for the period 2075–2095 (DEA, 2013). A general pattern of wetting over eastern South Africa is projected in the far future while a significant risk of dry conditions is predicted over the remainder of the country, particularly the south and west regions (DEA, 2013). The warming trend in South Africa has a strong signal, which is alarming; it is, therefore, imperative that our response to climate change is hard-hitting and effective.

Solar geoengineering is a proposal to cool the earth's surface by reflecting sunlight back to space, thereby reducing some of the effects of increasing Greenhouse Gases (GHGs) (Irvine et al. 2016). The prospect of Solar Radiation Management (SRM) by way of Stratospheric Aerosol Injection (SAI) is a commonly discussed approach, that is increasingly being investigated as a temporary measure to offset warming while countries implement mitigation measures to reduce emissions, such as transitioning to renewable energy (Matlakala, 2020). When volcanoes erupt, they release large quantities of sulphate aerosols into the stratosphere which grow into a stratospheric aerosol layer. This layer reflects incoming solar radiation which triggers a cooling effect over the Earth's surface (Cheng et al. 2019). SAI is based on the idea of mimicking this natural radiative forcing and involves the continuous injection of a gaseous sulphate precursor, most commonly sulphur dioxide (SO_2), into the stratosphere (Irvine et al. 2016) to cool the Earth's surface. The SO_2 oxidises

within weeks to form sulphuric acid, which condenses into aerosol particles (Irvine et al. 2016) and forms the aerosol layer, which will increase the reflection of solar radiation.

Previous research on SAI was regionally and globally focused with diverse outcomes (Odoulami et al. 2020). The analysis of the climatic response to SAI in Africa suggests an overall reduction in surface temperature and in total precipitation and an increase in the duration of dry spells in Southern Africa (Pinto et al. 2020). The impact of SAI on precipitation alone is less straightforward as SAI in Africa could trigger a decrease in summer rainfall and exacerbate rainfall reduction in localised areas in western and Southern Africa (Pinto et al. 2020). Odoulami et al. (2020) assessed the potential impact of SAI deployment on the Cape Town region in South Africa with a focus on the future risk of "*Day Zero"* level droughts, as experienced by the Western Cape in 2015–2017. They found that deploying SAI could decrease the risk of future "*Day Zero"* level droughts by about 90% (Odoulami et al. 2020).

These studies show that current research into the impact of SAI on the climate in Africa has been conducted at a regional scale with limited insights into its potential impact on climate extremes at local or country scales. Even though the Odoulami et al. (2020) local scale case study focuses on the impact of SAI on climate extremes, it focuses on a single drought event and assesses how SAI might influence the likelihood of such an event in the future. This study is novel in a South African context as it aims to assess the potential impact of SAI on projected changes in temperature and precipitation extremes over the country's climatic zones in the future (2075–2095). This will be done by analysing the "Stratospheric Aerosol Geoengineering Large Ensemble" (GLENS) Project datasets (Tilmes et al. 2018) to assess a potential future with and without SAI deployment in South Africa . In addition, this study will assess how changes in the injection characteristics (varying latitudes and altitudes) of sulphate aerosols would influence the impact of SAI on temperature and precipitation extremes in South Africa in the future.

There are seven chapters in this study. Chapter 2 is the literature review, which presents a synthesis of what climate extremes are, how climate extremes are changing in Southern Africa and in South Africa, vulnerabilities to climate change in South Africa, climate geoengineering options and their potential to mitigate warming and an overview of SAI impact on climate extremes on a global scale and in Africa. The chapter is concluded with an assessment of the ethics and governance of SAI.

Chapter 3 presents a description of South Africa's geography and topography and associated climate followed by the country's climatic zones. Chapter 4 discusses the data and methodology used in this study. Chapter 5 presents the results from the climate model simulations for (i) the spatial distribution of projected temperature and precipitation extremes and (ii) the projections over the country's climatic zones, both with and without SAI deployment. The implications of these findings for climate change vulnerability in South Africa with respect to water stress, agriculture, health and vulnerable communities, are discussed in Chapter 6. Lastly, Chapter 7 concludes this dissertation with an outline of the limitations and recommendations for future research into SAI.

2 CHAPTER 2 – LITERATURE REVIEW

2.1 BRIEF OVERVIEW ON CLIMATE EXTREMES

2.1.1 Definitions/categories of climate extremes

The IPCC (2012) refers to an extreme climate or weather event when the value of a climate variable goes beyond or beneath a threshold value that draws up to the upper or lower ends, or *tails* of observed values of the variable, or has a low probability of occurrence (generally less than 0.01 or 0.05). The IPCC identifies two categories of extreme climate events: the first is a single event, also called *extreme weather events* which are associated with changing weather patterns that occur in under a day to a few weeks. The second climate event refers to *compound events,* which refers to when two or more extreme climate events occur simultaneously or successively and results in an accumulation of numerous weather events over a longer time scale (IPCC, 2012; AghaKouchak et al. 2020). An example of a compound event is the accumulation of precipitation days with below-average rainfall over the course of a season which results in less than average accumulated rainfall, subsequently causing a drought (IPCC, 2012). The occurrence of climate or weather events, even if not considered *extreme* statistically, can still trigger or induce the critical crossing of a threshold in a larger physical, social, or ecological system, or transpire concurrently with other events to bring about extreme conditions or effects (IPCC, 2012). For example, a weather system such as a hurricane that is not considered *extreme* compared to other hurricanes could still have severe ramifications based on where and when it approached the land. The focus in this literature review is on different types of weather and climate extremes. The World Meteorological Organisation (WMO) Commission for Climatology Task Team (2018) has identified four types of extreme weather and climate events:

- extreme precipitation
- drought
- heat wave
- cold wave

An extreme precipitation event is defined as a distinct rainfall incident during which the total daily precipitation surpasses a given threshold outlined – in accordance with station-based data - for the relevant location, during a time period of one to several days (often less than one week) (WMO,

2018). The IPCC defines drought as a natural weather phenomenon referred to as a period of atypical dry weather that continues for long enough to induce a severe imbalance over the area or region's hydrological system (IPCC, 2018). There are four variations of drought: meteorological, agricultural, hydrological, and socioeconomic drought (WMO 2018).

A meteorological drought occurs when a location's atmospheric conditions lead to a prolonged absence or decrease of precipitation leading to any or a combination of the other types of droughts. The WMO Climatology Task Team (2018) therefore defines a drought based on meteorological aspects, as a period longer than a month of uncharacteristically dry weather, embodied by a prolonged deficiency of precipitation below a given threshold across a wide area. A meteorological drought could trigger an agricultural or hydrological drought. Agricultural drought is characterised by deficits in soil moisture, shortages in precipitation and increased evapotranspiration (WMO, 2018). A drought is considered hydrological when it occurs because of drained surface and or subsurface water resources (WMO, 2018). Socioeconomic droughts refer to an imbalance in supply and demand, or the impact of drought-induced water shortages on society such as poor health, and its economy such as crop losses (WMO, 2018).

The next extreme weather/climate event is a heat wave, which is defined as a region experiencing a minimum of three consecutive days during which the maximum, minimum and average daily temperature are hotter than usual during that region's warm cycle within the year based on local meteorological conditions (WMO, 2018). Lastly, a cold wave is characterised by a stark decrease in the maximum, minimum and daily average air temperatures near the surface across a large area below that area's given threshold for a minimum of two successive days during the cold season (WMO, 2018).

2.1.2 Methods used to study climate extremes

Changes in the Earth's climate system are assessed through a methodical comparison between climate observation and results from climate models using a variety of statistical methods (Knutson et al. 2017). This process describes "detection and attribution" studies which also assists in studying climate extremes and in determining whether climate variables, such as temperature and precipitation, are influenced by human activities or by natural variability (Knutson et al. 2017). The results from detection and attribution studies often inform policy makers in decisions surrounding

climate change adaptation (Knutson et al. 2017). The IPCC (2018) defines "detection" as the process of demonstrating that the climate or a system that has been impacted by the climate, has altered statistically and defines "attribution" as an evaluation of the relative confidence of the contribution of several causal factors to a climate-related event or change.

There are many techniques used in attribution science; one such technique is using coupled models (Stott et al. 2016). This approach involves acquiring data from multimodel ensembles which simulate the relative variable (e.g., precipitation if investigating a flood) with and without anthropogenic influences to gain insight into the extent to which human activities have contributed to the occurrence of the climate extreme (Stott et al. 2016). This approach generally provides fast-track assessments. Another approach is by using "sea-surface temperature forced atmosphere-only" models, which condition the climatic conditions at the time of the event by prescribing observed sea surface temperature anomalies into an atmosphere-only model (Stott et al. 2016). This approach is similar to the coupled models approach, however, it differs in that it could result in fewer biases and is able to simulate more ensemble members (Stott et al. 2016). A potential downfall of this approach is that it is not representative of ocean-atmosphere coupling and could therefore provide inaccurate results. Lastly, analogue-based approaches are also used to condition the climatic conditions at the time of an event by estimating the climatic conditions during past events under the same present-day large-scale circulation (Stott et al. 2016). Empirical approaches are applied directly to observations to estimate how anthropogenic influences are impacting the return time or probability of specific classes of events (Stott et al. 2016).

Extreme indices are often used in both observational and climate model datasets to establish climate and weather extreme thresholds that are relative to location. Extreme indices are quantified in two ways: the first relating to their probability of occurrence and the second relating to a specific (potentially impact-related) threshold (IPCC, 2012).

Indices commonly used to quantify temperature extremes include:

- the monthly maximum value of daily maximum temperature (TXx)
- the monthly minimum value of daily minimum temperature (TNn)
- the fraction of days with cold night time (TN10p) and cold day time (TX10p) temperatures (count of days where temperature is less than the 10th percentile)

- and warm night time (TN90p) and warm day time (TX90p) temperatures (count of days where the temperature is greater than the 90th percentile)
- and the warm spell duration index (WSDI)

Indices commonly used to quantify precipitation extremes include:

- the total wet-day rainfall (PRCPTOT)
- heavy precipitation days (R10mm)
- maximum one-day (RX1DAY) and five-day precipitation (RX5DAY)
- simple daily intensity index (SDII)
- precipitation due to very wet days (R95p) where daily wet day precipitation is greater than the 95th percentile
- count of the number of consecutive dry days (CDD) (IPCC, 2013)

Many of the abovementioned indices are quantified and measured according to the number of occurrences of the percentage, number, or fraction of days of the indicator that is beneath the 1st, 5th or 10th percentile, or exceeds the 90th, 95th or 99th percentile within a specified time frame in reference to the historical period (1961–1990) (IPCC, 2012). Other indices, such as RX1DAY and RX5DAY, are measured based on the mm of rainfall in the respective time period. The specified time frame used to measure indices could be a day, months, season (usually three months) or annual. The number of days that exceed a specified precipitation or temperature threshold informs on the characteristics of extremes such as frequency, magnitude, and persistence (NASEM, 2016).

2.1.3 How climate change is affecting climate extremes

The mechanisms which play a role in causing the occurrence of extreme weather and climate events are diverse and intricate (Wehrli et al. 2021). Weather and climate extremes are driven by a combination of dynamic components, relating to changes in large-scale atmospheric flows, and thermodynamic components, relating to changes in atmospheric moisture content (Emori and Brown, 2005). For example, heat waves develop from a combination of large-scale persisting anti-cyclonic weather systems and stagnant air conditions (Vautard et al. 2016). Two necessary causes of heavy precipitation events are the large-scale flow conditions, especially sustained zonal flow in Europe, and the atmosphere's thermodynamic capacity to hold water (Vautard et al. 2016). Another example of the role of dynamics and thermodynamics in driving extreme weather events is in the mid-latitudes where winter cold spells result from atmospheric conditions, which prevent anticyclonic formulation, and in the absence of meridional circulations and clouds, leads to radiative

cooling of the surface (Vautard et al. 2016). Additionally, the relationship between snow cover and radiation plays a role in regulating temperatures (Vautard et al. 2016).

The abovementioned examples showcase how dynamic and thermodynamic components play a role in driving weather and climate extremes. Human-induced climate change, or increased atmospheric warming, is impacting dynamic and thermodynamic components and subsequently, the magnitude, frequency, and intensity of weather and climate extremes (Palmer, 2013). Changes in thermodynamic components in relation to increased warming have resulted in increased atmospheric moisture content (Emori and Brown, 2005). It is likely that, since 1970, the increase in moisture content has resulted in a 5-10% effect on precipitation extremes (Trenberth, 2012). Since the 1950s, global warming has also triggered an increase in sea surface temperatures by 0.5-0.6°C which has caused 4% increase in atmospheric water vapour since the 1970s (Trenberth, 2012). These changes have been linked to increasingly warmer and more humid summers across the Northern Hemisphere (Wang et al., 2016).

Increasing atmospheric heating has caused upward trends in hot temperature extremes, downward trends in most cold extremes, and has exacerbated the intensity of hydroclimatic events, such as droughts and heavy precipitation events (Horton et al. 2015). Increased occurrences of extreme heat events have been observed over the mid-latitudes in response to the dynamic and thermodynamic effects of human-induced warming (Horton et al. 2015). Eastern Asia has experienced a ~60% decrease in the frequency of cold extremes over the period 1979-2013 (Horton et al. 2015). Thermodynamic changes are estimated to account for 35% of these changes while dynamic changes account for 58% (Horton et al. 2015). These atmospheric alterations have caused a decrease in the occurrence of the cyclonic circulations, which advect cold air towards the equator, subsequently inducing cold extremes (Horton et al. 2015). Should GHG emissions continue to increase and accumulate, the impacts of altered dynamic and thermodynamic forcing could be expecting to continue exacerbating hot and cold extremes, as well as precipitation extremes (Horton et al. 2015).

2.1.4 Impact of climate extremes on Earth and human societies

As of 2020, the average temperature of the Earth's surface has grown by 1.02°C since 1880 (NASA's Goddard Institute for Space Studies; NASA/GISS, 2020). The beginning of the industrial era has seen

drastic increases in the oceanic uptake of carbon dioxide (CO_2) which has led to amplified ocean acidification (IPCC, 2014). Ocean surface water pH has dropped by 0.1, equating to a 26.0% growth in ocean acidity (IPCC, 2014). The cryosphere has consequently undergone rapid global ice loss in mountains, the Greenland ice sheet, West Antarctica, and Arctic Sea ice (National Geographic, 2019). For example, the rate of annual Arctic Sea ice decrease between 1979–2012 was between 3.5–4.1% per decade (IPCC, 2014). The melting ice has led to an average sea level rise rate of 3.2 mm annually and an average increase of 0.19 m during the period 1901–2010, with an increasing pace in recent years (IPCC, 2014; National Geographic, 2019). The 75% of observed global average sea level rise since the beginning of the 1970s has been attributed to the combination of ocean thermal expansion from increased GHGs and glacier mass loss (IPCC, 2014). The disappearing ice has threatened the animal species that live on the ice; the Adélie penguin population in western Antarctica, for example, has decreased by 90% (National Geographic, 2019). Increasing temperatures are affecting most habitats of wildlife and plant species across the globe – numerous species such as alpine forests, foxes and some butterflies have been observed migrating northward and to higher altitudes where temperatures are cooler (National Geographic, 2019). Additionally, the average global precipitation has increased, despite some regions having experienced more severe droughts, leaving them increasingly vulnerable to the risk of wildfires, crop losses and water stress (National Geographic, 2019).

Climate extremes are posing a threat to economic growth, the durability of natural and built environments and to human health across the world (AghaKouchak et al. 2020). As an example, climate extremes cost the United States of America (USA) alone USD 1.5 billion in damages and near 10 000 deaths between 1980–2017 (AghaKouchak et al. 2020); natural disasters cost USD 306 billion in damages in 2017, making it the costliest year for the USA on record (AghaKouchak et al. 2020). The observed impact of increasing climate-induces extremes like floods, heat waves, wildfires, droughts and cyclones have brought to light how exposed and vulnerable many human systems and ecosystems are to the ongoing climate variability and change (IPCC, 2014). The significant fluctuations in the incidences, magnitude and extent of climate extremes that have been observed since 1950 are partly attributed to anthropogenic activities (IPCC, 2014). A primary way in which climate change has affected climate extremes is reflected in the observed global number of decreased cold days and nights and increased warm days and nights. The IPCC (2014) states that it

is *very likely* (90–100% probability (IPCC, 2010)) that since the 1950s, human activity has exacerbated the global scale intensity and frequency of daily temperature extremes. It is also *likely* (66–100% probability (IPCC, 2010)) that the probability of heat wave occurrences has more than doubled in numerous locations across the globe in response to human activities (IPCC, 2014). These alterations in the Earth's climate system are also associated with increased occurrences of droughts and wildfires (IPCC, 2014).

The IPCC (2014) states that it is likely that more land regions have experienced an increase in the frequency of heavy precipitation events than where heavy precipitation events have decreased. The recent trends of increasing extreme precipitation events are linked to increases in discharge in river catchments worldwide which have implications for escalating flooding at the regional scale (IPCC, 2014). The IPCC (2014) has also indicated that it is *likely* (66–100% probability (IPCC, 2010)) that extreme sea levels as seen during storm surges for example, have risen since 1970 because of the rise in mean sea levels (IPCC, 2014); these alterations in the Earth's climate system are associated with increased occurrences of floods and cyclones (IPCC, 2014). The occurrence of a single storm surge may not be considered extreme, but when combined they have significant repercussions (AghaKouchak et al. 2020). These are referred to, as previously mentioned, as *compound events* (AghaKouchak et al. 2020). The magnitude of compound events and the severity of the outcomes, increases with the rise in frequency of extreme events. The observed increase in impact from climate extreme across the globe reflects the increase in human exposure to natural hazards, because of rapid population growth and human development; it also directly reflects the vulnerability of current infrastructure systems to climate extremes (AghaKouchak et al. 2020). Climate change is therefore simultaneously increasing the magnitude, extent and severity of climate extremes and compound events. The urgency for action is louder than ever.

2.2 CLIMATE AND WEATHER EXTREMES IN A CHANGING ENVIRONMENT

2.2.1 Climate extremes in Southern Africa

For the period 1951-2010, a weak drying trend has been observed in eastern Zimbabwe, South Africa and Botswana while a weak wetting trend was observed over the western and central regions of South Africa and southern Namibia (Reason, 2017). The IPCC Fifth Assessment Report (AR5) states that it is very likely that all of Africa will continue to warm as the century progresses, with the

warming over subtropical Southern Africa projected to exceed that projected over equatorial Africa (Niang et al. 2014). This has been attributed to the projected poleward shift and intensifications of the subtropical anticyclones (Reason, 2017). Lastly, Southern Africa has experienced a simultaneous increase in the frequency of dry spells and an increasing trend in the intensity of daily rainfall (New et al. 2006). The 2015-2017 "*Day Zero*" drought in the City of Cape Town, South Africa has been attributed to the long-term poleward shift of the westerlies responsible for bringing winter rains to the area (Fitchett, 2021).

Since 1950, Southern Africa has experienced a trend toward enhanced aridity in conjunction with a 20% observed decrease in precipitation during austral summer (February-March-April) (Hoerling et al. 2006). Southern African austral summer rainfall is known to be sensitive to global sea surface temperatures and has shown to be a response to warming of the Indian Ocean, which is a consequence of increased GHG emissions (Niang et al. 2014; Hoerling et al. 2016). Additionally, the warmer waters have exacerbated atmospheric convection, subsequently driving subsidence drying across Africa (Hoerling et al. 2006). Shongwe et al. (2009) reached the conclusion that current rainfall trends in southern Africa are defined by exacerbated rainfall in northern Zambia, Malawi and northern Mozambique, while southwestern Southern Africa is characterised by more severe droughts. Evidence gained over the last few decades indicates that tropical cyclones have expanded their range moving poleward, subsequently affecting a more expansive surface area over Southern Africa (Fitchett, 2021). These findings reveal how climate extremes in Southern Africa have changed over the last few decades.

2.2.2 How climate extremes have impacted Southern Africa

Climatically, Southern Africa as a region is experiencing warming at a rate that is faster than the global average (Bauer and Scholz, 2010). This, in tandem with the fact that Southern Africa's population is one of the world's most socio-economically vulnerable, highlights how exposed the region is to the changing climate (Bauer and Scholz, 2010). Southern Africa is vulnerable to various climate extremes with the four primary climate disasters being droughts, wildfires, floods, and storm surges (Davis-Reddy and Vincent, 2017). The region has experienced a total of 491 of these climate disasters during 1980–2015, which affected an estimated 140 million people and caused 110,978 fatalities, leaving 2.47 million people without homes (Davis-Reddy and Vincent, 2017). The

socio-economic impact of extreme weather events to Southern Africa Development Community (SADC) countries are wide-ranging from direct impacts, such as loss of life, to secondary impacts, such as the loss of livelihoods (Davis-Reddy and Vincent, 2017). The abovementioned four categories of climate disasters have collectively cost Southern Africa an estimated USD10 billion in economic damages between 1952–2016, of which USD 3.4 billion was associated with droughts and USD 3.3 billion with floods (Davis-Reddy and Vincent, 2017). The period between 1980–2015 saw floods being the most frequent climate extreme, with the costliest storms in the region costing South Africa USD 15 million in losses in 2009 (Guha-Sapir et al. 2016). Droughts were the costliest economically, in terms of lives affected and fatalities, with storms most responsible for displacement and injuries (Davis-Reddy and Vincent, 2017).

In South Africa wildfires affected about 57 000 people in Cape Town in March 2015, whilst a hail event in Gauteng on 28 November 2013 brought about losses exceeding R1.6 billion in insurance claims in the motor vehicle and property sectors (PwC, 2014). The negative socioeconomic impact of weather and climate-related extremes in Southern Africa and South Africa, have evidently increased and will only worsen during the twenty-first century as the frequency and magnitude of climate extremes increase (Davis-Reddy and Vincent, 2017). Extreme climate events have evidently caused extensive damage to SADC countries. It is very likely that the impact of these events will worsen in the future because of the warming climate; subsequently the vulnerability of people living in the region will increase to the adverse effects of climate change. The economic consequences of climate extremes are interlinked with social aspects, as rapid population growth and urbanisation in SADC countries are intensifying the region's vulnerability to climate extremes. The projected changes in temperature and precipitation extremes are anticipated to negatively affect the region's infrastructure, human well-being, access to water, human settlements, and food security (Davis-Reddy and Vincent, 2017). Climate change has also altered the timing of phenological events, or annually recurrent biological events, which is an effective bio-sensitive indicator of climate change (Fitchett, 2021). For example, South African scientists have noted that apple and pears in the southwestern Cape have been flowering earlier than is usual (Fitchett, 2021). Delays in the sardine run along the south coast of KwaZulu-Natal province have also been observed, and linked to increasing sea surface temperatures (Fitchett, 2021). Aside from altering the natural environment,

shifts like these in phenological events have implications for agriculture, the economy, and tourism (Fitchett, 2021).

Southern Africa's population majorly resides in rural areas and are the most exposed to climate change, which is intensified by existing socioeconomic conditions such as extreme poverty, high pre-existing disease burden, local conflict, poor governance, restrained access to services and resources, technological exclusion, food and water insecurity, education barriers and gender inequality (UNECA, 2010). Rural economies in Southern Africa rely heavily on natural resources for livelihood maintenance which leaves them predominantly sensitive to the direct shocks of climate change (UNECA, 2010). Sectors that are central to rural development like biodiversity and ecosystems, water resources, and agriculture (UNECA, 2010), are also those that are already directly affected by climate change; thus, leaving the economies of SADC countries increasingly susceptible to climate change. For example, more than 60% of Mozambique's population, and the country's poorest communities, live along the extensive coastline (Irish Aid, 2018), which was ravaged for the first time by two severe tropical cyclones in 2019 within six weeks (UNICEF, 2019). Tropical Cyclones Idai and Kenneth left 2.5 million Mozambicans in need of humanitarian assistance, 160,927 people displaced, 223,947 houses destroyed, 6,768 cholera cases, and 715,378 hectares of crop damaged (UNICEF, 2019).

The "IPCC Special Report on the impact of global warming of 1.5°C" (IPCC SR1.5) suggests that Southern Africa will undergo a general decrease in precipitation in addition to severe heating and consequent heat stress (IPCC, 2018). The SR1.5 brings to light that Southern Africa's projected drying trend would exacerbate the region's exposure to desertification and consequent rises in the magnitude, frequency and duration of drought. The anticipated increase in water stress and subsequent decrease in food availability is expected to be the most hard-hitting outcome of the projected changes in climate extremes. More specifically, reductions in cropping areas that are suitable for growing maize, cocoa and sorghum and the following rise in yield losses could lead to food insecurity (IPCC, 2018). Additionally, Muthige et al. (2018) showed that projected decreases in tropical cyclones and tropical lows over the south-west Indian Ocean under global warming of various levels would decrease precipitation over the southern, central and northern regions of

Mozambique as well as over the Limpopo River Basin, suggesting increased vulnerability for agricultural production in the region.

2.2.3 Climate extremes in South Africa: observed and projected changes

The observed climate trends in South Africa between 1960–2010 suggest a significant overall increase in the frequency of annual hot extremes, and a decrease in the frequency of annual cold extremes, especially in the country's western and northern interior (Department of Environmental Affairs; DEA, 2013). The harshest warming trends have been observed in two regions within South Africa. Firstly, the dry western region, particularly the Northern Cape and Western Cape (DEA, 2017). Davis et al. (2016) found that the arid Namaqualand region located in western South Africa experience a +1.4°C increase in minimum temperatures and a +1.1°C increase in maximum temperatures, in addition to a significant increase in the occurrence of anomalously warm days and decrease in cool days. The second region, which has experienced the harshest warming in the country is the north-east region around Limpopo and Mpumalanga which extends southwards to KwaZulu-Natal's east coast (DEA, 2017). The latter region's observed rate of warming has been 2°C per century, which exceeds by two-fold the global rate of warming (DEA, 2017). Additionally, Kruger et al. (2019) note that stronger warming trends are reflected in northeast South Africa. An exception to these observed trends is the significant decrease in minimum temperatures over the central interior over the period 1960–2010 (Mackellar et al. 2014).

On the other hand, the observed rainfall trends across the country are mixed. There is an overall decrease in rainfall across all hydrological zones in South Africa during autumn (Limpopo/Olifants and Inkomati, Pongola-Umzimkulu, Vaal, Orange, Mzimvubu-Tsitsikamma, and Breede-Gouritz/Berg) (DEA, 2013); additionally, observed annual rainfall significantly decreases across the country, particularly over eastern South Africa and the south coast region (DEA, 2013; Reason, 2017). The observed trends in annual rainfall for the period 1921–2015, however, reveal an upward trend in total annual rainfall across the central southern interior and to a degree, northern South Africa (DEA, 2017). These trends were reflected primarily during the summer rainfall season, especially over the southern Drakensberg region (DEA, 2013; Reason, 2017). Kruger (2007) also found that, for the period 1910-2004, annual precipitation increased significantly over the central interior of the country and over the North West Province. Conversely, northern Limpopo shows a

negative trend in total annual rainfall mostly characterised by decreasing autumn rainfall (DEA, 2017). The general reduction in the annual number of rainy days, however, points concurrently to longer dry spells and increased intensity in rainfall events (DEA, 2013). These conditions provide evidence that the frequency of extreme weather events in South Africa is rising, as heat wave conditions occur more commonly, and the duration of dry spells has slightly increased (DEA, 2017).

It is worth noting that flood and storm conditions were more prominent than drought conditions in South Africa between 1991–2014 (DEA, 2017). This is because the country was not impacted by the effects of El Niño events between the 1991–1992 and 2015–2016 (DEA, 2017). South Africa subsequently experienced above-average rainfall conditions during those two decades with limited drought conditions (DEA, 2017). The overall observed trends in temperature and precipitation extremes across South Africa are projected to keep on playing out over the course of the twenty-first century.

South Africa has developed "Long-Term Adaptation Scenarios" (LTAS) for the purpose of assessing and understanding the possible impacts of and adaptation options to climate change. One LTAS projected an increase in warming of 3–6°C by 2081–2100 relative to 1986–2005, across South Africa (Ziervogel et al. 2014). More specifically, projections under the RCP8.5 (business as usual) scenario reveal that the minimum and maximum temperatures could increase by under 1°C along South Africa's coastal areas and by 1–2°C across the country's interior by 2015–2035 (DEA, 2013). Kruger et al. (2019) found that warm spells are projected to increase while cold spells decrease in South Africa over the period 2006–2095. Over the same period, RCP8.5 is projected to trigger a decrease in cold nights by -1.5–2.5% per decade while warm nights would increase by over +2.5% per decade (Kruger et al. 2019). Similarly, cool days are projected to decrease by -1.5–2.5% per decade while hot days would increase by over +2.5% per decade (Kruger et al. 2019). The warmest night and hottest day of the year are projected to increase by over +0.3°C per decade in South Africa while

The projected changes (direction and magnitude) in precipitation are, however, less certain over the country (Ziervogel et al. 2014). The mixed rainfall projections indicate a moderate to significant increase in rainfall during winter and spring for the south Western Cape and the Cape south coast in the far future (DEA, 2013). Rainfall is projected to increase over South Africa's eastern and central interior regions in the far future, particularly during summer (DEA, 2013; DEA, 2017). Hewitson and

Crane (2006) found that the country's convective region specifically, which covers the eastern and central plateau and the Drakensberg Mountains is projected to experience enhanced summer rainfall. Malherbe et al. (2013) found that the projected northward shift of tropical cyclone tracks would result in reduced flood events over the Limpopo River Basin located in north-east South Africa and more flood events in Mozambique. This could have serious implications for Limpopo River Basin's water balance, subsequently impacting those rural populations in the region with agricultural livelihoods (Malherbe et al. 2013). Projections for the mid- and near-futures are not as well developed as that of the far-future because they indicate an overall mixed signal of either a wetting or drying trend across the country (DEA, 2013). A significant drying trend is projected over eastern South Africa, and it is probable that autumn will become drier in the far future (DEA, 2013). The strong signal about the warming trend in South Africa is alarming and it is therefore imperative that our response to climate change is hard-hitting and effective.

Regarding extreme events, South Africa is anticipated to experience increased incidences of heat waves, dry spells, high fire danger days and flood events, in comparison with the historical reference of 1971–2000 (DEA, 2017). On the other hand, incidences of cold waves and intense thunderstorms are expected to decrease (DEA, 2017). Heat waves are not common events in present-day Southern Africa as most regions experience less than five heat wave days annually. The frequency of heat waves is projected to increase to eight days or more annually, primarily over South Africa's central interior and minimally around coastal areas (DEA, 2017). More specifically, Mbokodo et al. (2020) found that South Africa's coastal areas are projected to experience an increased frequency, more than 50%, of short heat waves (between 3–4 days on average) in the far future (2070–2099). They found that longer lasting heat waves would occur over the country's interior (Mbokodo et al. 2020). Dry spells are expected to increase during the period 2021–2050 under low and high mitigation scenarios. Eastern and southern South Africa are most vulnerable to fire danger as these areas experience less than twenty high fire danger days annually. The forested regions in the Western and Eastern Cape, Mpumalanga and Limpopo Provinces are projected to experience between 10–30 high fire danger days annually (DEA, 2017). Perren et al. (2020) found that the southward shift of the Southern Hemisphere westerlies, since the 1950s, has deterred the primary moisture-laden storm tracks from continental areas. This has been associated with increased droughts and wildfires

in western South Africa, which they predict will increase in severity in response to the poleward movement of the Southern Hemisphere westerly winds (Perren et al. 2020).

Flood events are not common in most regions of the country and on average, experience less than one average flood event annually; the frequency of large-scale flood events is projected to increase over South Africa's eastern escarpment and along the east coast (DEA, 2017). Following the general projected decrease in precipitation across the country, the incidences of thunderstorm events are expected to drop across most of South Africa under the low mitigation scenario between 2021–2050 in reference to 1971–2000 (DEA, 2017). Projections indicate that it is, however, probable that intense thunderstorm events will increase over eastern and north-eastern South Africa (DEA, 2017). Lastly, cold waves most commonly occur over the country's central interior regions between 5–8 days per year on average and are projected to decrease by 2–3 days per year under low and high mitigation scenarios (DEA, 2017).

2.2.4 South Africa's vulnerabilities to climate change

The "Notre Dame Global Adaptation Initiative" (ND-GAIN), which ranks the vulnerability and readiness to adapt to climate change of 181 countries by using 45 climate indicators, ranks South Africa as the 80th least vulnerable country and the 81st country that is the least ready for climate change (ND-GAIN, 2018). South Africa's vulnerability to climate change might seem relatively manageable, but there is room for enhanced readiness to better the country's ability to adapt to increased warming (ND-GAIN, 2018). As a developing country, South Africa is challenged with finding a balance between enhancing economic growth and transformation, while sustainably utilising natural resources and responding to climate change (DEA, 2017). As a water-stressed country with an annual rainfall of 500 mm, climate change could have harsh consequences for South Africa's water resources (Dennis and Dennis, 2011); this makes water the central medium through which the effects of climate change are being felt in the country (Department of Water Affairs, 2013). Increasing levels of water quality, availability and stress are compounded by matters of population growth and socio-economic development (Dennis and Dennis, 2011) – South Africa is a country associated with the burden of disease which makes health a predominant issue and vulnerability to climate change (Chersich et al. 2018). The most noticeable effect of climate change in the country is extreme climate events such as the Western Cape drought between 2015–2017.

However, increases in vector-borne diseases are becoming more distinguished (Chersich et al. 2018). This extends to increased outbreaks in food- and water-borne diseases (Chersich et al. 2018). These climate change effects amplify the vulnerabilities of the country's pre-existing vulnerable groups – rural subsistence farmers, women, children, the elderly, fishing communities and populations living in informal settlements (Chersich et al. 2018).

South Africa's National Climate Change Adaptation Strategy (DEA, 2017; Department of Environment, Forestry and Fisheries: DEFF, 2019) identified several key social, economic and biophysical factors that make the country most vulnerable to climate change. The first is South Africa's *unreliable and increasingly uncertain access to water*. Climate change will only amplify the uncertainty surrounding access to water for agricultural, domestic and industrial purposes (DEA, 2017). This vulnerability factor is crucial given that the country is already water stressed, suffers from rainfall variability on a year-to-year basis and the uneven distribution of groundwater and freshwater resources. (DEA, 2017). In addition, there is evidence of deteriorating water quality in the country's main river systems, groundwater resources and reservoirs; these water sources underpin the country's economic and social development (DEA, 2017). This once again highlights the centrality of water availability in South Africa's susceptibility to climate change, with agricultural productivity and livestock identified as other key vulnerabilities (DEA, 2017). Future changes in temperature and rainfall variability put various livestock and crop production capabilities at risk, trigger an increased demand for irrigation and leave crops and livestock more vulnerable to pests and disease; thus, people with agriculture livelihoods are exposed and vulnerable to climate change (DEA, 2017).

A number of LTAS examples indicate that regions in western South Africa are likely to become less capable of producing maize (DEA, 2017). Regions in the Western Cape that are suitable for viticulture could be significantly reduced, or begin to shift to cooler and higher altitudes, the deciduous fruit industry in the Western Cape could be at risk due to projected decrease in runoff and more areas will be at risk to damage by chilo (a pest attracted to sugarcane and tropical crops) and codling moth, which damage high-value temperature fruits such as pears (DEA, 2017). The country's biomes and ecosystems are too, vulnerable to plentiful non-climatic pressures such as human land use, bush encroachment, invasive plants and shifting wildfire regimes (DEA, 2017).

Climate change is anticipated to amplify the effect of these stressors on biomes and ecosystems, making them more vulnerable to climate change.

Climate change poses a severe threat to human health in South Africa as climate extremes take an increasingly harsh toll on property, infrastructure, and human life (DEA, 2017). Leading causes of mortality in the country include chronic diseases, conditions related to poverty, HIV/AIDS and injuries (Wright et al. 2014). These factors – intertwined with the nation's substantial levels of unemployment, inequality and food and water insecurity – are increasingly vulnerable to the direct and indirect impacts of rising temperatures and South Africa's economy is therefore considerably vulnerable and exposed to climate change (DEA, 2017). The economy is already threatened, both directly and indirectly, by veld fires, floods, and droughts (and tropical depressions over the Limpopo River Basin during wet summers (Malherbe et al. 2014)), which are projected to amplify in magnitude and frequency as the climate changes (DEA, 2017). The cost implications for the country are severe, for example, fire damage cost the forestry sector USD 3–9 million between 1980–2002 but cost the same sector between USD 6–52 million between 1980–2010 due to the accumulation of burnt land from 5 000–20 000 ha in 2002, to 9 000–70 000 ha in 2002 (DEA, 2017). South Africa's National Climate Change Adaptation Strategy (DEA, 2017) also identified the productivity and health of South Africa's labour force as another key vulnerability to climate change given that the country is highly dependent on its strong human capital and there is a wide range of stressors that could reduce labour capacity, especially negative climate-induced health impacts. The changing climate can affect human health both directly through exposure to floods and rising temperatures, and indirectly through exposure to climate-induced disease distribution shifts (DEA, 2017). Individuals with pre-existing health conditions are also more susceptible to climate change, for example, those with cardiovascular diseases are more susceptible to heat stress (DEA, 2017).

According to South Africa's National Climate Change Adaptation Strategy (DEA, 2017thethe long-term implications of spatial planning during South Africa's apartheid era are an underpinning reason for the country's disjointed urban communities and extreme poverty. These informal urban settlements have been left significantly exposed to climate change as an outcome of poor infrastructure and inefficient construction materials, high population density, poor service delivery, lack of funds, resources and insurance for weather-related damages and predisposition to fires and

floods (DEA, 2017). Communities living in rural locations are also highly exposed to climate change, weather extremes and to inadequate water supply (DEA, 2017). A large proportion of these communities are dependent on rain-fed agriculture which leaves them exposed to the projected increases in rainfall variability and water stress (DEA, 2017). Lastly, coastal communities are increasingly exposed to financial vulnerabilities as rising sea levels are resulting in real estate loss, value reduction of properties situated on beaches, damaged infrastructure and reduced tourism (DEA, 2017).

South Africa's energy systems and infrastructure are key vulnerabilities to climate change (DEA, 2017). Over 90% of South Africa's electricity is supplied through coal-fired generation, which is environmentally unsustainable and water intensive. This poses a threat to the country's future energy security and highlights the urgent need to look to renewable energy options. Climate change poses various challenges of damage and loss to the country's energy system and public infrastructure as extreme weather events increase in incidences and magnitude.

Although various types of renewable energy are the best options for climate change mitigation, South Africa's National Climate Change Adaptation Strategy (DEA, 2017) notes that renewable energy is concurrently susceptible to climate change. This is because renewable energy sources rely on, and are subsequently affected by, climatic conditions (particularly wind power, hydropower and solar photovoltaic power). Climate change projections should therefore inform renewable energy plans and implementation to decrease their susceptibility to the changing climate (DEA, 2017). South Africa's heavy dependence on carbon-intensive industries and coal leaves the country especially helpless to shifts in global carbon and trade systems (DEA, 2017). As one of the world's top twenty GHG emitters, South Africa will suffer the consequences of a global economy that is carbon-constrained (DEA, 2017). Lastly, South Africa's National Climate Change Adaptation Strategy (DEA, 2017) identified that the country is also vulnerable to climate-induced supply chain disruptions as the changing climate affects raw materials produced in sectors such as water, agriculture, and energy. Supply chain uncertainties and climate change stressors that impact consumers could simultaneously reduce consumer spending, subsequently hindering economic development (DEA, 2017).

2.3 CLIMATE GEOENGINEERING

2.3.1 An overview of climate geoengineering

Solar geoengineering is a proposed climate intervention with the potential to be impactful. "*Climate geoengineering"* (CG) refers to a large-scale intervention in the Earth's environment (atmosphere, soils and oceans) to reduce or offset the effects of alterations in atmospheric chemistry (Geoengineering Monitor; NAS, 1992) CG options have been proposed to mediate the effects of increased GHG emissions, and to complement climate change mitigation (Lenton and Vaughan, 2009; Lawrence et al. 2018). Lawrence et al. (2018) state that the current outlined efforts by signatories to the Paris Agreement to mitigate warming are not enough to limit warming to 1.5°C. Thus, researchers across the globe are looking to assess the potential of deploying proposed CG options that would alter Earth's radiative energy budget (Lawrence et al. 2018). This budget refers to the net balance between incoming (shortwave) radiation and outgoing (longwave) radiation which largely determines Earth's average surface temperature (Lenton and Vaughan, 2009). CG aims to remedy current and potential future energy budget imbalances. There are two main ways to do this. The first is to reduce the quantity of shortwave radiation that the Earth absorbs through radiative forcing techniques or SRM. The second is to increase and enhance the amount of longwave radiation that the Earth emits through various Greenhouse Gas Removal (GGR) techniques (Lenton and Vaughan, 2009; Lawrence et al. 2018). Most CG techniques, therefore, fall into two main categories: SRM or Solar Geoengineering and GGR or Carbon Geoengineering. Figures 1 and 2 display an overview of CG options, which are discussed in the following sections, while Figure 3 shows the effectiveness and affordability of these options.

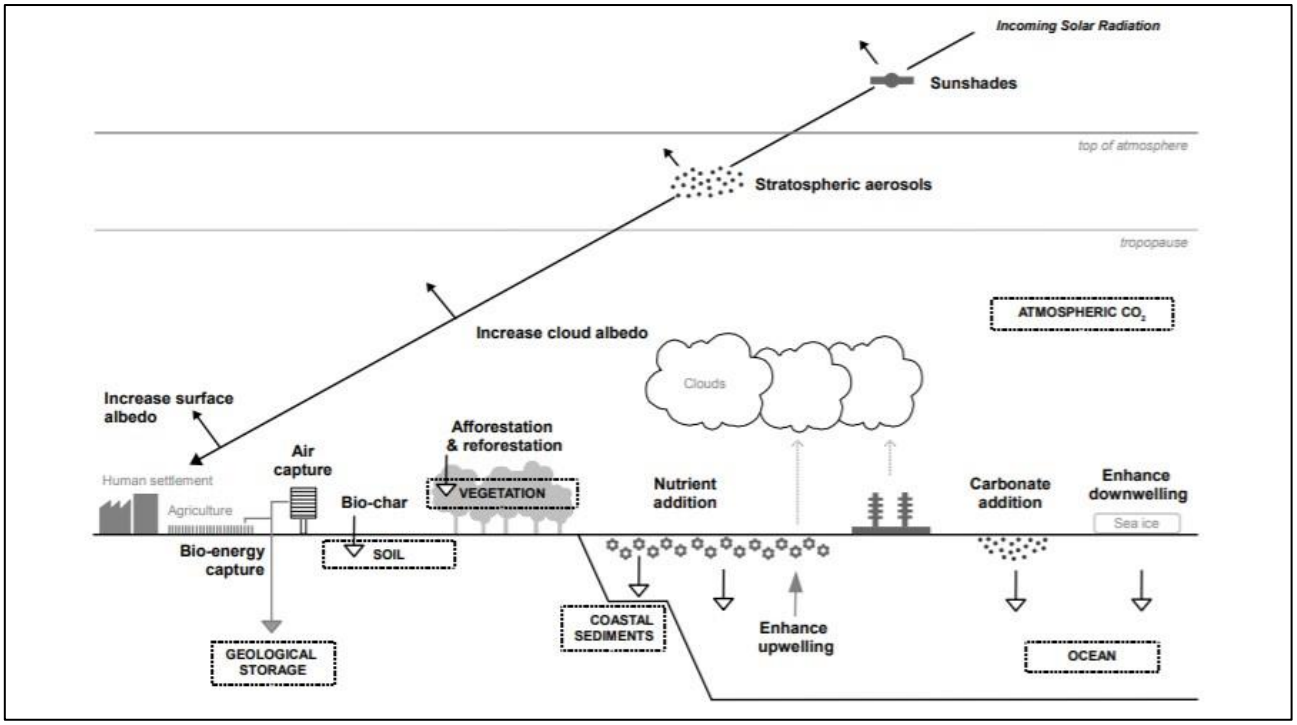

Figure 1. Schematic diagram of various geoengineering techniques of Solar Radiation Management and Greenhouse Gas Removal climate geoengineering techniques (Lenton and Vaughan, 2009).

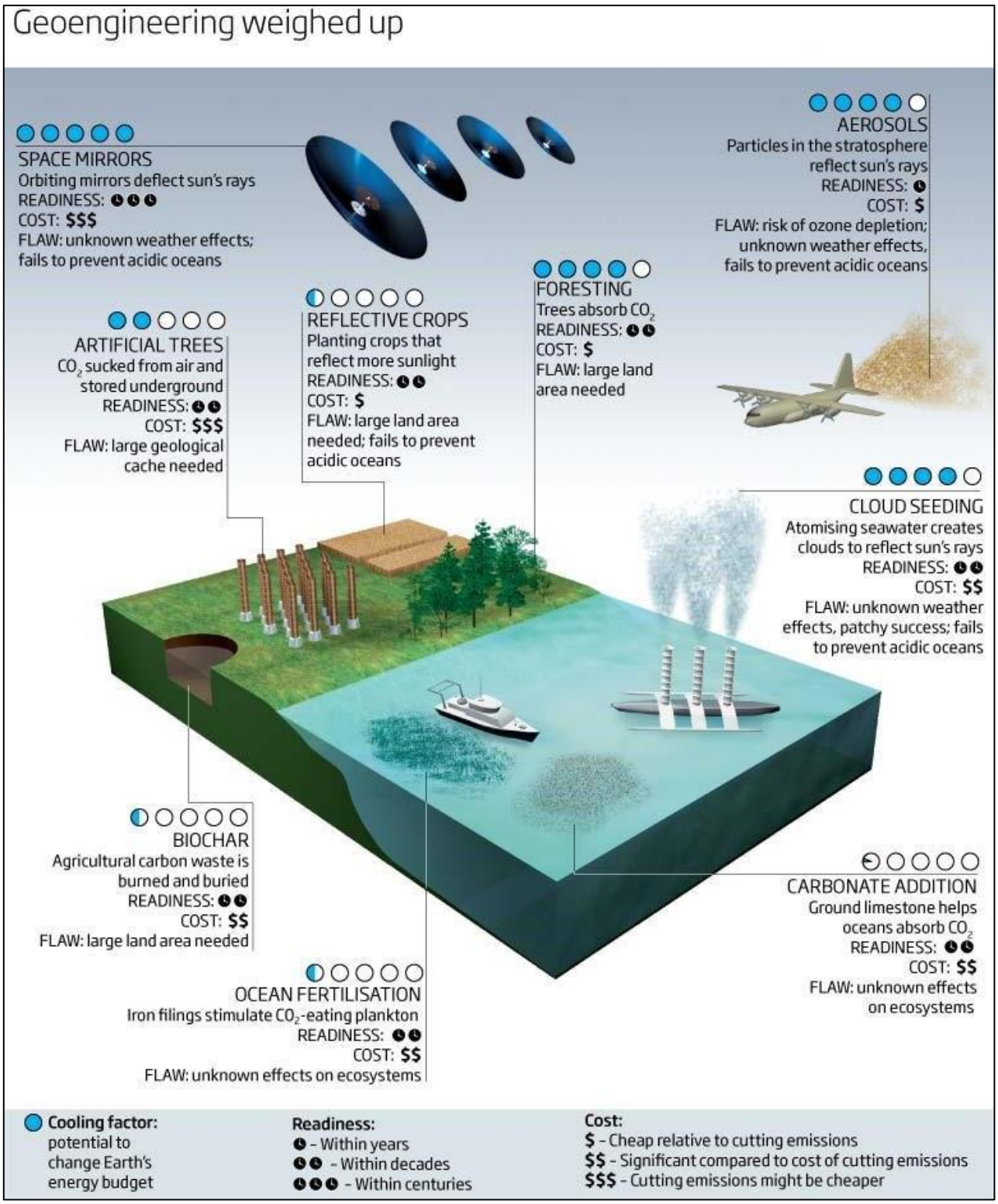

Figure 2. Visual representation of Solar Radiation Management and Greenhouse Gas Removal climate geoengineering techniques showing their cooling potential, technological readiness and cost relative to cutting down emissions (Maxey, 2015).

2.3.2 Solar Radiation Management (SRM)

Shortwave radiative CG options or SRM techniques include Marine Cloud Brightening (MCB), sunshade geoengineering or space reflectors, Cirrus Cloud Thinning (CCT), Stratospheric Aerosol Injection (SAI) and other techniques that enhance surface albedo (Lenton and Vaughan, 2009; Lawrence et al. 2018). MCB involves the injection of sea salt particles to supply cloud condensation nuclei into the marine boundary layer to seed low-altitude clouds which will enhance cloud albedo (Irvine et al. 2016; Lawrence et al. 2018). CCT proposes the injection of ice nuclei into cirrus clouds to freeze supercooled droplets in the clouds, causing the droplets to grow into large ice particles, which leave the clouds and cause the cirrus clouds to reduce in thickness and lifetime (Irvine et al. 2016; Lawrence et al. 2018). The idea of CCT is based on the fact that cirrus clouds, warm the Earth as they absorb and reemit longwave radiation, rather than reflecting incoming shortwave radiation and cooling the Earth's surface (Lawrence et al. 2018). Another technique – sunshade geoengineering – suggests the placement of large mirrors in space to reflect incoming shortwave radiation to decrease the quantity of radiation that reaches the Earth's surface. Lastly, the prospect of SRM by means of SAI is a commonly discussed approach that is increasingly being investigated as a temporary measure to offset warming – while countries simultaneously implement mitigation measures to reduce emissions, such as transitioning to renewable energy (Matlakala, 2020).

In their assessment of the radiative forcing potential of CG options, Lenton and Vaughan (2009) concluded that SAI is one of the CG techniques with the greatest potential to contribute to cooling the climate back towards its pre-industrial state. It is also a cost-effective option as Smith (2020) estimates that the average direct costs of SAI deployment in a program through to the end of the twenty-first century would be USD 18 million per 1°C of warming avoided. Figure 2 shows that SAI has the greatest potential to cool the Earth, followed by space mirrors or sunshade geoengineering. Figure 3 shows the high effectiveness and affordability of SAI.

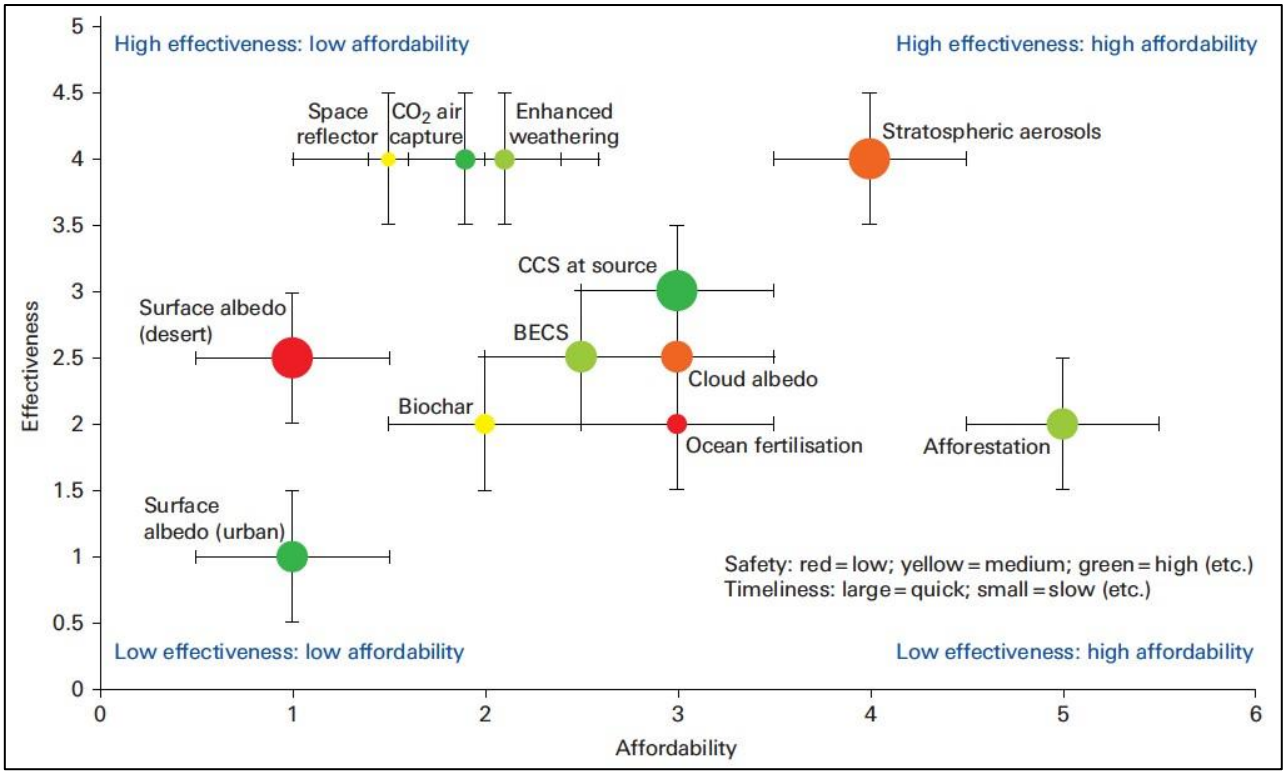

Figure 3. Evaluation of effectiveness and affordability of various Solar Radiation Management and Greenhouse Gas Removal climate geoengineering techniques (The Royal Society, 2009). The numbers on the y-axis represent a numerical rating of the potential effectiveness of the various climate geoengineering techniques with 5 being "very good" and 1 being "very poor" (The Royal Society, 2009). Similarly, the numbers on the x-axis represent a rating of the estimated affordability of the relevant climate geoengineering techniques with 6 being "high affordability" and 1 being "poor affordability" (The Royal Society, 2009).

2.3.3 Greenhouse Gas Removal (GGR)

Carbon Geoengineering options, or GGR techniques, have the potential to contribute to achieving net zero or net negative CO_2 emissions (Lawrence et al. 2018). A significant proportion of GGR proposals are biomass- and mineralisation-based techniques and other abiotic techniques (Lawrence et al. 2018). Biomass-based techniques aim to utilise photosynthesis to remove CO_2 from the atmosphere (Lawrence et al. 2018). The most common options are afforestation and reforestation, which increase and enhance carbon sinks by expanding forest cover and forest density in areas that are deforested or were previously non-forested (Lawrence et al. 2018). Another technique – "Biomass Energy with Carbon Capture and Storage" (BECCS) – has two parts. The first turns plant material into bioenergy, which can be used to produce liquid or hydrogen fuels or for

electricity generation (IPCC, 2018). The second part captures the CO_2 that is released during energy production before it reaches the atmosphere and stores it underground (IPCC, 2018).

Integrated assessment model scenarios indicate that BECCS has the potential to remove enough CO_2 from the atmosphere to restrict warming to 2°C (Lawrence et al. 2018). Soil carbon enrichment is a GGR technique with growing interest due to the capability of soil to absorb up to 500 Gt (CO_2) by 2100 if it is scaled up and more widely used (Lawrence et al. 2018). Burying or ploughing biochar – a stable form of carbon that is generated through high temperature (about 900°C) gasification or through medium temperature pyrolysis (>350°C) of biomass in an environment with low oxygen – into agricultural soils is a technique that could enrich soil carbon content (Lawrence et al. 2018). Another GGR technique is *Ocean Iron Fertilisation* (OIF) which aims to enhance ocean sinks by fertilising regions that are iron-deficient to stimulate phytoplankton growth and expand the accrual carbon flux to the deep ocean (Lawrence et al. 2018). Other biomass-based GGR techniques include accelerating peatland development and submerging timber biomass beneath anoxic wetlands, both of which have been estimated to have a limited CO_2 removal capacity of less than 100 Gt (CO_2) by 2100 (Lawrence et al. 2018).

GGR proposals also largely include mineralisation-based and abiotic techniques (Lawrence et al. 2018). There are two primary approaches to abiotic techniques to stimulate ocean alkalinisation and terrestrial weathering by scattering weathering materials across wide ranges of open space (Lawrence et al. 2018). The second approach is "*Direct Air Carbon Capture And Storage"* (DACCS), which captures CO_2 in a closed space or inbuilt machinery (Lawrence et al. 2018). Ocean alkalinisation has been proposed as a technique to counteract ocean acidity by either distributing crushed rock into surface water around coastlines, or by spreading limestone powder into ocean regions where upwelling occurs (Lawrence et al 2018). This will in turn increase ocean uptake of CO_2. There are two approaches to enhancing terrestrial weathering. The first, ex situ techniques, involves scattering silicate rocks which have been mined and ground over large open areas – specifically warm, humid regions – to increase the exposed surface area and to accelerate the uptake of CO_2 (Lawrence et al. 2018). The second approach, in situ techniques, is similar to ocean alkalinisation as it is based on GGR through forms of underground geochemical or geological sequestration (Lawrence et al. 2018). The alternative abiotic technique, DACCS, captures CO_2

directly from the air and stores it in enclosed spaces such as submarines or spaceships (Lawrence et al. 2018). DACCS is designed to consume less land or water surface area than other GGR techniques; however, it is costly (Lawrence et al. 2018). Lenton and Vaughan (2009) assessed the radiative forcing potential of different CG options and found that the discussed longwave radiation CG options, particularly CO_2 capture and storage, biochar production and afforestation, combined with ongoing mitigation efforts, have the potential to return CO_2 back to pre-industrial levels by 2100.

2.4 STRATOSPHERIC AEROSOL INJECTION (SAI)

2.4.1 Overview of SAI

When a volcano erupts, an enormous volume of sulphate aerosols is released into the stratosphere which grows into a stratospheric aerosol layer. This layer reflects a small quantity of incoming solar radiation and triggers a cooling impact on the Earth's surface (Cheng et al. 2019). SAI is based on the idea of mimicking this natural radiative forcing and involves the continuous injection of a gaseous sulphate precursor, most commonly sulphur dioxide (SO_2), into the stratosphere (Irvine et al. 2016) to cool the Earth's surface. The gaseous precursor is injected into the stratosphere instead of the troposphere because stratospheric aerosols have a longer lifetime, therefore, reducing the injection rate (English et al. 2012). The injected SO_2 oxidises within weeks to form sulphuric acid, which condenses into aerosol particles; the aerosols then coagulate and form a mass onto which the gaseous precursor (SO_2), condenses and accumulates into larger aerosol particles (Irvine et al. 2016). These particles form the aerosol layer which will enhance the reflection of solar radiation. The greater the quantity of SO_2 injected, the less sunlight is reflected back into space; this is because the process of aggregation shifts the distribution of the aerosols to particles that are larger and less reflective (Irvine et al. 2016). It is therefore imperative that the size of the aerosol particles be considered because it determines three factors:

- how efficiently light particles are scattered (with approximately 0.1 micron being the most effective particle size)
- how much the aerosols heat the stratosphere (because too much heating could, to a certain degree, weaken the scattering effect)
- particle size determines aerosol lifetime, as bigger particles deposit faster than smaller particles

(Irvine et al. 2016).

The geoengineering design – injection rate, mass and location strategy – of SAI deployment is crucial in determining the climate outcomes and effectiveness. Injecting SO_2 into the equatorial stratosphere would generate a world-wide aerosol layer because the Brewer-Dobson circulation (which rises in the tropical stratosphere and falls in the higher latitudes), would disperse the aerosols globally (Irvine et al. 2016). The injection of SO_2 from a point source would be rapidly distributed zonally as a result of strong regional flows in the stratosphere (Irvine et al. 2016). The zonal distribution would also distribute the aerosols in a poleward direction, but at a slower rate than that of an injection in the equatorial stratosphere. The altitude of aerosol injection is also important; the higher the point of injection, the longer the lifetime of the aerosols (Irvine et al. 2016). There is an overall agreement among modelling studies that injection altitudes at about five kilometres above the tropopause have greater success in decreasing global mean surface temperatures than injection locations at lower altitudes (Tilmes et al. 2018).

2.4.2 Impact of SAI on the global climate

Numerous climate modelling simulation studies have investigated how the location of SO_2 injection could impact the climate and distribution of aerosols (Tilmes et al. 2018). MacMartin et al. (2017) found that using four injection locations (15°S, 30°S, 15°N and 30°N), achieves three degrees of freedom of Aerosol Optical Depth (AOD) and subsequently, a spatially uniform AOD distribution across the globe. Studies which have used a single injection location at the equator found that SAI overcools the tropics in relation to the higher latitudes (MacMartin et al. 2017). MacMartin et al. (2017) also found that over and above balancing the global mean temperature, the three additional degrees of freedom with using the four abovementioned injection locations can be useful in balancing the equator to pole temperature gradient and the interhemispheric temperature gradient. Sun et al. (2020) compared the projected impact of two SAI injection locations, tropical and Arctic aerosol injection, on global monsoon precipitation. They performed ten 140-year modelling experiments for both locations. CO_2 was increased by 1% each year and sulphate aerosols were injected – from 10 to 100 Tg/year – into the lower stratosphere annually. The results indicated that tropical SAI was 50% more efficient in subduing global warming (by -0.6 °C per 10 Tg/yr) than Arctic SAI (by -0.3 °C per 10 Tg/year). Their findings also revealed that tropical SAI reduces precipitation on a global scale, whereas Arctic SAI triggers precipitation to decrease in the Northern

Hemisphere and to increase in the Southern Hemisphere (Sun et al. 2020). Their study showcases how the SAI experiment design can impact climate outcomes.

Most modelling studies have assessed the projected impacts of SAI on temperature and precipitation (Halstead, 2018). These studies indicate that SAI cannot undo the effects of increased GHGs, but it is consistently projected to reduce temperature and precipitation anomalies over most regions across the globe, when compared to future climate projections in a world without SAI deployment (Halstead, 2018). There is general consensus that SAI could cool the Earth within months after beginning deployment; however, continuous replenishment would be necessary to sustain its cooling effect (Halstead, 2018). Additionally, SAI could minimise the risk of destruction to positive feedback loops and tipping points if SAI were to be deployed for the purpose of reducing the magnitude and rate of warming (Halstead, 2018). For example, Tjiputra et al. (2020) investigated how SAI would impact large-scale land carbon and ocean cycles using an Earth system model under RCP8.5 between 2020 and 2100. They found that SAI enhances land carbon uptake in regions that are dominated by shrubbery, grassland and tropical and boreal forest, resulting in an average decrease in temperature (Tjiputra et al. 2015). SAI was also found to enhance ocean carbon uptake by almost 10% which results in a ~15% decrease in atmospheric CO_2 by 2100. Although SAI is not projected to significantly modify projected ocean surface pH (Matthews et al. 2009; Keller et al. 2014), the increased ocean carbon uptake is consequently anticipated to accelerate ocean acidification, especially in water deeper than 2000 m in the North Atlantic Ocean. Lastly, their study revealed that SAI would delay sea ice melt in the Northern and Southern Hemisphere's polar regions.

Many other researchers have investigated the relationship between SAI and glacial activity and sea level rise. Lee et al. (2019) investigated the projected impact of SAI deployment on permafrost and ecosystems at high-latitude and found that SAI could play a role in slowing down permafrost degradation. They found that regional variations in temperature and precipitation resulted in variations in the timing and rate of permafrost degradation of up to 40 years (Lee et al. 2019). Additionally, Moore et al. (2019) studied the projected impact of SAI deployment on the Greenland Ice Sheet and found that SAI could reduce ice sheet mass loss by 15–20% by 2070 compared to a world under the RCP4.5 scenario. They note that a combination of GHG mitigation and climate

geoengineering would be necessary to maintain the Greenland Ice Sheet as close as possible to its present-day state.

2.4.3 Regional impacts of SAI on the climate in Africa

Previous research on SAI were regionally and globally focused, with diverse outcomes (Odoulami et al. 2020). The analysis of the climatic response to SAI in Africa suggests an overall reduction in surface temperature, total precipitation and in the duration of dry spells over Southern Africa (Pinto et al. 2020). The impact of SAI on precipitation alone is less straightforward as SAI in Africa could trigger a decrease in summer rainfall, whilst causing rainfall to increase in certain regions in Africa and worsening rainfall reduction in parts of western and Southern Africa (Pinto et al. 2020).

Da-Allada et al. (2020) investigated the effect of SAI on the West African Summer Monsoon rainfall. They found that, without SAI under the RCP8.5 scenario, precipitation is projected to increase by +44,76% over the Northern Sahel (NSA), +19,74% over the Southern Sahel (SSA), and +5.14% over the West African Region (WAR) during the monsoon period. Under SAI deployment, relative to the baseline period (2010-2029), precipitation would be unaffected over NSA, while the SSA and WAR regions would experience a reduction in rainfall by -4.06% and -10.87% during the monsoon period, respectively.

Karami et al. (2020) conducted a further investigation into the impact of SAI on climate extremes. They studied how SAI would impact the storm track changes and subsequently, precipitation patterns in North Africa and the Middle East. Numerous modelling studies have projected that storm tracks will shift poleward in response to increased GHGs. Kaspi and Tamarin (2017), using an ensemble of CMIP5 models under RCP8.5, found that the Atlantic storm track will shift poleward by 1.2° and the Southern storm track by 1.6°. This means that the Mediterranean, North Africa and the Middle East would experience a significant reduction in precipitation (Karami et al. 2020). Deploying SAI could partly offset the anticipated storm track shift, subsequently offsetting decreases in precipitation that would result in response to increasing GHGs (Karami et al. 2020). Keeping

precipitation closer to present-day levels would reduce environmental stresses, especially water stress which is one of the most serious concerns in North African regions (Karami et al. 2020).

Abiodun et al. (2021) investigated the potential implications of SAI on drought risk management over Africa's major river basins. They found that SAI could reduce the Standardized Precipitation Evapotranspiration Index (SPEI) droughts by decreasing temperatures and subsequently, lower atmospheric demand, and could trigger an increase in the Standardized Precipitation Index (SPI) droughts by decreasing precipitation (Abiodun et al. 2021). The Lake Chad (located in Niger, Nigeria, Cameroon and Chad) and Senegal river basins could experience the highest decrease in the frequency of SPEI droughts, while the Juba-Shibelli basin (located in Ethiopia, Somalia and Kenya) could experience the greatest increase in the frequency of SPEI droughts (Abiodun et al. 2021). SAI deployment could therefore decrease the gap between SPEI and SPI drought projections which could assist in reducing uncertainty surrounding droughts but could also limit opportunities for drought risk mitigation by causing an increase in the lower limit of drought projections (Abiodun et al. 2021).

Odoulami et al. (2020) conducted a local-scale investigation into the potential impact of SAI deployment on the Cape Town region in South Africa with a focus on the future risk of *Day Zero* level droughts, as experienced by the Western Cape in 2015–2017. They found that deploying SAI could decrease the possibility of *Day Zero* level drought occurrences by up to 90% in the future, in comparison to a future under RCP8.5 (Odoulami et al. 2020). Their results showed that SAI could contribute to minimising rainfall reduction in the south Western Cape region by offsetting the projected southward shift in westerlies and keeping them similar to present-day conditions – and by reversing the projected upward trend of the Southern Annular Mode (SAM) (Odoulami et al. 2020). Aside from the Odoulami et al. (2020) local-scale case study which focused on the impact of SAI on a single drought event, the studies presented here showcase that current research on the impact of SAI on the climate over Africa have been conducted at a regional scale with limited insights into the impact of SAI on climate extremes at local or country scales.

2.4.4 Ethics and governance of SAI

The ethics and governance of SAI are increasingly being debated as part of the growing interest in SAI. Lenferna et al. (2017) conducted an ethical and scientific analysis related to carrying out climate

response tests and SAI deployment. In their analysis, they consider the following factors to be central ethical principles to SAI deployment:

- distributive justice
- consent and compensation
- intent

Distributive justice is an important ethical consideration because the impact of SAI may potentially be geographically unevenly and or disproportionately distributed (Lenferna et al. 2017). In addition to this ethical consideration is the possibility that the negative side effects of SAI could most harshly affect populations that are marginalised, vulnerable and have the smallest capacity to adapt to the repercussions of climate change (Lenferna et al. 2017). These populations often have no voice in political discussion and debate surrounding climate change decisions, such as the prospect of SAI deployment. The second ethical consideration outlined by Lenferna et al. (2017) – consent and compensation – is based on the necessity of obtaining a form of meaningful consent from all people who will be affected by SAI influences, to warrant robust political legitimacy for SAI deployment. This consideration extends to the question of whether those negatively affected by the side effects of SAI should be compensated, and if so, by whom. Consent, however, may be more challenging to obtain if compensation is excluded (Lenferna et al. 2017). Claims of compensation are further complicated due to the existing scientific uncertainties surrounding the differing regional effects of SAI. Lastly, it is crucial to consider the type of intent behind a SAI intervention (Lenferna et al. 2017). Intent is morally relevant in SAI considerations because it enables a clearer understanding of its policy relevance. Lenferna et al. (2017) conclude their analysis by stating that these epistemological and ethical nuances and challenges should be considered in relation to the struggles prevalent in the current and projected climate crisis.

Halstead (2018) discussed whether SAI should be investigated based on the ethical notion that the prospect of lowering existential risk is of tremendous moral importance. He identifies relevant environmental and security gains and risks of SAI research and deployment. These environmental benefits are that SAI is projected to reduce most regional temperature and precipitation anomalies compared to a future world without SAI deployment. The other environmental benefit is that SAI could lessen the risk of destruction to positive feedback loops and tipping points. Halstead (2018) identifies termination shock as an environmental risk; he argues, however, that the probability of

termination shock has been overemphasised. He asserts that termination shock poses catastrophic risks if the stratospheric aerosol layers are very thick, but this risk could be eliminated through the engineering of moderately thick aerosol layers. He continues that termination shock could be avoided by gradually phasing out SAI when the time arrives, rather than abruptly halting it. Halstead closes the environmental aspect of SAI by shedding light on the fact that there are unknown benefits and risks associated with SAI. He proposes that the unknown risks can be reduced firstly, by investing in SAI climate modelling and secondly, by gradually phasing in SAI deployment to avoid risks of extreme CG.

It is also important to consider how SAI would be governed because the efficiency, effectiveness and climate outcomes of SAI would be strongly influenced by political choices (Halstead, 2018). Halstead (2018) discusses factors surrounding SAI governance and identifies the security risks and benefits of SAI – the primary benefit being that SAI inhibits the security risks related with global warming. He finds three security risks, which are: *direct military use of SAI*, *unilateral deployment* and *the politicisation of weather and unilateral withdrawal*. The direct use of SAI by the military is a transparent security risk that could be reduced if research funders were to place firm restrictions on research around weaponising SAI. The prospect of unilateral SAI deployment poses both a security risk and governance challenges because a potential outcome is the politicisation of the weather. The effectiveness and climate outcomes of SAI depend therefore on continuous agreement by all nations or parties involved over a time period as long as a century. There is a wide range of actors capable of deploying SAI due to its low cost; for example, an alliance of states, single states or even billionaires. This poses a security risk because the actors could make decisions to suit their own interests or that of their own nation, which could result in outcomes that are substandard or even harmful to particular regions. Regional damage consequently opens the door to interstate conflict. Halstead (2018) supported that the risk of a unilateral deployment is however overstated because it is likely that the current SAI cost estimates are substantially underestimated, which ultimately shrinks the potential pool of players capable of SAI deployment. The unilateral deployment of SAI may pose a serious risk in that, if an influential actor or coalition of actors were strongly opposed to SAI, they could use military threat or counteract SAI effects to discourage SAI deployment. Ultimately, the existential risks posed by unilateral deployment are negligible because

they could not trigger a nuclear war, which is the greatest manmade existential threat (Halstead 2018).

The primary governance challenges outlined by Halstead (2018), are rooted in the potential for SAI to politicise weather and the possibility of unilateral withdrawal. For SAI to be effective, it would need to be deployed for extended time periods. Strong global agreement during this time would be crucial in order to sustain SAI deployment and its effects. However, the door for unilateral withdrawal opens with the probability that some countries or regions may be harmed by the negative effects of SAI, despite the overall harm that SAI would reduce. Furthermore, there is the possibility that some countries would experience an upsurge in hostile weather events because of climate change. The blame for these events could be placed on SAI by political members or the public, even though that may not be the true cause. This risk could be reduced if trust in climate and probabilistic models was high. In addition, compensation (as mentioned earlier) could help reduce this governance challenge. Despite the reduction in security risks of climate change, century-long global cooperation is essential and central to effectively deploy and sustain SAI.

2.5 SUMMARY OF LITERATURE REVIEW

This literature review has shown the following:

- A trend towards enhanced aridity over Southern Africa has been observed over Southern Africa since 1950, in addition to a 20% decrease in austral summer precipitation (Hoerling et al. 2006). The IPCC AR5 states that the region is projected to continue warming as the century progresses.
- The observed climate trends in South Africa between 1960–2010 suggest a significant overall increase in the frequency of annual hot extremes, and a decrease in the frequency of annual cold extremes, with the harshest warming occurring over western and north-east South Africa (Department of Environmental Affairs; DEA, 2013).
- Rainfall trends in South Africa have been mixed, however, an overall decreasing trend over the country's six hydrological zones has been observed (especially over the south coast and eastern regions) (DEA, 2013).

- Warm spells are projected to increase while cold spells decrease in South Africa over the period 2006–2095 (Kruger et al. 2019). The mixed rainfall projections indicate a moderate to significant increase in rainfall during winter and spring for the south Western Cape and the Cape south coast in the far future (DEA, 2013). A significant drying trend is projected over eastern South Africa and it is probable that autumn will become drier in the far future (DEA, 2013).
- Regarding extreme events, South Africa is anticipated to experience increased incidences of heat waves, dry spells, high fire danger days and flood events, in comparison with the historical reference of 1971–2000 (DEA, 2017). On the other hand, incidences of cold waves and intense thunderstorms are expected to decrease (DEA, 2017).
- As a water-stressed country, increased incidences of dry spells and decreased precipitation could exacerbate water scarcity (DEA, 2017). Heat waves could affect the work force, and subsequently the economy (DAE, 2017). Rising temperatures are affecting the timing of phenology, and subsequently, agricultural production, the economy, food security and tourism (DEA, 2017). Additionally, hot temperatures have implications for human health, livestock and crop production and infrastructure.
- South Africa's vulnerable communities are the most vulnerable to the adverse effects of climate change.
- Solar geoengineering is a proposed climate intervention with the potential to be impactful. SAI, a commonly discussed geoengineering technique, is based on the idea of mimicking the natural radiative forcing that occurs when a volcano erupts (Irvine et al. 2016). It involves the continuous injection of a gaseous sulphate precursor, most commonly sulphur dioxide (SO_2), into the stratosphere (Irvine et al. 2016) to cool the Earth's surface.
- Previous research on SAI has been focused on regional or global scales, with diverse outcomes (Odoulami et al. 2020). More research is needed to inform policy makers about debates surrounding SRM. If South African policy makers want to engage with the policy and ethical debates around geoengineering, further research could assist in understanding the implications of SAI for the country.

Considering the abovementioned, this study aims to assess the potential impact of SRM through SAI on projected temperature and precipitation extremes in South Africa using climate model simulations from the GLENS Project. More specifically, this proposal wants to: (i) Evaluate the ability of GLENS to simulate temperature and precipitation over South Africa and the climatic zones in South Africa; (ii) assess the impact of SAI on temperature and precipitation extremes over climatic zones in South Africa in the future; and (iii) assess how changes in the injection characteristics (varying latitudes and altitudes) of sulfate aerosols would influence the impacts of SAI on temperature and precipitation extremes in South Africa in the future.

3 CHAPTER 3 – STUDY AREA

3.1 GEOGRAPHICAL LOCATION AND TOPOGRAPHY

Located at the southernmost tip of Africa, South Africa stretches between 22–35°S latitude and 17–33°E longitude (GCIS, 2019). The country is encompassed by the Atlantic Ocean in the West and the Indian Ocean in the South and the East, and shares borders in the North with Eswatini, Mozambique, Zimbabwe, Botswana and Namibia (GCIS, 2019). The Kingdom of Lesotho is landlocked within eastern South Africa (GCIS, 2019). South Africa's topography is characterised by two geographical features, the interior plateau and the land that lies between the coast and the plateau (GCIS, 2019). Figure 4 displays the boundary between these two areas which is a continuous relief feature called the *Great Escarpment* ranging from 1 500 m above sea level in the south-west Roggeveld scarp, to 3 482 m above sea level in the Drakensberg Mountain Range (GCIS, 2019). The inland plateau refers to the southward extension of the African plateau from the Sahara Desert that is distinguished by open plains and has a mean altitude of 1 200 m above sea level (GCIS, 2019). The narrow coastal belt ranges in width from 80–240 km in the South and East to 60–80 km in the West and is in part responsible for South Africa's sharp topographic gradients (Reason, 2017). This region has three key subdivisions: the western plateau slopes, the eastern plateau slopes and the Cape Fold Belt and adjacent regions (GCIS, 2019). South Africa's topography influences the track and development of numerous weather systems, which has resulted in distinct rainfall and vegetation gradients across the country (Reason, 2017). This gradient is categorised into numerous climatic zones across the country which is displayed in Figure 4.

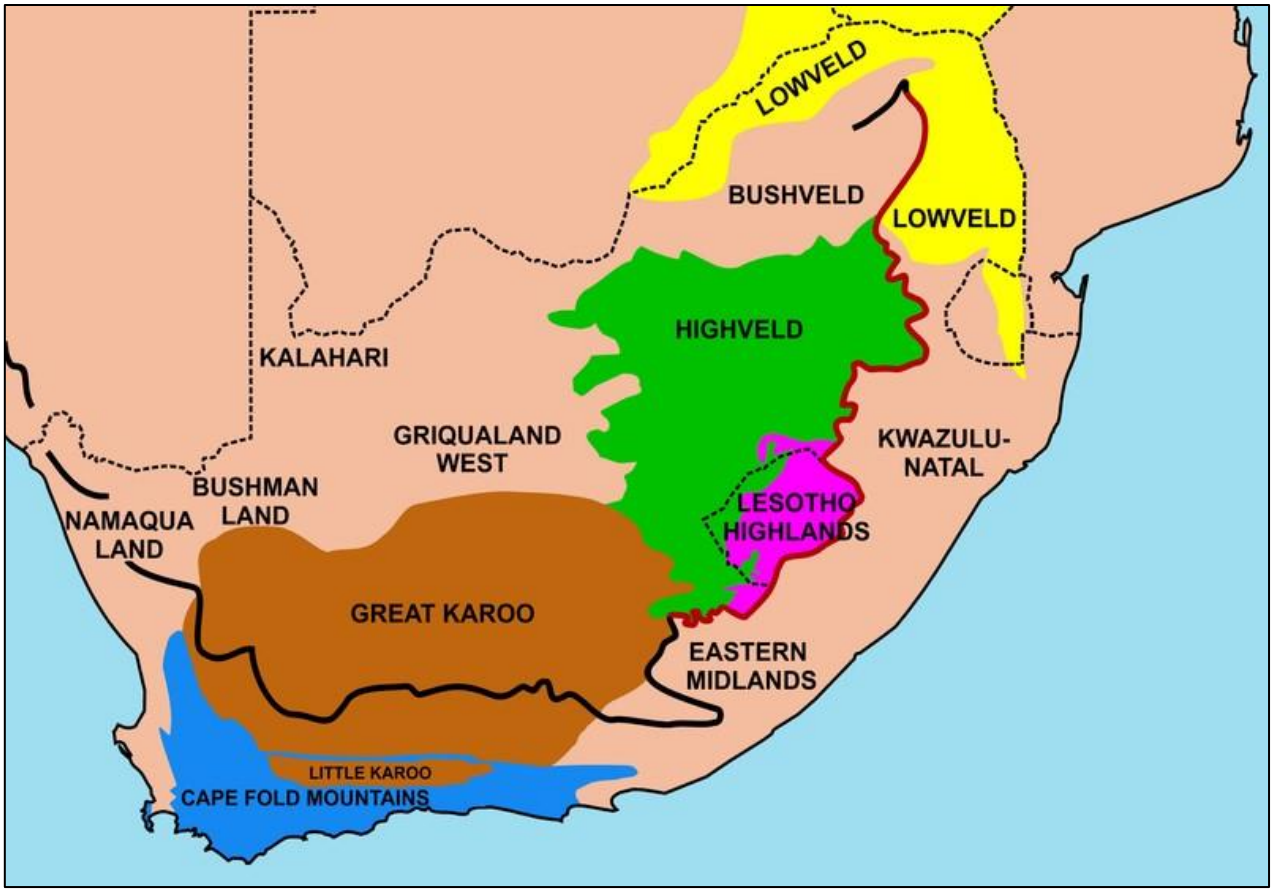

Figure 4. Important geographical regions in South Africa: the thick black line outlines the Great Escarpment and the red line indicates the Drakensberg (Oggmus, 2014).

3.2 THE CLIMATE OF SOUTH AFRICA

The combination of South Africa's subtropical location, topographical features and Atlantic and Indian Ocean surroundings, account for the country's warm temperature conditions (GCIS, 2019). The country has an average annual temperature of 17.54°C and the annual seasonal temperature cycle climaxes during the austral summer in January at 30°C and reaches a minimum at -2°C in July (World Bank Group, 2016). The interior plateau is cooler and regulates the temperature as it generally maintains the summer average to less than 30°C, and results in temperatures dipping below freezing point in certain parts (GCIS, 2019). South Africa's average annual rainfall is 469.86 mm (World Bank Group, 2016) and the majority of the country receives its rainfall during summer between October and March, aside from the south-western region which has a winter rainfall season and the far south which has year-round rainfall (Reason, 2017). The cold Benguela Current flowing in the Atlantic Ocean along the West Coast cools the air above the ocean which retains

minimal moisture, whereas the warm Agulhas Current in the Indian Ocean along the country's east coast causes the air to be warm, unstable and humid, resulting in an increase in rainfall (Reason, 2017). The highest rainfall in South Africa, therefore, occurs around the east coast (Reason, 2017). South Africa's latitudinal position is dominated by a belt of three semi-permanent subtropical highs – South Atlantic Anticyclone (SAA), the South Indian Ocean Anticyclone (SIA) and the Kalahari High – which are responsible for most of the country having dry winters (Reason, 2017).

Interannual and longer variations in rainfall are caused mainly by the El Niño Southern Oscillation (ENSO), the Indian Ocean Dipole (IOD), the Southern Annular Mode (SAM) or Antarctic Oscillation (AAO) (Reason, 2017). ENSO is a coupled ocean-atmosphere climatic event specific to the equatorial Pacific Ocean which occurs every 2–7 years (Reason, 2017), and is considered to be the dominant mode of interannual variability in the tropics. El Niño (La Niña) events are characterised by a warming (cooling) of Sea Surface Temperatures (SSTs) in the eastern and central tropical Pacific Ocean and a weakening (strengthening) of the easterly winds (National Weather Service, n.d.). In eastern and north-eastern South Africa, El Niño (La Niña) events result in high (low) pressure systems, warmer (cooler) SSTs in the Indian Ocean, offshore (onshore) winds and subsequently decreased (increased) rainfall (Reason et al. 2002). A strong positive relationship between El Niño events and severe droughts in South Africa has been observed (Mackellar et al. 2014). The south-western region in South Africa receives winter rainfall; Philippon et al. (2011) found that the years when this region has received high seasonal rainfall correlate with the occurrence of El Niño events and are the result of extended wet spells in and around Cape Town and increased incidences of wet spells extending past 33° North. The opposite result was found for La Niña events (Philippon et al. 2012). The SAM is another mode of atmospheric variability that contributes to the south-western region's winter rainfall (Reason et al. 2005). SAM is a fundamental mode of tropospheric circulation variability (Reason et al. 2005) between the midlatitudes and high latitudes of the Southern Hemisphere through the oscillation of atmospheric pressure between the southern midlatitudes and the Antarctic region (Driver, P. 2014). A negative SAM event (in South Africa) is characterised by an intensification of the subtropical jet stream just above the south-western Cape region and significant cyclonic anomalies extending over the region from the south-west Atlantic Ocean, and subsequently wetter winters (Reason et al. 2001). Reason et al. (2005) found that six of the seven wettest winters in the south-western region between 1948–2004 transpired during a negative SAM

phase, and the driest winters occurred during a positive SAM phase. Lastly, the IOD is a naturally occurring coupled ocean-atmosphere climatic event that influences the global climate (Reason, 2017). Positive IOD events are characterised by warmer sea surface temperatures in the south-west Indian Ocean, resulting in above-average rainfall in parts of Southern Africa and enhancing the effect of El Niño over South Africa (New et al. 2014). El Niño events are also amplified by the Madden-Julian Oscillation (MJO), an intraseasonal eastward movement of clusters of large-scale convective low pressure systems in the tropics, lasting between 30–60 days and resulting in a further reduction in rainfall (New et al. 2017). South Africa's regional location and land-sea distribution have resulted in pronounced climate variability across seasonal, interannual and longer time scales.

3.3 CLIMATIC ZONES IN SOUTH AFRICA

The potential outcomes produced by SAI deployment across the country's main climatic zones will be explored to attain deeper insight into how SAI could affect climate extremes. There are various classifications of climatic zones in South Africa. Two of them are analysed in this section.

The first identified six climatic zones in South Africa are based on annual total rainfall and variations in rainfall seasonal cycles (Figure 2a; African Development Bank: ADB 2018). These identified regions are the Southwestern, Eastern/Central, Northern/Central, Western/Central, Southern and Transitional regions (Figure 2 a). The Southwestern region is characterised by winter rainfall with mean annual rainfall ranging between 300–1200 mm from north to south with low interannual variability and an average temperature of 17°C with an inter-seasonal range of 11°C (ADB, 2018). The Eastern/Central region is characterised by summer rainfall with mean annual rainfall ranging between 600 mm to more than 1000 mm from the west to the east coast with low interannual variability and an average temperature of 17°C with an inter-seasonal range of 10°C (ADB, 2018). The Northern/Central region transitions from the high rainfall Eastern/Central region and is characterised by summer rainfall with mean annual rainfall ranging between 400–600 mm with moderate interannual variability (ADB, 2018). The region is characterised by an average temperature of 20°C with an inter-seasonal range of 10°C (ADB, 2018). The arid Western/Central region is characterised by summer rainfall with an annual rainfall averaging below 400 mm and strong interannual variability (ADB, 2018). The region has an average temperature of 19°C with an

inter-seasonal range of 12°C (ADB, 2018). The Southern region is distinguished by all-year around rain with mean annual rainfall ranging between 400–600 mm and low interannual variability (ADB, 2018). The region has an average temperature of 17°C with an inter-seasonal range of 10°C (ADB, 2018). Lastly, the most arid Transitional region is characterised by summer rainfall with mean annual rainfall remaining below 250 mm and strong interannual variability (ADB, 2018). The region has an average temperature of 18°C with an interseasonal range of 12°C (ADB, 2018).

The second identified nine homogenous rainfall regions in Southern Africa (Figure 5. b; Landman and Goddard 2005). These nine homogenous rainfall regions in Southern Africa (Figure 5. b) are the southwestern Cape; south coast; Transkei; KwaZulu–Natal coast; Lowveld; north-eastern Highveld; central interior; western interior; northern/western Botswana (Landman and Goddard, 2005). The twelve climatic zones identified by Nemakononi (2020) by superimposing the zones in the Figures 5. a) and 5. b) and are presented in Figure 5. c).

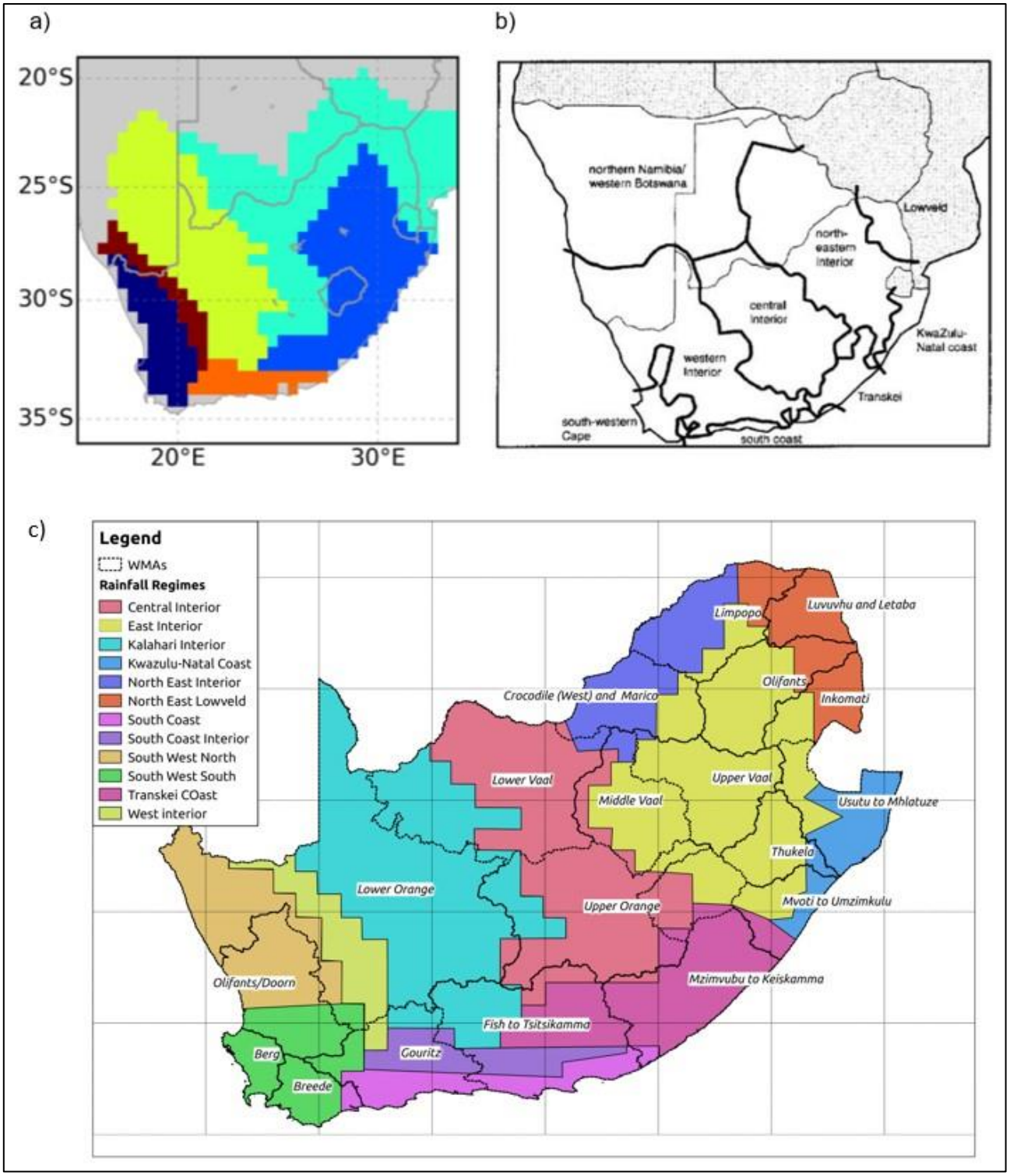

Figure 5. Rainfall and temperature regions in South Africa. (a) Map displaying the six identified rainfall and temperature regions in South Africa (World Development Bank, 2018). (b) The nine homogenous rainfall regions identified in Southern Africa (Landman and Goddard, 2005). (a). and (b). were superimposed to create (c), representing South Africa's climatic zones (Nemakononi, 2020), which will be used in this study. The titles on the map in (c)

represent South Africa's water management areas to which water resources are allocated (Statistics South Africa, 2010).

Table 1. The names and abbreviates of the climatic zones to be analysed

ABBREVIATION	CLIMATIC ZONE
CEI	Central Interior
EAI	East Interior
NAI	Kalahari Interior
KNC	KwaZulu-Natal Coast
NEI	North East Interior
NEL	North East Lowveld
SCO	South Coast
SCI	South Coast Interior
SWN	South West North
SWS	South West South
TCO	Transkei Coast
WEI	West Interior
SAF	South Africa

4 CHAPTER 4 – DATA AND METHODOLOGY

This chapter provides an overview of the data and methodology used in this study. The section begins with a description of the various datasets used in this study, where the datasets were sourced from and how they were processed. This is followed by Table 2 which presents a summary of the datasets used. The section moves forward with a description of the methodology used in this study: a model evaluation, an assessment of the projected changes in temperature and precipitation extremes with and without SAI deployment, and a comparative analysis consisting of three components. These components include a comparison of the feedback experiments to the baseline period (2010–2030), a comparison of the control future to the baseline period (2010–2030) and a comparison of the feedback experiment with the control future experiment.

4.1 DATA

This research used two types of datasets: observation datasets and climate model simulations. To validate the GLENS model simulations, this study used observation temperature data from the "Climate Research Unit" (CRU TS4.03; Harris et al. 2014, Harris and Jones 2020) and precipitation data from the "Climate Hazards Group Infrared Precipitation with Stations" (CHIRPS; Funk et al. 2015). The CRU TS4.03 data are monthly high-resolution (0.5° x 0.5°) gridded fields which are built from observational data on a monthly basis that is calculated from daily data by National Meteorological Services and additional external groups (Harris and Jones, 2020). The CRU TS4.03 dataset contains variables such as potential evapotranspiration (PET), cloud cover, frost day frequency, monthly mean temperature, diurnal temperature range, vapour pressure and monthly maximum and minimum temperatures (Harris & Jones, 2020). The CHIRPS dataset is a quasi-global (50°S–50°N), high-resolution (0.05° x 0.05° degree), daily, pentadal and monthly precipitation dataset, which was constructed to monitor agricultural drought and terrestrial environmental changes on a global scale (Funk et al. 2015). Both annual and seasonal precipitation and temperature data over South Africa during 1990–2009 were extracted and used to validate the model's performance over the same period.

The climate model simulation data used in this study is from the *Stratospheric Aerosol Geoengineering Large Ensemble* (GLENS) project (Tilmes et al. 2018). The GLENS project provides a large ensemble of stratospheric sulphate aerosol geoengineering simulations from the *National*

Centre for Atmospheric Research (NCAR) *Community Earth System Model (CESM1), which used the Whole Atmosphere Climate Community Model* (WACCM) as its atmospheric component (CESM1(WACCM); Mills et al. 2017). The GLENS project includes three main experiments: historical, control and feedback simulations. The historical experiment is a single-member simulation that runs between 1990–2009. The control experiment consists of twenty simulations under the RCP8.5 during the period 2010–2030 (baseline period) with three simulations extended up to 2097 (Kravitz et al. 2019). The feedback experiment that runs between 2020–2099 is a twenty-member ensemble simulation in which SO_2 is simultaneously injected at four latitudes: 30°S, 15°S, 15°N and 30°N at 180°E into the stratosphere (Kravitz et al. 2019). Each injection occurs in a single grid cell at a 25 km altitude at 15°N and 15°S latitude and a 22.8 km altitude at 30°N and 30°S latitude, with the rate of injection being dynamically attuned for the duration of the simulation run to maintain the following three systems of measurement of surface air temperature at 2020 levels: pole-to-equator gradient, global average temperature and inter-hemispheric difference (Irvine and Keith, 2020). Additionally, two other feedback experiments available in the GLENS project were considered in this project: Feedback Equator (Feedback_Eq) and Feedback Low (Feedback_Low).

Feedback_Eq is a three-member ensemble that simulates a single injection of SO_2 at the Equator at a height of 20–25 km above the ground to sustain mean surface temperatures at 2010–2030 levels for the period 2020-2099 (Kravitz et al. 2019). The last feedback simulation (Feedback_Low) is also a three-member ensemble that simultaneously injects SO_2 at 1 km above the tropopause into the stratosphere at the same four latitudes as in the feedback simulation to maintain mean surface temperatures at 2010–2030 levels for the period 2020-2099 (Kravitz et al. 2019). This study used three ensemble members in each simulation to maintain consistency. The three feedback experiments that were used in this study, each with differing altitude and/or injection location characteristics, can be used to recognise regional and seasonal changes in the climate, in addition to changes in climate extremes and variability (CESM, n.d.). Varying injection characteristics were also used to identify existing limits to SAI (CESM, n.d.). Table 2 presents a summary of the GLENS simulations that were used in this study.

Table 2. Summary of GLENS simulations used in this study

GLENS EXPERIMENTS	SO_2 INJECTION CHARACTERISTICS		SIMULATION PERIOD	ENSEMBLE SIZE
	ALTITUDE	LOCATION		
Historical	-	-	1990–2009	1
Control	-	-	2010–2030 (of which 3 members are extended to 2097)	3
Feedback	25 km above ground	15°N, 15°S latitude (at 180°E longitude)	2020–2099	3
	22.8 km above ground	30°N, 30°S latitude (at 180°E longitude)		
Feedback_Eq	20-25 km above ground	0° (at the equator)	2020–2099	3
Feedback_Low	1 km above tropopause	15°N, 15°S, 30°N, 30°S (at 180°E longitude)	2020–2099	3

4.2 METHODOLOGY

4.2.1 Model evaluation

It is necessary to evaluate the model to assess how accurate its simulations are in comparison with observations. The model accuracy is indicative of how often the model makes correct predictions (Rawat, 2019). Pinto et al. (2020) assessed the CESM1(WACCM) model performance in relation to the CRU observed temperature and CHIRPS observed rainfall estimates for the historical reference period 1981–2009 over four regions in Africa (Southern Africa, East Africa, West Africa and Central Africa). They found that the model reproduces the spatial distribution of the meteorological patterns of precipitation and temperature well, with good levels of agreement for both variables (Pinto et al. 2020). The model also reproduced the temperature and precipitation seasonal cycles well (Pinto et al. 2020). They, however, noticed that the model overestimates average temperature in all regions throughout the year, in addition to overestimating temperature and

precipitation in sub-Saharan Africa. They also found that the overestimation of the magnitude of rainfall is relatively higher over the Central and Southern African regions (Pinto et al. 2020). As the research here focused specifically on South Africa, it was necessary that the model be evaluated again in this study to assess its ability to simulate key climatic variables such as precipitation and temperature over the country. The model evaluation therefore assessed how well the historical simulations of precipitation and temperature in GLENS reproduce the spatial distribution and seasonal cycle (austral winter and summer) of precipitation and temperature over South Africa and the climatic zones in the country over the common period 1990–2009, in comparison to CHIRPS and CRU respectively. This model evaluation could be improved in many ways but for the sake of time it was limited to seasonal distribution of precipitation and temperature.

4.2.2 Projected changes in precipitation and temperature extremes

The second step in the methodology was to assess the future projected changes in temperature and precipitation extremes across South Africa's climate zones (Figure 5. c) in future climates with and without SRM for the period 2075–2095, against the baseline period (2010–2030). This was done by comparing the Feedback and Control simulations for the future period (2075–2095) with simulations from the Control baseline period (2010–2030). This was to inform the potential impact of SAI on temperature and precipitation extremes across the climatic zones in South Africa. The difference between the future with and without SAI was also assessed to explore the effectiveness of SAI. These changes were evaluated by using a selected number of extreme precipitation and temperature indices from the "Expert Team on Climate Change Detection and Indices" (ETCCDI) (Table 3). The ensemble means were used to display the scale of the projected changes for the calculated indices and the number of ensemble members that agree with the direction (sign) of the projected changes informed on the level of agreement of the ensemble (Pinto et al. 2020).

Table 3. List of extreme temperature and precipitation indices used in this study

TEMPERATURE INDICES		**PRECIPITATION INDICES**	
INDEX	DESCRIPTION	INDEX	DESCRIPTION
TNN	Monthly minimum value of daily minimum temperature (°C)	PRCPTOT	Total wet-day rainfall (mm)

TXX	Monthly maximum value of daily maximum temperature (°C)	R10MM	Days when rainfall is at least 10 mm (days)
TN10P	Fraction of days with cold night-time temperatures (%)	RX1DAY	Maximum amount of rain that falls in one day (mm)
TN90P	Fraction of days with warm night-time temperatures (%)	RX5DAY	Maximum amount of rain that falls in five consecutive days (mm)
TX10P	Fraction of days with cool day time temperatures (%)	CDD	Longest dry spell or maximum number of consecutive days when rainfall is less than 1.0 mm (days)
TX90P	Fraction of days with hot day time temperatures (%)	R95P	Total annual amount of rainfall from very wet days (mm)
WSDI	Number of days contributing to a warm period where the period has to be at least 6 days long (days)		

The final step in the methodology was a comparative analysis consisting of three components: a comparison of the feedback experiments to the baseline period (2010–2030), a comparison of the control future to the baseline period (2010–2030) and a comparison of all three feedback experiments with the control future experiment.

5 CHAPTER 5 – RESULTS

5.1 MODEL EVALUATION

This model evaluation assesses how well the historical simulations of precipitation and temperatures (maximum and minimum) in the CESM1(WACCM) – used in the GLENS project – reproduce the spatial distribution and seasonal cycle of precipitation and maximum and minimum temperatures over South Africa (SAF) and the twelve climatic zones in the country (Figure 6), over the common reference period 1990–2009 (Figure 7 and 8), in comparison to CHIRPS and CRU respectively.

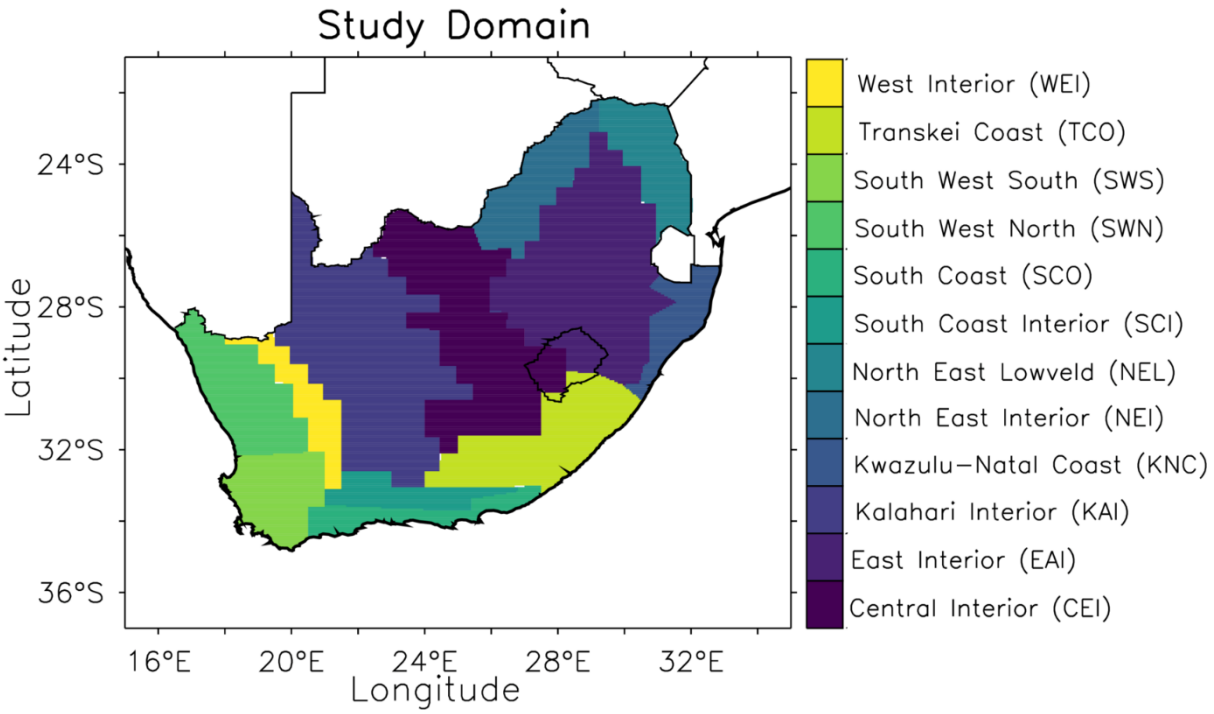

Figure 6. South Africa's twelve climatic zones as represented in the climate model data. More on these climatic zones is provided in section 3.3 and Figure 5.

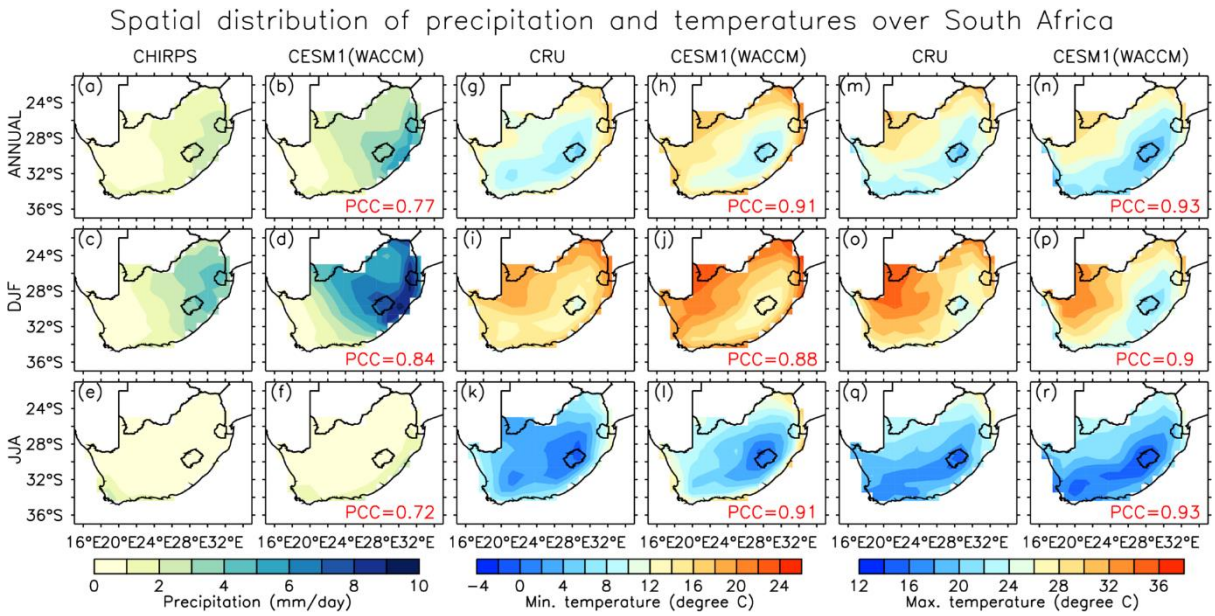

Figure 7. Spatial distribution of annual mean and seasonal (austral summer and winter) means of precipitation, minimum and maximum temperatures as observed by CHIRPS and simulated by CESM1(WACCM) model during 1990–2009 over South Africa. The pattern or spatial correlation between observed and simulated patterns is PCC. The observations were regridded to the same spatial resolution as the model using bilinear gridding.

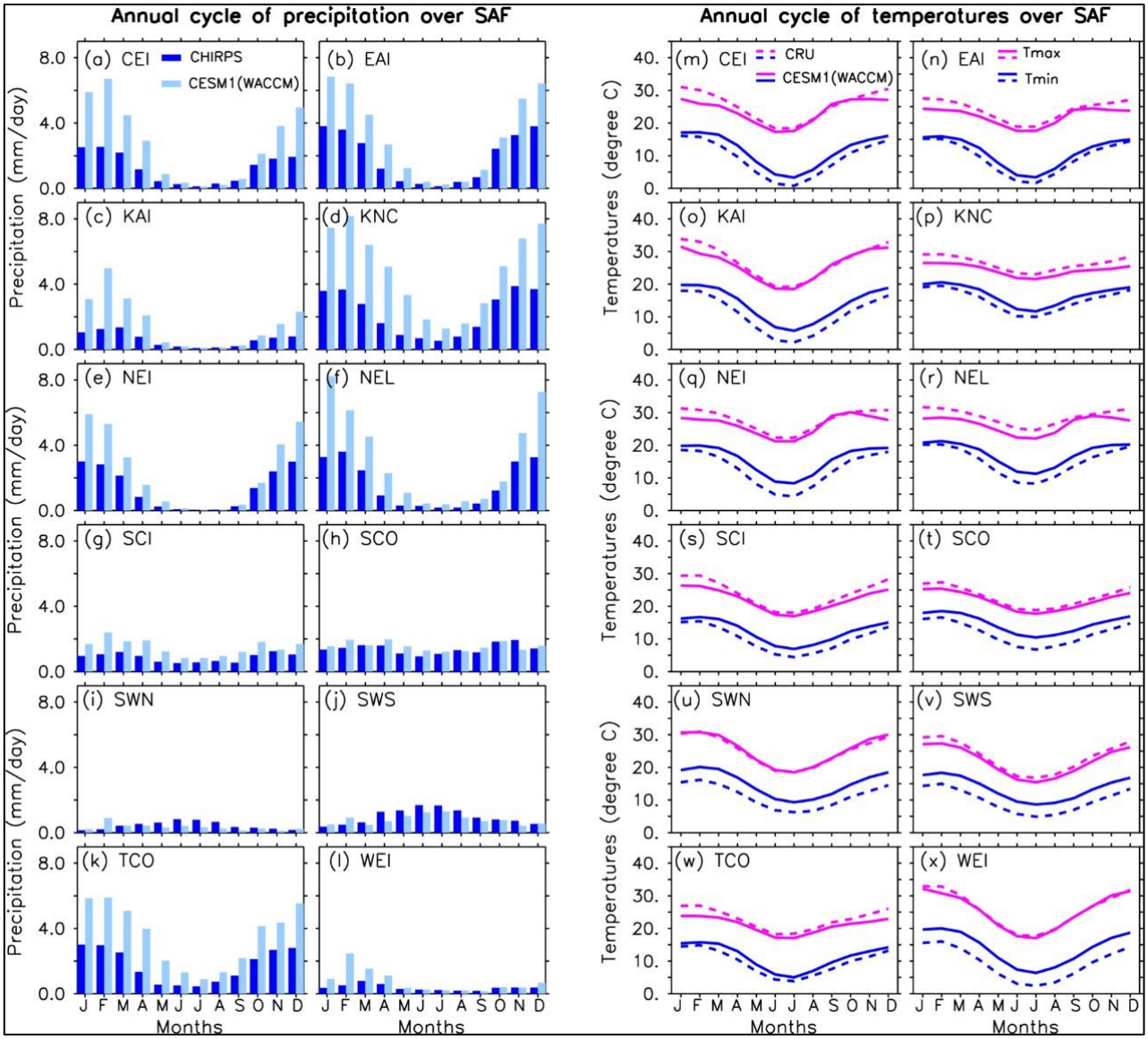

Figure 8. Annual cycle of precipitation and the minimum and maximum temperatures over the climatic zones in South Africa as observed by CHIRPS and simulated by CESM1(WACCM) over the period 1990–2009.

Twelve climatic zones characterising SAF are considered in this study based on a combination of South Africa's homogenous rainfall regions, annual total rainfall and rainfall seasonal variations (Figures 7 and 8). The CESM1(WACCM) model reproduced well the spatial distribution of annual and seasonal (austral winter or JJA and summer or DJF) mean precipitation as observed over South Africa. The model reproduces well the observed gradient in the annual and summer mean precipitation over SAF, which increases from the western and south-western coast to the East. The pattern correlation coefficient (PCC) ranging between observed and simulated precipitation is high,

ranging between 0.77 and 0.84 (Figure 7). Despite the good level of agreement between observed and simulated precipitation over SAF, the model overestimates the annual and summer spatial distribution of precipitation over the regions with peak precipitation located in north-east SAF and along the south-west coast of SAF. The regions where precipitation is overestimated have a summer rainfall season. The seasonal cycle of precipitation (Figure 8) is well reproduced by the model across the country's climatic zones. The SAF zone (Figure 8) shows that overall, the model reproduces well the country's mean precipitation – especially during winter – and tends to overestimate summer precipitation. Figure 8 shows that the model simulates well the seasonal cycle over the climatic zones of the country along the south coast (SCO and SCI), particularly in winter. Precipitation is slightly underestimated in the SWN and SWS climatic zones, both of which have a winter rainfall season. The model tends to overestimate precipitation in the remaining climate zones, which all have a summer rainfall season, particularly KAI, CEI, TCO, EAI, NEI, and NEL. The discrepancies observed in the model's ability to simulate the spatial distribution (Figure 7) agree with those in the seasonal cycle (Figure 8). Firstly, the regions where summer rainfall is overestimated in Figure 8 coincide with the corresponding climatic zones in Figure 8. Secondly, the eastern coastline where precipitation is slightly overestimated in Figure 8 coincides with the corresponding climatic zones – TCO and KNC – in the seasonal cycle (Figure 8). Thirdly, the underestimated rainfall in south-western SAF reflected in Figure 8 coincides with the corresponding climatic zones (SWN and SWS) in the seasonal cycle (Figure 8). The overall high levels of agreement between the spatial distribution and seasonal cycle of precipitation reflect well on the model's consistency in reproducing the observed precipitation across South Africa.

The model simulates well the spatial distribution of annual and seasonal mean of minimum and maximum temperatures over SAF (Figure 7). The PCC calculated between CRU and the model are high and range from 0.88 to 0.93 (Figure 7). Despite the strong spatial agreement between observed and simulated temperatures over SAF, the model tends to overestimate the annual, summer, and winter mean of minimum temperatures and underestimate the observed mean of maximum temperatures across the country (Figure 7). Maximum temperatures are underestimated in central SAF, in addition to the northern eastern regions of the country. Figure 8 (annual cycle of temperatures over SAF) shows that the model's ability to simulate the seasonal cycle of observed mean maximum temperatures across the country's climatic zones is good. The model well

reproduces the mean of maximum temperatures across all climatic zones, especially during winter in the TCO, WEI, CEI, KAI, NEI, SCI, SCO, SWN, and SWS climatic zones. The model does, however, tend to slightly underestimate maximum temperatures in summer in a few climatic zones, particularly TCO, CEI, EAI, KAI, KNC, NEI, NEL, and SCI. Conversely, the model tends to overestimate the mean of minimum temperatures in most months of the year over the climatic zones (Figure 8). The discrepancies observed in the model's ability to simulate the spatial distribution (Figure 7) tend to agree with those in the seasonal cycle (Figure 8). The areas where the mean of maximum summer temperature is underestimated coincide with the corresponding climatic zones in Figure 8. Secondly, the annual mean of minimum temperatures across SAF is overestimated by the model both in the spatial distribution (Figure 7) and the seasonal cycle (Figure 8) over all the climatic zones. The consistency between the spatial distribution and seasonal cycle of maximum and minimum temperatures reflects well on the model's capability to simulate observed maximum and minimum temperatures across South Africa.

The overall high levels of agreement between simulation and observation for temperature and precipitation indicates that the CESM1(WACCM) has a good ability to reproduce the CHIRPS precipitation and CRU maximum and minimum temperature datasets during 1990–2009.

5.2 PROJECTED CHANGES IN THE SPATIAL DISTRIBUTION OF CLIMATE EXTREMES

5.2.1 Projected changes in climate extremes over South Africa under RCP8.5

5.2.1.1 Precipitation

The spatial distribution of GHG-induced alterations in extreme precipitation indices over SAF in 2075–2095 relative to the baseline period (2010–2030), is shown in the middle left-hand column in Figure 9. The impact of increased GHGs on precipitation extremes varies spatially across the country. Widespread decreases in the annual spatial distribution of all extreme precipitation indices, except for the maximum length of dry spells (CDD), are projected across the country. The area moving from the central interior (where there is high agreement among the model's ensemble members), to western SAF could become less vulnerable to flood conditions under RCP8.5 as decreases are projected for the number of heavy precipitation days (R10MM; up to -4 days/year), the daily maximum amount of precipitation (RX1DAY; up to -8 mm/day), the maximum consecutive 5-day

precipitation (RX5DAY; up to -12 mm/5-day) and the total annual amount of rainfall from very wet days (R95P; up to -30 mm/year). In contrast, the projected decrease in the total wet days precipitation (PRCPTOT; up to -80 mm/year) suggests increased vulnerability to drier conditions. Areas where PRCPTOT is projected to decrease are often associated with increases in CDD, and vice versa. All ensemble members agree that Western SAF would experience a substantial increase in CDD, exceeding +20 days/year in some places. North-eastern SAF is projected to experience a decrease in R10MM (up to -4 days/year), R95P (up to -30 mm/year) and PRCPTOT (up to -80 mm/year). These findings agree with Muthige et al. (2018) who found that the Limpopo River Basin, located in northeast SAF, would experience decreased precipitation due to projected declines in tropical cyclones and tropical lows over the south-west Indian Ocean under various global warming levels. On the other hand, Eastern SAF and the eastern coastline are areas projected to experience increases for RX1DAY (up to over +8 mm/day) and RX5DAY (up to over +16 mm/5-day). Likewise, PRCPTOT (up to +100 mm/year) and R10MM (about +4 days/year) would increase along the eastern coastline. All ensemble members agree that the latter, R10MM, would increase (by +4 days/year on average) in the central interior. These findings align with the previous reporting that eastern SAF will experience an increase in thunderstorm events (DEA, 2017), and indicates that the region will grow increasingly vulnerable to extreme precipitations and flood conditions. Lastly, CDD is projected to decrease (up to -12 days/year) slightly in eastern SAF and along the southern and south-eastern coastline.

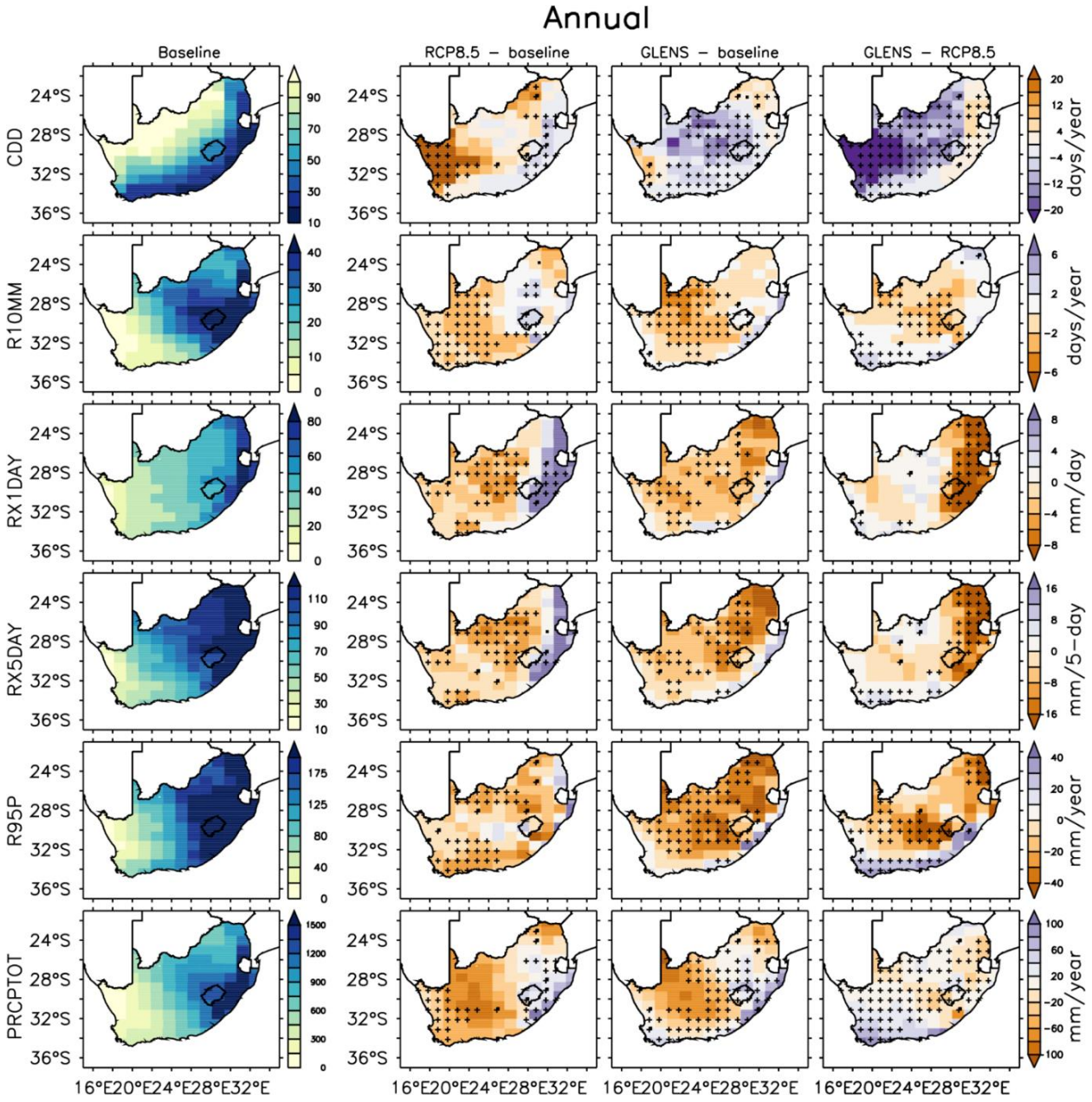

Figure 9. The ensemble mean of annual extreme precipitation indices over South Africa for the present-day or baseline period (2010–2030; left-side column) as simulated by the CESM1(WACCM) model in the Geoengineering Large Ensemble (GLENS) project. Mean projected impacts of GHG-induced warming under RCP8.5 (RCP8.5-baseline; middle left-hand column) and of stratospheric aerosol injection or SAI (GLENS – baseline; middle right-hand column) on annual extreme precipitation indices over South Africa in 2075–2095 relative to the baseline period (2010–2030). Mean annual impact of SAI on projected annual precipitation indices under RCP8.5 (GLENS – RCP8.5; right-hand column). The '+' signs indicate areas where all ensemble members agree on the sign of the projected change.

The projected impact of increased GHGs on extreme precipitation reveals that while regions such as western and north-eastern SAF would become vulnerable to drying conditions (increased CDD and decreased PRCPTOT), others such as parts of eastern SAF and the eastern coastline could become more vulnerable to extremely wetter conditions (increased R10MM and R95P). The projected future dry conditions in this study agree with the IPCC SR1.5 which shows that Southern Africa is projected to experience a drying trend in response to GHG-induced warming (IPCC, 2018). The risks associated with drought include desertification and increased wildfires, while those associated with wetter conditions include flooding and storm surges. Increases in these climate extremes would have overlapping and wide-ranging implications for a number of building blocks that underpin social and economic development in the country. These include human health, agriculture and livelihoods, irrigation, biodiversity and water supply and availability (DEA, 2017). The impact of increased GHGs on precipitation extremes highlights the country's susceptibility to the adverse impact of climate change.

In summer, increased GHG emissions are projected to intensify precipitation extremes over SAF for the period 2075–2095 with reference to the 2010–2030 baseline period (Figure 10). All ensemble members agree on the projected increases in PRCPTOT (more than +20 mm/month on average) and R10MM (up to +1.5 days/month) in summer over the central interior moving east and north-eastward under the RCP8.5 scenario (Figure 10). This result aligns with Hewitson and Craig (2006) who found that South Africa is projected to experience enhanced summer precipitation over the country's convective region covering the eastern and central plateau and the Drakensberg Mountains. While increases are projected in east and north-east SAF, GHG-induced warming would decrease PRCPTOT (up to -12 mm/month) and R10MM (up to -0.5 days/month) in the west and south-west SAF, a region characterised by winter rainfall season. Similar to the projected impact of GHG-induced warming on annual precipitation extremes, increased summer PRCPTOT is associated with decreased CDD and vice versa. Western SAF is projected to experience the highest increase in CDD (more than +5 days/month), while the central interior moving east- and north-eastward would experience decreased CDD by up to -2 days/month. There is a high level of agreement among the model's ensemble members that CDD would increase over most of western SAF. An increase in RX1DAY (up to over +5 mm/day) and RX5DAY (up to over +10 mm/5-day) is projected over north-east SAF and the eastern coastline, whilst they are projected to decrease (by up to -3 mm/day and

-6 mm/5-day respectively) over the rest of the country. This finding suggests that eastern and north-eastern SAF would grow increasingly vulnerable to flood conditions during summer while western SAF would experience drier summer conditions under RCP8.5.

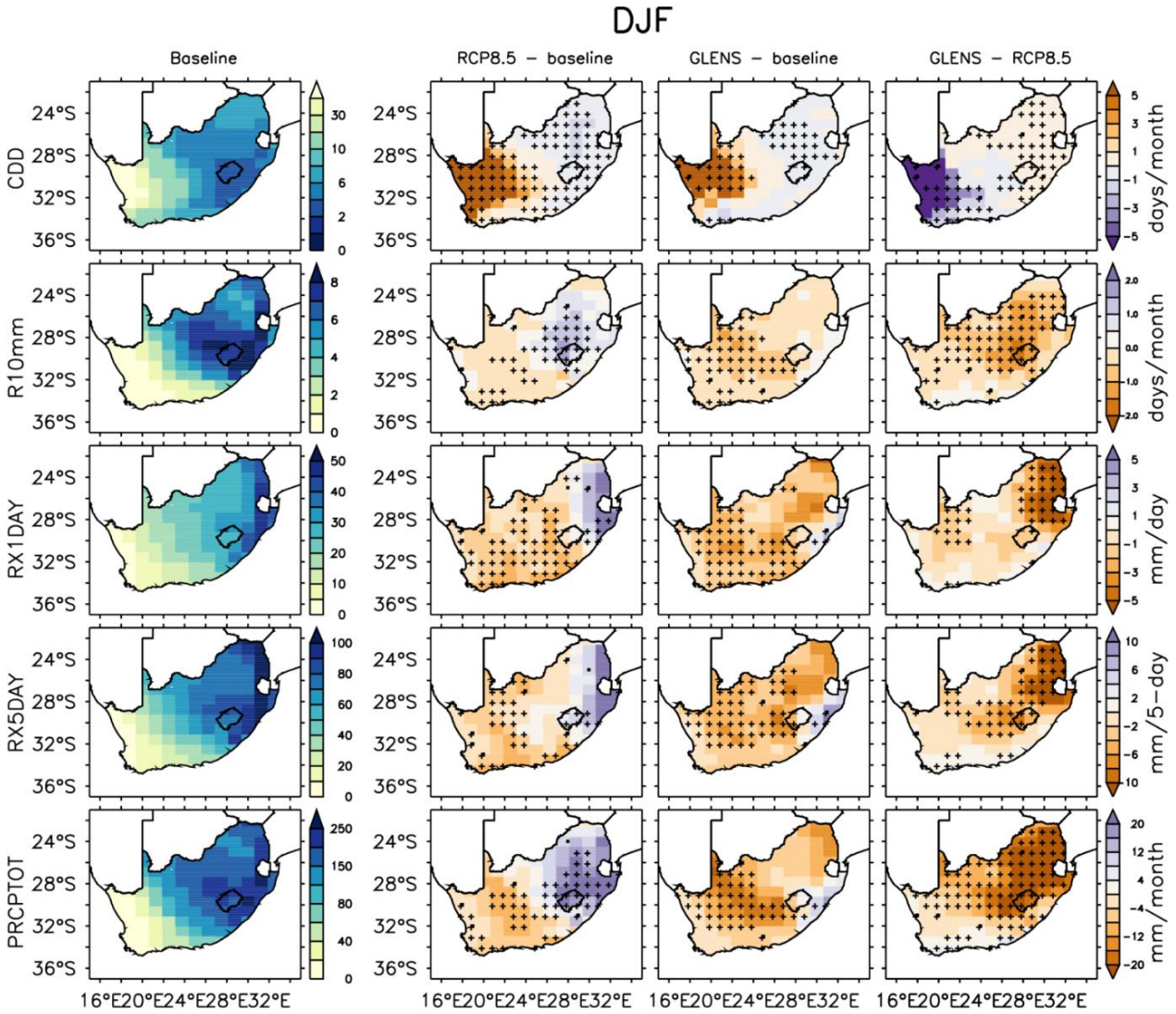

Figure 10. The ensemble mean of extreme precipitation indices during summer (DJF) over South Africa for the present-day or baseline period (2010–2030; left-side column) as simulated by the CESM1(WACCM) model in the Geoengineering Large Ensemble (GLENS) project. Mean projected impacts of GHG-induced warming under RCP8.5 (RCP8.8-baseline; middle left-hand column) and of stratospheric aerosol injection or SAI (GLENS – baseline; middle right-hand column) on annual extreme precipitation indices over South Africa in 2075–2095 relative to the baseline period (2010–2030). Mean annual impact of SAI on projected summer precipitation indices under RCP8.5 (GLENS – RCP8.5; right-hand column). The '+' signs indicate areas where all ensemble members agree on the sign of the projected change.

The impact of GHG-induced warming on winter precipitation extremes indicates that north-east and south-west SAF would experience dryer winters in the future, while the south-eastern coastline is projected to experience wetter conditions (2075–2095; Figure 11). The projected changes in the spatial distribution of R10MM, RX1DAY, RX5DAY and PRCPTOT are relatively consistent, with varying degrees of change in a few areas. The maximum projected increase in precipitation extremes is located along the south-eastern coast for R10MM (up to over +0.2 days/month), RX1DAY (up to over +2 mm/day), RX5DAY (up to over +4 mm/5-day) and PRCPTOT (up to over +8 mm/month). Decreases are projected over north-eastern and south-western SAF for R10MM (up to over -0.2 days/month), RX1DAY (up to -1 mm/day), RX5DAY (up to -2 mm/5-day) and for PRCPTOT (up to -4 mm/month). The central interior remains largely unaffected. Lastly, CDD is projected to decrease extensively by more than -8 days/month over the central interior moving north-eastward and south-eastward. All ensemble members agree on the projected decrease in CDD over these regions. The signal for CDD in north-western SAF is mixed as decreases are projected in some areas (up to -6 days/month) while increases (up to +8 days/month) are projected in other areas. There is a high level of agreement that the remainder of the country would experience decreased CDD (-2 days/month on average). These findings suggest that south-western SAF, a winter rainfall region, is likely to experience drier winters in the future. Odoulami et al. (2020) explained that the cold fronts that bring austral winter rainfall over this region are correlated with anti-cyclonic circulation systems in the mid-latitude westerlies, which bring rainfall to this region as they expand towards the equator. Increased GHG emissions are projected to trigger a southward shift of the westerlies, thereby reducing winter rainfall in south-western SAF (Odoulami et al. 2020). Similarly, Perren et al. (2020) noted that the southward shift of the Southern Hemisphere westerlies since the 1950s has deterred the primary moisture-laden storm tracks from continental territories. This has been correlated with increased droughts and wildfires in western South Africa, which they predict will increase in severity in response to the poleward movement of the Southern Hemisphere westerly winds (Perren et al. 2020).

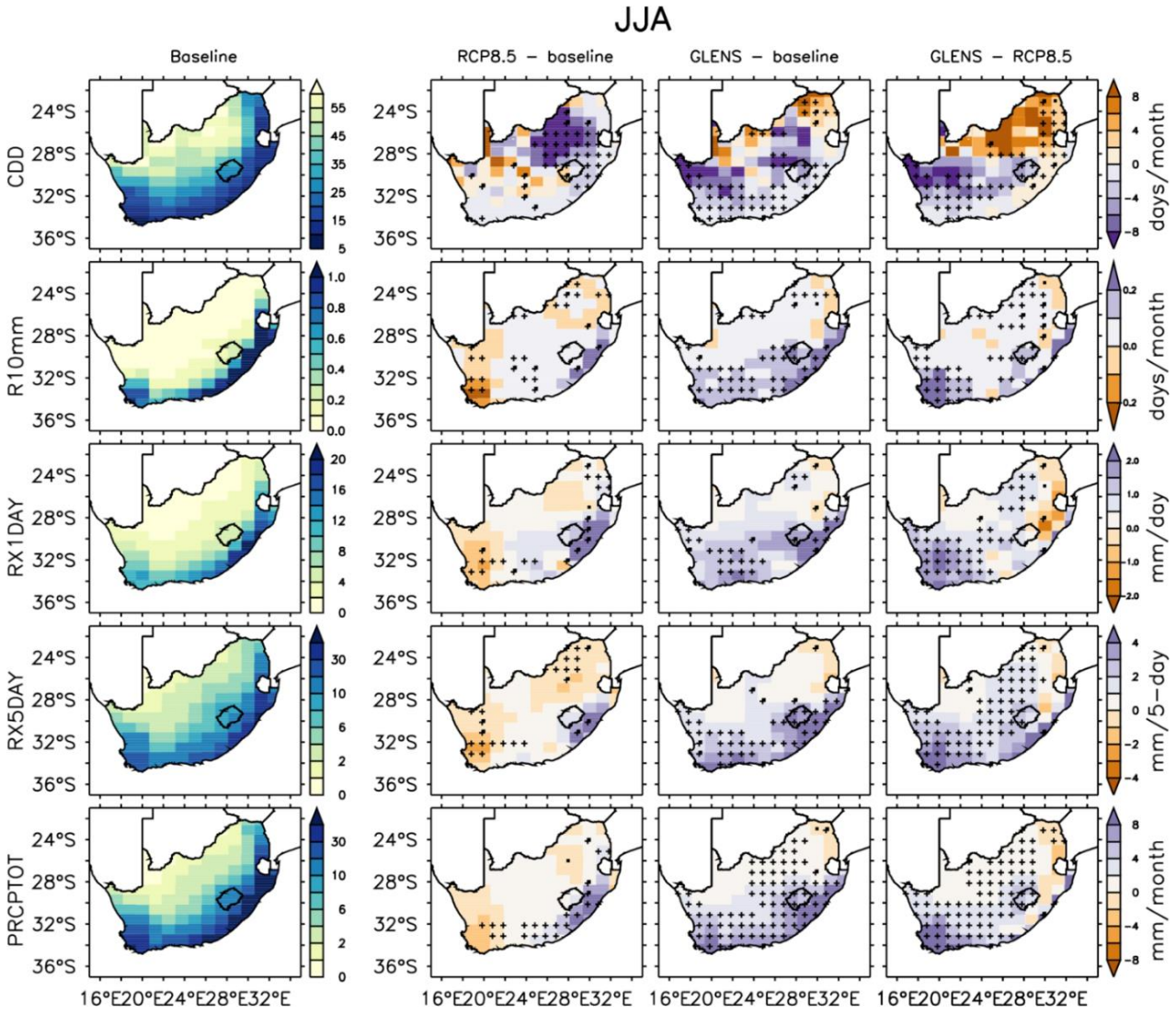

Figure 11. The ensemble mean of extreme precipitation indices during winter (JJA) over South Africa for the present-day or baseline period (2010–2030; left-side column) as simulated by the CESM1(WACCM) model in the Geoengineering Large Ensemble (GLENS) project. Mean projected impacts of GHG-induced warming under RCP8.5 (RCP8.8-baseline; middle lefthand column) and of stratospheric aerosol injection or SAI (GLENS – baseline; middle right-hand column) on annual extreme precipitation indices over South Africa in 2075–2095 relative to the baseline period (2010–2030). Mean annual impact of SAI on projected winter precipitation indices under RCP8.5 (GLENS – RCP8.5; right-hand column). The '+' signs indicate areas where all ensemble members agree on the sign of the projected change.

5.2.1.2 Temperature

The spatial distribution of GHG-induced annual changes in extreme temperature indices over South Africa in 2075–2095 relative to 2010–2030, is shown in the middle left-hand column of Figure 12.

The country's temperature response to RCP8.5 shows an increase in all hot temperature extremes with varying degrees of magnitude, with high level of agreement on the projected sign of change among the model's ensemble members. The projected spatial distribution for annual warm spell duration (WSDI) and in the frequency of warm days (TX90P) are similar with the largest projected increase over the central interior moving northward (up to over +160 days/year and up to +60%, respectively) and the smallest increase along SAF's coastline (up to +40 days/year and up to +20%, respectively). These findings suggest that the central interior would be the most vulnerable to hot temperature extremes while the areas along the coastline would be less vulnerable. Similarly, the largest increase in the hottest day temperature (TXX) is projected over the central interior moving north-eastward (up to over +6°C), while the smallest increase would be along the country's coastline (up to +4°C). East and north-east SAF are also projected to experience substantial increases in the annual coldest night temperature (TNN) (up to over +5°C), while west and south-west SAF would experience increased TNN (up to +4°C) to a slightly lesser extent. These findings are supported by the LTAS from the IPCC AR5 which projected an increase in warming of 3-6°C by 2081-2100 relative to 1986-2005, across SAF (Ziervogel et al. 2014). The projected spatial distribution for the frequency of warm nights (TN90P) is similar to that of TXX and TNN, with the largest projected increase occurring over east and north-east SAF (up to over +70%) and the smallest over west and south-west SAF (up to +60%). Lastly, nationwide decreases are projected in the frequency of cold nights (TN10P) (between –5 and –8%) with southern and south-western SAF experiencing the largest decrease in TN10P. In addition, the frequency of cold days (TX10P) is projected to decrease by up to -8% across the entire country, aside from south-western and north-easternmost SAF where TX10P would decrease by up to -6%. Overall, these results suggest that increased GHGs are projected to cause nationwide increases in hot temperature extremes.

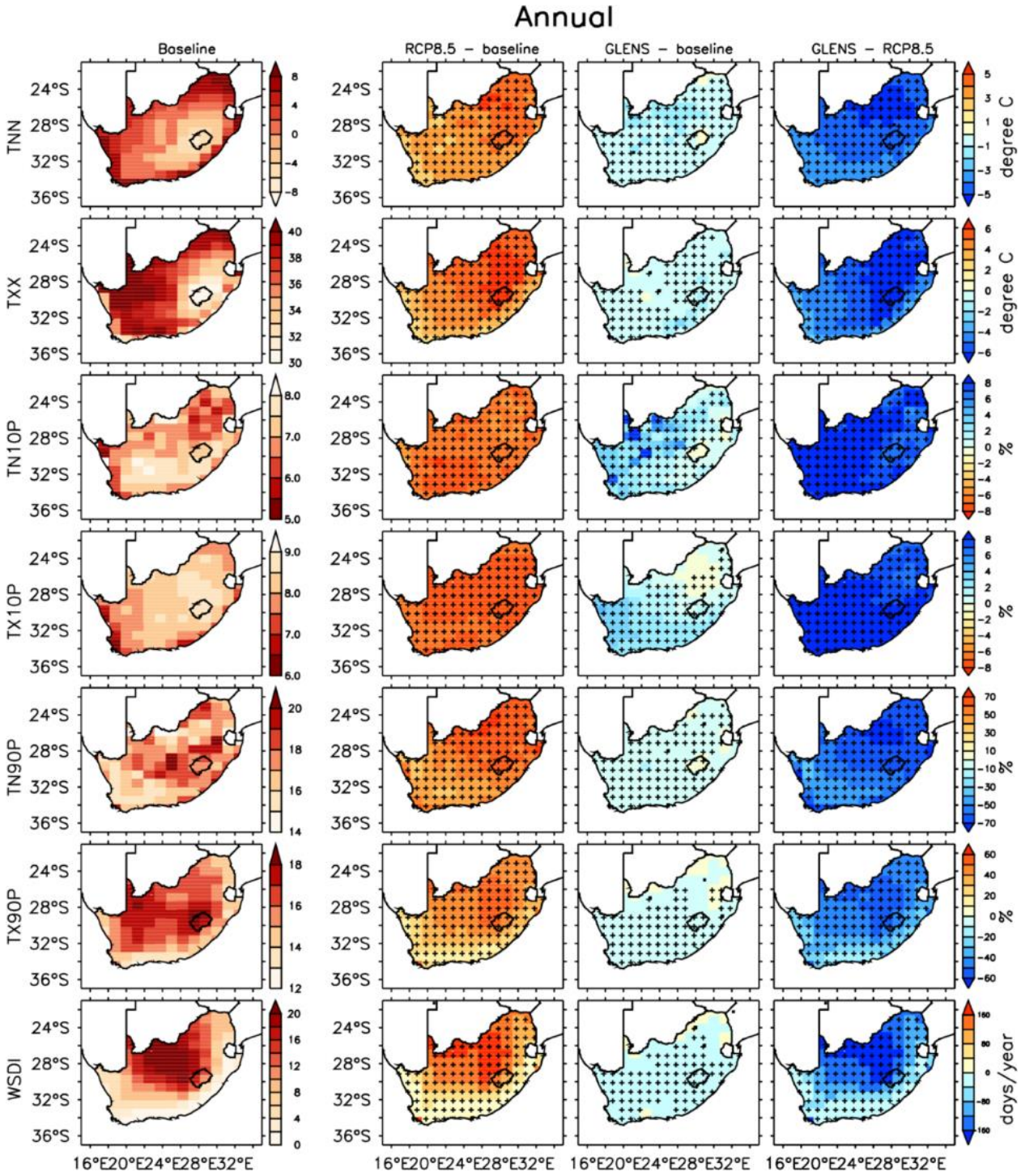

Figure 12. The ensemble mean of annual extreme temperature indices over South Africa for the present-day or baseline period (2010–2030; left-side column) as simulated by the CESM1(WACCM) model in the Geoengineering Large Ensemble (GLENS) project. Mean projected impacts of GHG-induced warming under RCP8.5 (RCP8.8-baseline; middle left-hand column) and of stratospheric aerosol injection or SAI (GLENS – baseline; middle right-hand column) on annual extreme precipitation indices over South Africa in 2075–2095 relative to the baseline period (2010–2030). Mean annual impact of SAI on projected

annual extreme temperature indices under RCP8.5 (GLENS – RCP8.5; right-hand column). The '+' signs indicate areas where all ensemble members agree on the sign of the projected change.

In summer, RCP8.5 is projected to increase (decrease) all hot (cold) temperature extremes nationwide, but with varying magnitude (Figure 13; middle left-hand column). All ensemble members agree on the projected sign of change for all indices across the entire country. Figure 13 (middle left-hand column) shows that SAF's central interior is projected to experience substantial increases in TXX (up to over +5°C), TN90P (up to over +60%) and TX90P (up to over +40%) and decreases in TX10P (up to over -8%). Following the central interior, north-east and north-west SAF are projected to be the second-most vulnerable to increases in hot temperature extremes as these are anticipated to experience increased TNN (up to +4°C), TXX (up to +5°C), TN90P (up to +60), TX90P (up to +40%) and decreased TX10P (up to -8%). These findings suggest that SAF's interior regions moving northward are projected to grow increasingly vulnerable to hot temperature extremes during summer. The country's coastal regions are projected to experience noticeably smaller increases in TXX (up to +3°C), TN90P (up to +60% on average), TX90P (about +20% on average) compared to the rest of the country, suggesting that coastal regions would be less vulnerable to increased GHG emissions.

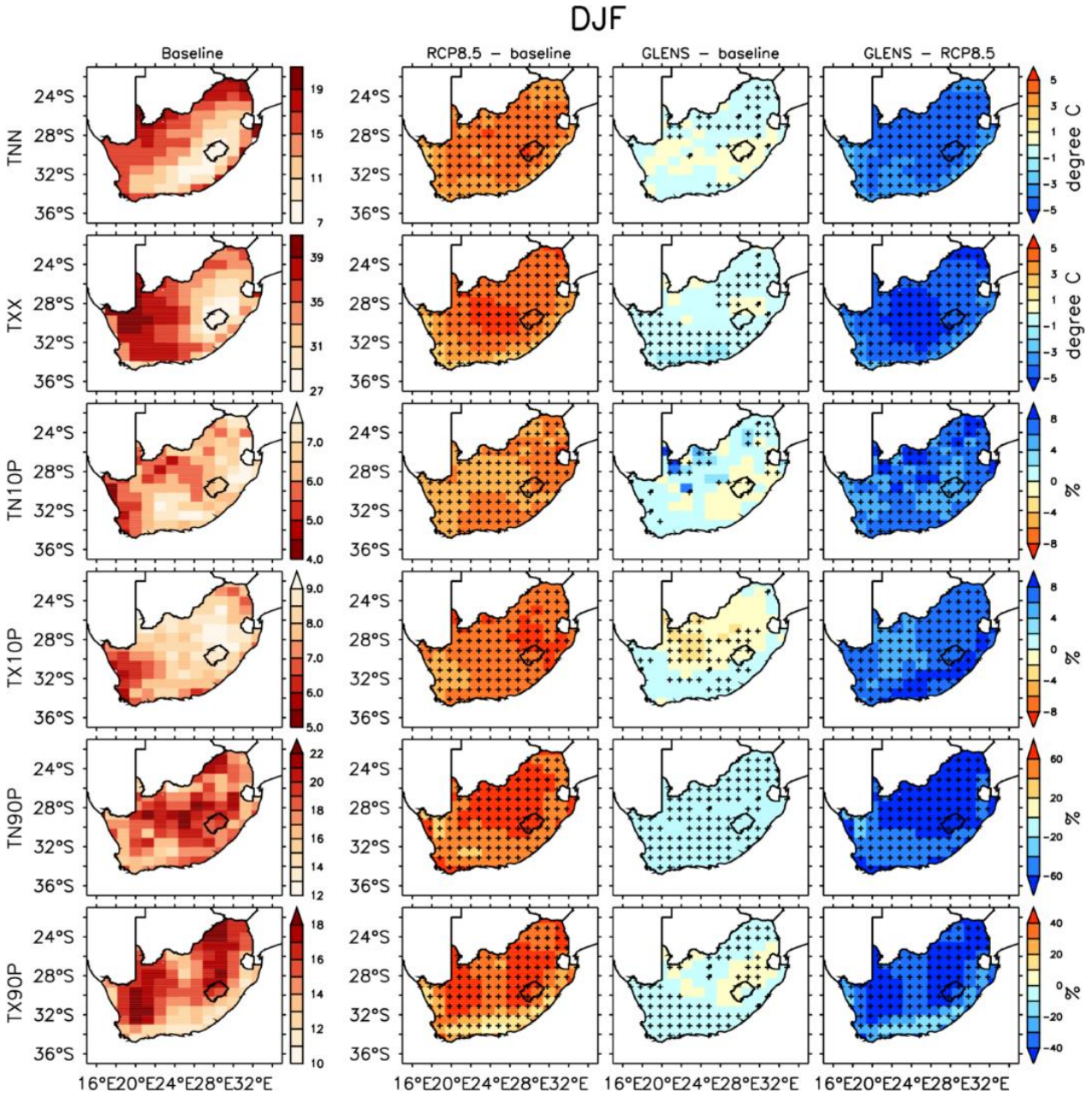

Figure 13. The ensemble mean of extreme temperature indices during summer (DJF) over South Africa for the present-day or baseline period (2010–2030; left-side column) as simulated by the CESM1(WACCM) model in the Geoengineering Large Ensemble (GLENS) project. Mean projected impacts of GHG-induced warming under RCP8.5 (RCP8.8-baseline; middle left-hand column) and of under stratospheric aerosol injection or SAI (GLENS – baseline; middle right-hand column) on annual extreme temperature indices over South Africa in 2075–2095 relative to the baseline period (2010–2030). Mean annual impact of SAI on projected summer precipitation indices under RCP8.5 (GLENS – RCP8.5; right-hand column). The '+' signs indicate areas where all ensemble members agree on the sign of the projected change.

The middle left-hand column in Figure 14 shows that increased GHG emissions are projected to trigger nationwide warming over SAF during winter. There is a high level of agreement on the sign of the projected changes across the entire country for all indices. The area covering the central interior moving north-eastward is projected to experience substantial increases in TNN (up to over +5°C), TXX (up to +6°C), TN90P (up to +60%) and TX90P (up to over +50%), suggesting that this region would be the most vulnerable to hot temperature extremes during winter near the end of the century (2075-2095) relative to the baseline period (2010-2030). Western and south-western SAF, on the other hand, would be the most vulnerable to increased warming as these regions have the largest projected decreases in TN10P and TX10P (both by up to -8%), while the rest of the country would experience less decreased TN10P and TX10P (both by up to -6%). South-western SAF in particular is projected to experience the smallest increase in TNN (up to +3°C), TXX (up to +3°C), TN90P (between +20-40%) and TX90P (up to +20%). These findings suggest that the entire country would become more vulnerable to hot temperature extremes during winter under RCP8.5, with the central interior and north-east SAF being the most vulnerable to hotter temperature extremes while western and south-western SAF would experience fewer cold days and nights and more hot extremes.

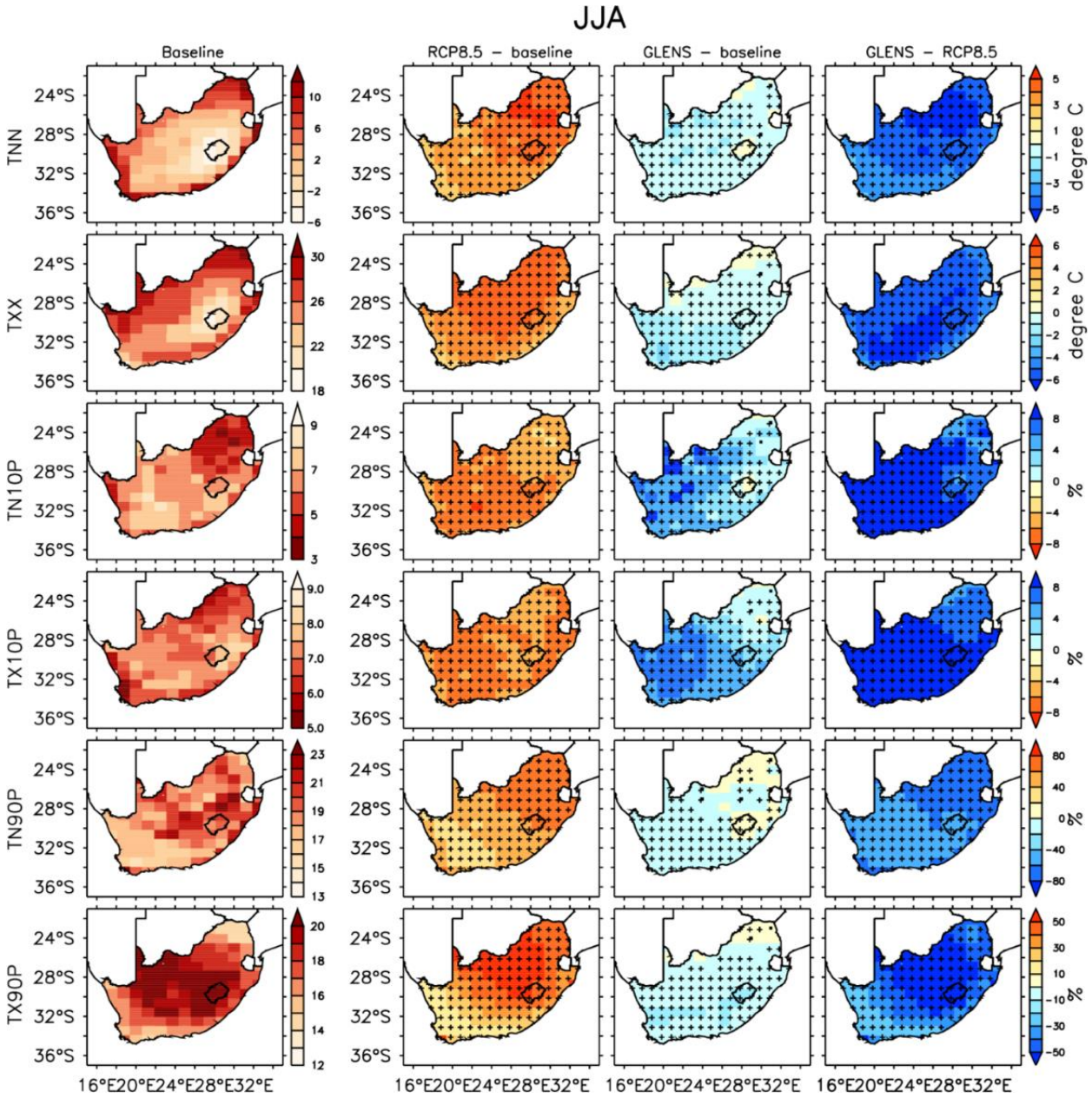

Figure 14. The ensemble mean of extreme temperature indices during winter (JJA) over SAF for the present-day or baseline period (2010–2030; left-side column) as simulated by the CESM1(WACCM) model in the Geoengineering Large Ensemble (GLENS) project. Mean projected impact of GHG-induced warming under RCP8.5 (RCP8.8-baseline; middle left-hand column) and of stratospheric aerosol injection or SAI (GLENS – baseline; middle right-hand column) on annual precipitation indices over South Africa in 2075–2095 relative to the baseline period (2010–2030). Mean annual impact of SAI on projected winter extreme temperature indices under RCP8.5 (GLENS – RCP8.5; right-hand column). The '+' signs indicate areas where all ensemble members agree on the sign of the projected change.

5.2.2. Projected impact of SAI on climate extremes over South Africa

5.2.2.1 Precipitation

The middle right-hand column in Figures 9 (annual), 10 (summer) and 11 (winter), shows the projected impact of SAI on precipitation extremes in SAF in the future (2075–2095) with reference to the 2010–2030 baseline period. SAI would cause widespread decreases in precipitation due to overall projected decreases in R10MM, RX1DAY, RX5DAY, R95P and PRCPTOT (Figure 9). CDD is projected to decrease over most of the country in response to SAI, aside from northeast SAF and part of the western coastline where it would increase.

The majority of SAF is projected to experience decreases (to varying degrees) in annual R10MM, RX1DAY, RX5DAY, R95P and PRCPTOT, under SAI deployment. North-eastern SAF is projected to experience the most substantial decreases in RX1DAY (up to -8 mm/day), RX5DAY (up to over -16 mm/5-day) and R95P (up to over -40 mm/year) while the area covering the central interior moving west- and north-westward would experience the largest decreases in R10MM (up to -6 days/year) and PRCPTOT (up to -100 mm/year). The impact of SAI on RCP8.5 is prominent in the central interior moving north-eastward, where SAI would exacerbate the projected annual decrease in precipitation extremes under RCP8.5 for R10MM (up to -4 days/year), R95P (up to over -40 mm/year) and PRCPTOT (up to -60 mm/year) (Figure 9; right-hand column). SAI would, however, offset the projected decrease under RCP8.5 over south-western SAF and parts of the southern coastline by increasing R10MM (up to +4 days/year), R95P (up to +40 mm/year) and PRCPTOT (up to +100 mm/year) (Figure 9; right-hand column). These results suggest that, overall, SAI would simultaneously decrease vulnerability to flood conditions whilst increasing dry conditions across most of the country. The only areas projected to experience increased precipitation extremes are those along the eastern coastline as increases are projected for R10MM (up to +4 days), RX1DAY (up to +6 mm/day), RX5DAY (up to +16 mm) and R95P (up to +40 mm) (Figure 9; middle right-hand column). PRCPTOT (up to over +100 mm) is also projected to increase. These results indicate that under SAI, this region could become wetter and potentially more vulnerable to flooding. A benefit of SAI deployment is the projected decrease in CDD across most of the country by up to -4 days/year on average, and by up to -16 days/year over parts of the central interior. All ensemble members agree on the projected decrease in CDD over the central interior moving south and south-westward

and parts of north-east SAF. Pinto et al. (2020) found that the impact of SRM is 23.5% effective for CDD over Southern Africa, which aligns with the findings of this study. On the other hand, CDD increases substantially by up to +12 days/year over north-eastern SAF and parts of the western coastline showing that the response of CDD to SAI in the country is mixed.

The response of precipitation extremes to SAI during summer (Figure 10) is similar to the annual response as SAI is projected to cause a nationwide decrease in precipitation extremes, suggesting simultaneous decreased vulnerability to flood conditions and enhanced drying conditions. During summer, nationwide decreases (except for parts of the eastern coastline) are projected for R10MM (-1 day/month), RX1DAY (up to -5 mm/day), RX5DAY (up to -10 mm/5-day) and PRCPTOT (up to over -20 mm/month) (Figure 10; middle right-hand column). All ensemble members agree on the projected SAI-induced decrease in precipitation extremes in areas covering the central interior moving westward. Figure 10 (middle right-hand column) shows that eastern SAF (except for the eastern coastline), in particular would experience decreased vulnerability to flood conditions as SAI is projected to decrease R10MM (up to -0.5 days/month), RX1DAY (up to -5 mm/day) and RX5DAY (up to -8 mm/5- day). In addition, the region would simultaneously experience dryer conditions in response to SAI due to the projected decrease in PRCPTOT (up to -16 mm/month). The right-hand column in Figure 10 shows that SAI would exacerbate the reduced precipitation extremes over eastern and north-eastern SAF (by up to -1.5 days/month for R10MM, up to over -5 mm/day for RX1DAY, up to over -10 mm/5-day for RX5DAY, up to over -20 mm/month for PRCPTOT, and by up to +1 day/month for CDD). Comparable to the annual response of precipitation extremes to SAI, the eastern coastline is projected to increase RX1DAY (up to +3 mm/day), RX5DAY (up to +10 mm/5-day) and PRCPTOT (up to +16 mm/month) during summer. All ensemble members agree that CDD increases in the west (up to over +5 days/month). Western is an area where SAI would, however, offset the projected RCP8.5 impact on CDD by up to over -5 days/month (Figure 10; right-hand column). The remainder of the country would experience decreased CDD (-1 day/month) (Figure 10; middle right-hand column). The consistent response of precipitation extremes to SAI during summer suggests that SAF would experience dryer summers in the future, except for the eastern coastline, which would become more prone to wetter summers and more vulnerable to flood conditions.

The response of precipitation extremes to SAI during winter (Figure 11) is relatively consistent as SAF's coastline and the surrounding areas are projected to experience increased R10MM (up to over +0.2 days/month), RX1DAY (up to over +2 mm/day), RX5DAY (up to over +4 mm/5-day) and PRCPTOT (up to over +8 mm/month) (Figure 11; middle right-hand column). All ensemble members agree on the projected increase in precipitation extremes over south-west SAF and along the eastern coastline in response to SAI deployment. SAI offsets the projected drying impact under RCP8.5 over south-west SAF by increasing R10MM (up to over +0.2 days/month), RX1DAY (up to over +2 mm/day), RX5DAY (up to over +4 mm/5-day) and PRCPTOT (up to over +8 mm/month) (Figure 11; right-hand column). Similarly, all simulations agree that SAI would offset the projected decrease under RCP8.5 over parts of north-east SAF for R10MM (by up to +0.1 day/month) and RX1DAY (by up to +1 mm/day) (Figure 11; right-hand column). Lastly, SAI is projected to cause a widespread decrease in CDD (up to -6 days/month on average) during winter which agrees with areas where PRCPTOT is projected to increase (southern SAF and extending to south-west and south-east SAF). All ensemble members agree on the projected substantial increase in CDD (by up to over +8 days/month; Figure 11, middle right-hand column) over parts of north and north-east SAF. SAI would enhance the projected decrease in CDD under RCP8.5 in northern and north-eastern SAF by up to over +8 days/month and enhances the projected decrease under RCP8.5 by up to over -8 days/month in western SAF (Figure 11; right-hand column). These findings reveal that, overall, SAI is projected to increase flooding conditions along SAF's coastline and the surrounding areas during winter, while vulnerability to drought conditions would reduce over most of the country aside from northern-most SAF where drought vulnerability could increase.

The projected changes in the spatial distribution of precipitation extremes in response to SAI experiments with different injection characteristics, Equatorial SAI and Lower SAI, are similar to that of the GLENS feedback experiments shown in Figures 9, 10 and 11. All SAI experiments are projected to trigger widespread decreases in heavy precipitation extremes. There are, however, slight variations in the intensity and magnitude of these changes under Equatorial SAI and Lower SAI. A more detailed analysis can be found in the Appendices (Figures A1, A2 and A3).

5.2.2.2 Temperature

The middle right-hand column in Figures 12 (annual), 13 (summer) and 14 (winter), shows the projected impact of SAI on temperature extremes for the period 2075–2095. SAI is projected to cause a nationwide cooling effect due to annual decreases in TNN, TXX, TN90P, TX90P and WSDI and increases in TN10P and TX10P. All of the model's ensemble members agree on the sign of the projected changes over most regions of the country.

Figure 12 (middle right-hand column) shows that SAI is projected to trigger nationwide decreases for TNN (up to -2°C), TXX (about -1°C on average but up to -3°C), TN90P (up to -10%), TX90P (up to -10%), WSDI (up to -40 days/year), and increases for TN10P (up to over +8%) and TX10P (up to +4%). There are, however, localised areas in north-east SAF where TX90P would increase (up to +10%) and TX10P would decrease (up to -1%). There is a high level of agreement among the model's ensemble members on the projected sign of change for all indices across most regions of the country. The right-hand column in Figure 12 shows that SAI would substantially offset the projected warming impact under RCP8.5 by up to over -5°C for TNN, up to over -6°C for TXX, up to over -70% for TN90P, up to -60% for TX90P, up to over -160 days/year for WSDI, and up to over +8% for both TN10P and TX10P. The regions projected to undergo the largest increases in hot temperature extremes under RCP8.5, east and north-east SAF, are the regions where SAI would most largely offset the projected increase under RCP8.5 on these temperature extremes. All of the model's ensemble members agree on the cooling potential of SAI across the entire country for all extreme temperature indices (Figure 12; right-hand column). These findings reveal that SAI deployment could be effective in triggering an annual nationwide cooling effect over SAF or the period 2075-2095 relative to the baseline period (2010-2030).

Figure 13 (middle right-hand column) shows that temperature extremes are mainly projected to decrease under SAI during summer. TN90P is projected to decrease over the entire country by up to -20%, suggesting fewer hot nights. SAI is projected to induce widespread decreases in TNN (up to -1°C) over north-east and south-western SAF. In contrast, SAI would slightly increase TNN (about +1°C) over parts of the eastern coast and central interior moving southward. SAI is projected to trigger a nationwide decrease in TXX by up to -1°C, except over localised parts of eastern and north-western SAF where TXX increases by about +1°C. TN10P is projected to increase (about +2% on average but up to +8%) in north, north-east and south-west SAF and decreases (up to -2%) from the

central interior to the south-east (across the Drakensberg Mountain Range) and over parts of western SAF. In contrast, TX10P increases (up to +2%) along the country's coastal regions and the surrounding interior and decreases (up to -4%) over the remainder of SAF. Although the majority of the central interior and northern SAF are projected to experience the largest decreases in TX10P (by up to -4%), the magnitude of decrease is less under SAI than under RCP8.5 (up to over -8%). The right-hand column (Figure 13) confirms the effectiveness of SAI which could offset the projected decrease in TX10P under RCP8.5 by up to +8%. These findings also highlight that south-west SAF is projected to experience a simultaneous increase in the frequency of cold days and cold nights in response to SAI. Similarly, all ensemble members agree that both north-east and south-west SAF would experience a projected decrease (up to -20%) for TN90P and TX90P in response to SAI, suggesting cooler summers over this region. TX90P is projected to decrease (up to -10%) in south-west SAF and to increase (up to +10%) in parts of the central interior moving eastward and over parts of north-west SAF. Although parts of SAF are projected to experience increases in hot temperature extremes in response to SAI, the magnitude of projected change is less with SAI than without SAI. This can be seen in the right-hand column (Figure 13) which shows that SAI offsets the projected increase in temperature extremes under RCP8.5 across the entire country by up to -5°C for TNN, up to over -5°C for TXX, up to over -60% for TN90P, up to over -40% for TX90P, and up to over +8% for both TN10P and TX10P. The deployment of SAI could, therefore, be beneficial in causing cooler summers over SAF than without SAI for the period 2075-2095 relative to the baseline period (2010-2030).

The projected response of winter temperature extremes to SAI are similar to the annual response as SAI would trigger a nationwide cooling across all indices (Figure 14; middle right-hand column). The north-easternmost part of SAF is the exception as the region is projected to experience localised increases in TXX (up to +1°C), TN90P (up to +20%) and TX90P (up to +10%). TN90P is also projected to increase (up to 20%) near the Drakensberg Mountain Range around eastern SAF. Aside from these localised increases, SAF is projected to experience colder winters in response to SAI. This is particularly relevant over western and south-western SAF where all of the model's ensemble members agree that SAI would induce substantial decreases in TXX (up to -3°C), TN90P and TX90P (both by up to -20%) and increases in TN10P (up to over +8%) and TX10P (up to +8%). SAI most largely offsets the impact of RCP8.5 for TXX, TN10P and TX10P in western and south-west SAF

(Figure 14; right-hand column). Similarly, the central interior and eastern SAF are largely impacted as SAI substantially offsets the RCP8.5 effect on TNN (up to over -5°C), TN90P (up to -80%) and TX90P (up to over -50%). It can be inferred from these findings that SAI deployment would induce a positive cooling impact over SAF during winter for the period 2075-2095 relative to the baseline period (2010-2030).

The projected changes in the spatial distribution of temperature extremes in response to SAI experiments with different injection characteristics, Equatorial SAI and Lower SAI, are similar to that of the GLENS feedback experiments shown in Figures 12, 13 and 14. All SAI experiments are projected to trigger a widespread cooling effect over the country. There are, however, slight differences in the intensity and magnitude of these changes under Equatorial SAI and Lower SAI. A more detailed analysis can be found in the Appendices (Figures A4, A5 and A6).

5.3 PROJECTED IMPACT OF SAI ON CLIMATE EXTREMES OVER SOUTH AFRICA'S CLIMATIC ZONES

5.3.1 Precipitation

The projected changes in extreme precipitation indices over South Africa's climatic zones for the period 2075–2095 relative to 2010–2030, in response to RCP8.5 are shown in the left column of Figures 15 (annual), 16 (summer) and 17 (winter). Figure 15 shows that most climatic zones (except EAI, KNC, and NEL) are projected to experience annual decreases in precipitation extremes and increases in CDD under RCP8.5. Projected annual decreases for R10MM (between -0.5 and -3 days/year), RX1DAY (between -1 and -4 mm/day), RX5DAY (between -3 and -8 mm/5-day) and R95P (between -10 and -20 mm/year) across the remaining climatic zones (CEI, KAI, NEI, SCI, SCO, SWN and WEI) suggest reduced vulnerability to flooding conditions in the future (2075-2095) under RCP8.5. KNC is the only zone that is projected to experience increases in R10MM (about +2 days/year), RX1DAY (about +13 mm/day), RX5DAY (about +20 mm/5-day), R95P (about +18 mm/year) and PRCPTOT (about +70 mm/year). Similarly, EAI, NEL and TCO would experience increased heavy precipitation extremes. NEL is projected to experience larger increases in RX1DAY (about +8 mm/day) and RX5DAY (about +17 mm/5-day) than EAI and TCO which would experience increased RX1DAY (up to +4 mm/day) and RX5DAY (up to +5 mm/5-day) to a lesser extent. These findings suggest that these eastern climatic zones (NEL, EAI and TCO) would grow increasingly vulnerable to flooding conditions under RCP8.5. Annual and summer CDD are projected to increase

across most climatic zones, with the largest increases occurring over SWN (up to over +30 days/year), WEI (about +25 days/year) and SWS (up to +15 days/year). Areas projected to experience increased CDD generally correspond to areas with decreased PRCPTOT. Figures 15 (annual) and 16 (summer) show that PRCPTOT is projected to decrease over most climatic zones (between -20 and -80 mm/year and between -2 and -10mm/month, respectively). These findings indicate that SAF is projected to grow vulnerable to drier conditions under RCP8.5.

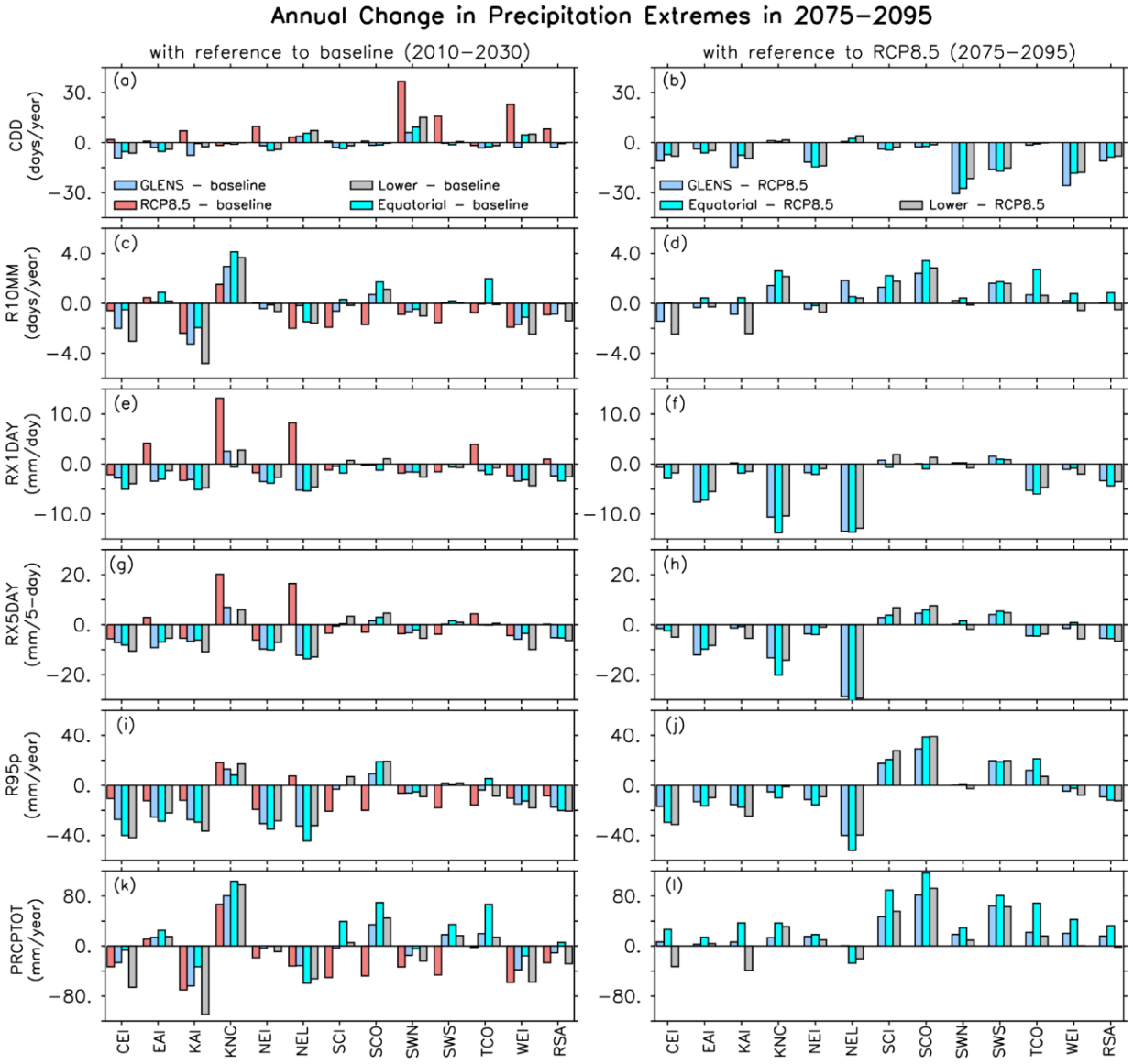

Figure 15. Bar graphs showing the mean projected changes in annual characteristics of precipitation extremes over South Africa's climatic zones in the future (2075–2095) with and without SAI as simulated by CESM1(WACCM) in the Geoengineering Large Ensemble (GLENS) project. Three SAI experiments with different injection characteristics are used: GLENS feedback experiment or GLENS (light blue), Equatorial SAI (cyan) and Lower SAI (light grey). The

graphs on the left indicate the projected changes with SAI (SAI - baseline) and without SAI (RCP8.5 - baseline) relative to the baseline (2010–2030), while the graphs on the right indicate the impact of SAI on projected temperature extremes under RCP8.5 in 2075–2095 (SAI - RCP8.5).

Figure 16 shows that there is variation in how precipitation extremes across SAF's climatic zones respond to RCP8.5 during summer. Eastern and north-eastern climatic zones (EAI, KNC and NEL) would experience more heavy precipitation extremes due to projected increases in R10MM (up to +0.7 days/month), RX1DAY (up to about +4.5 mm/day) and RX5DAY (up to +12 mm/5-day), suggesting a projected increase in vulnerability to flooding conditions. PRCPTOT is also projected to increase by up to +20 mm/month over all of the eastern climatic zones (CEI, EAI, KNC, NEI and NEL), indicating slightly wetter future summer conditions. On the other hand, the remaining climatic zones (CEI, KAI, NEI, SCI, SCO, SWN, SWS, TCO and WEI) are projected to experience decreased summer R10MM (between -0.05 and -0.2 days/month), RX1DAY (between -0.05 and -3 mm/day), RX5DAY (between -0.1 and -5 mm/5-day) and PRCPTOT (between -0.1 and -7 mm/month). During winter, projected changes in precipitation extremes across the climatic zones vary less as EAI, KNC, SCI, SCO and TCO would experience increased RX1DAY (up to +2 mm/day), RX5DAY (up to +2 mm/5-day) and PRCPTOT (up to +5 mm/month) (Figure 16). Contrastingly, climatic zones characterised by winter rainfall, SWN and SWS, would experience slight decreases in RX1DAY (up to -1 mm/day), RX5DAY (up to -2 mm/5-day) and PRCPTOT (up to -3 mm/month). Lastly, CDD is projected to decrease across most zones (up to -7 days/month), aside from KAI, SWN and WEI where it is projected to increase slightly (up to +2 days/month).

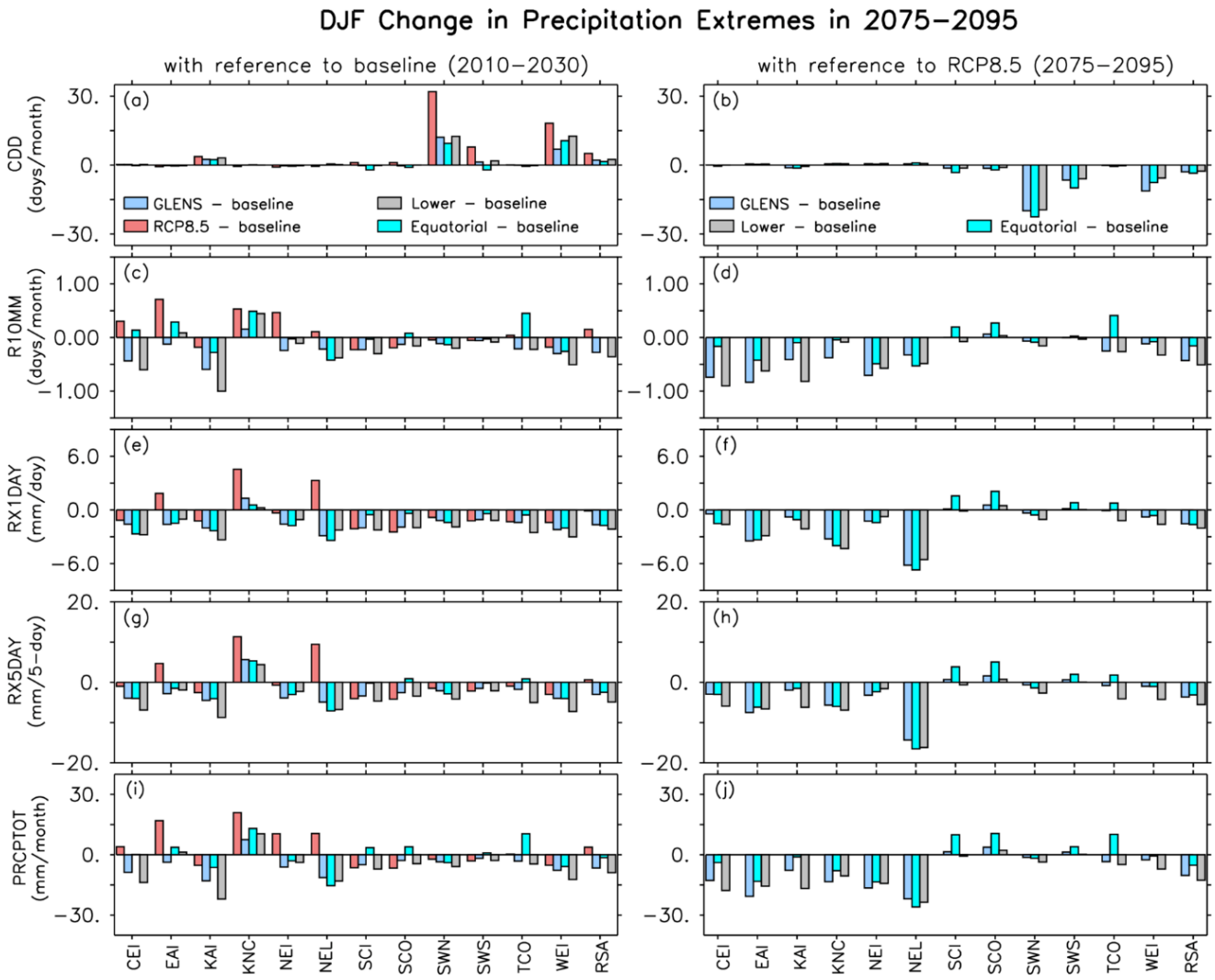

Figure 16. Bar graphs showing the mean of projected changes in characteristics of precipitation extremes during summer (DJF) over South Africa's climatic zones in the future (2075–2095) with and without SAI as simulated by CESM1(WACCM) in the Geoengineering Large Ensemble (GLENS) project. Three SAI experiments with different injection characteristics are used: GLENS feedback experiment or GLENS (light blue), Equatorial SAI (cyan) and Lower SAI (light grey). Graphs on the left indicate the projected changes with SAI (SAI – baseline) and without SAI (RCP8.5 – baseline) relative to the baseline (2010–2030), while the graphs on the right indicate the impact of SAI on projected temperature extremes under RCP8.5 in 2075–2095 (SAI - RCP8.5).

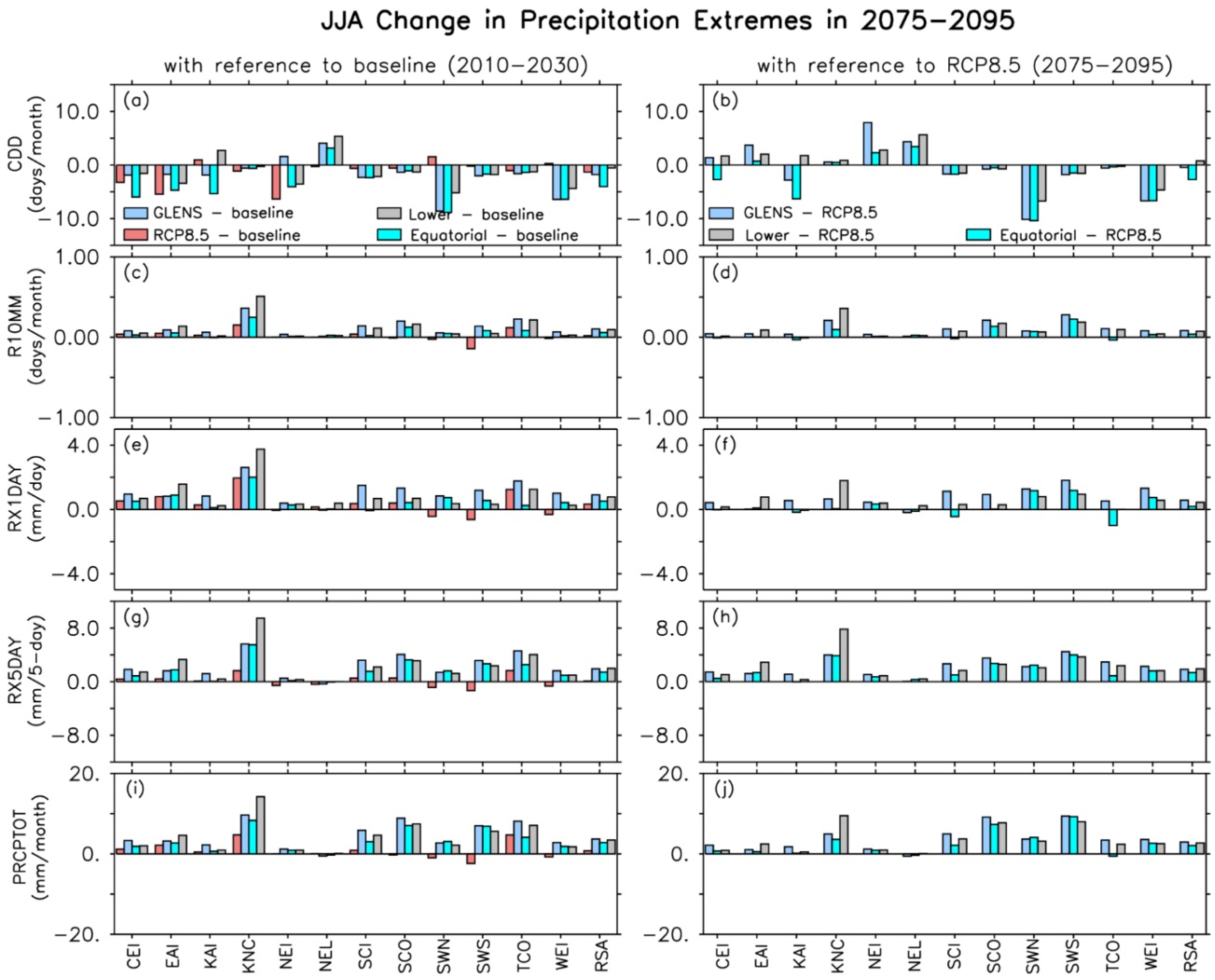

Figure 17. Bar graphs in the figure above show the mean of projected changes in characteristics of precipitation extremes during winter (JJA) over South Africa's climatic zones in the future (2075–2095) with and without SAI as simulated by CESM1(WACCM) in the Geoengineering Large Ensemble (GLENS) project. Three SAI experiments with different injection characteristics are used: GLENS feedback experiment or GLENS (light blue), Equatorial SAI (cyan) and Lower SAI (light grey). Graphs on the left indicate the projected changes with SAI (SAI – baseline) and without SAI (RCP8.5 – baseline) relative to the baseline (2010–2030), while the graphs on the right indicate the impact of SAI on projected temperature extremes under RCP8.5 in 2075–2095 (SAI - RCP8.5).

All SAI experiments are projected to decrease annual extreme precipitation indices across most climatic zones. Figure 15 shows that GLENS, Equatorial and Lower SAI would trigger less precipitation extremes than a future without SAI under RCP8.5 only. Decreases are projected for R10MM (up to -5 days/year), RX1DAY (up to -6 mm/day), RX5DAY (about -18 mm/5-day) and R95P

(up to about -45 mm/year), which suggests reduced vulnerability to flood conditions. PRCPTOT would also decrease (by up to -110 mm/year) in response to all SAI experiments, implying drier conditions in the future. Eastern climatic zones (CEI, EAI, KAI and NEI) are projected to experience the greatest decrease in heavy precipitation extremes (RX1DAY, RX5DAY and R95P) in response to all three SAI experiments. Lastly, SAI would prompt slight decreases in CDD across most climatic zones (except NEL and SWN) by up to -7 days/year, suggesting reduced vulnerability to drought conditions.

During summer, SAI would decrease R10MM (up to -1 day/month), RX1DAY (up to -3 mm/day), RX5DAY (up to -9 mm/5-day) and PRCPTOT (up to -20 mm/month) (Figure 16). Lower SAI would cause the greatest decrease, while GLENS and Equatorial SAI would cause a similar magnitude of decreases in precipitation extremes. CDD would decrease slightly (or not change) across most climatic zones, aside from KAI, SWN and WEI where it would increase (up to +14 days/month). Figure 17 shows that winter precipitation extremes in most climatic zones respond consistently to all SAI experiments as increases are projected for R10MM (up to +0.5 days/month), RX1DAY (up to almost +4 mm/day) and RX5DAY (up to +9 mm/5-day). GLENS and Lower SAI would cause the largest increases in these precipitation extremes, particularly over western climatic zones (SCI, SCO, SWN, SWS, TCO, WEI) and KNC, suggesting a projected increase in the vulnerability to flooding conditions during winter. Lastly, CDD would decrease across most climatic zones in response to all SAI experiments, with Equatorial SAI causing the greatest decrease (up to -10 days/month). The concurrent projected increase in PRCPTOT (up to +17 mm/month), most largely in response to GLENS and Lower SAI, indicates wetter winters for most of SAF's climatic zones. Overall, the results suggest that a future with SAI (especially Lower SAI) would reduce vulnerability to annual and summer flood conditions over climatic zones mainly characterised by summer rainfall (CEI, EAI, KAI, NEI, NEL), more than a future without SAI under RCP8.5. GLENS and Lower SAI, on the other hand, would cause slightly wetter winter conditions, over climatic zones characterised by winter rainfall (SWN and SWS) and all-year-round rainfall (SCI and SCO) compared to a future without SAI and under RCP8.5 only.

The right-hand column in Figures 15, 16 and 17 show the impact of all SAI experiments on RCP8.5 on precipitation extremes over SAF's climatic zones. All SAI experiments are projected to exacerbate

the projected decrease of annual precipitation extremes under RCP8.5 by up to -13 mm/day for RX1DAY, up to -30 mm/5-day for RX5DAY and up to -50 mm/year for R95P, across most climatic zones (Figure 15; right hand column). GLENS and Lower SAI would most largely exacerbate the projected decrease in these precipitation extremes under RCP8.5, especially over central (CEI, EAI, KAI) and eastern (NEI and NEL) climatic zones. Similarly, Lower SAI, in particular, would exacerbate the projected decrease in R10MM under RCP8.5 by up to -2.5 days/year over CEI, EAI, KAI, NEI, SWN and WEI. On the other hand, SAI is projected to offset the projected decrease in R10MM under RCP8.5 by up to +3 days/year over western climatic zones (SCI, SCO, SWN, SWS, TCO and WEI). SAI would also offset the projected decrease in PRCPTOT under RCP8.5 over all climatic zones, with the largest impact occurring over western SAF climatic zones (SCI, SCO, SWS, TCO and WEI) by up to almost +120 mm/year. These findings indicate that SAI would be effective in preventing dryer annual conditions. Equatorial SAI would most largely offset the projected decreases in R10MM and PRCPTOT. In addition, all SAI experiments would offset the projected increase in annual and summer (Figures 15 and 16; right-hand column) CDD by up to -30 days/year and -22 days/month respectively, over all climatic zones (aside from KNC and NEL). GLENS and Equatorial SAI would be the most effective in offsetting the projected increase in CDD under RCP8.5. These findings suggest that SAI would effectively decrease SAF's vulnerability to drought conditions.

Figure 16 (right-hand column) shows that all SAI experiments would exacerbate the projected decrease in precipitation extremes under RCP8.5 across most climatic zones during summer by up to almost -1 day/month for R10MM, up to about -6 mm/day for RX1DAY, up to -18 mm/5-day for RX5DAY and up to -25 mm/month for PRCPTOT. Lower SAI would most largely exacerbate the projected decrease in these precipitation extremes under RCP8.5, particularly for eastern climatic zones (CEI, EAI, KAI and KNC). Equatorial SAI would, however, offset the projected decreases under RCP8.5 over SCI, SCO, SWS and TCO by up to +0.5 days/month for R10MM, up to +2 mm/day for RX1DAY, up to +5 mm/5-day for RX5DAY and up to +13 mm/month for PRCPTOT. All three SAI experiments would most largely offset the projected increase in summer CDD over western SAF climatic zones (SCI, SCO, SWN, SWS and WEI) by up to -25 days/month. Figure 17 (right-hand column) shows that all SAI experiments would offset the projected decrease in winter precipitation extremes across most climatic zones under RCP8.5 by less than +0.3 day/month for R10MM, up to +2 mm/day for RX1DAY, up to +8 mm/5-day for RX5DAY, up to +10 mm/month for PRCPTOT and up

to -10 days/month for CDD. GLENS would offset the projected decrease in precipitation extremes under RCP8.5, especially in western SAF climatic zones (SCI, SCO, SWN, SWS, TCO and WEI). These results suggest that SAI would have contrasting effects on seasonal precipitation extremes by inducing overall dryer summers and wetter winters.

5.3.2 Temperature

The projected changes in extreme temperature indices over South Africa's climatic zones during 2075–2095 relative to 2010–2030, in response to RCP8.5 is shown in the left column of Figures 18 (annual), 19 (summer) and 20 (winter). The projected response of annual and seasonal temperature extremes across SAF's climatic zones to RCP8.5 are consistent as all climatic zones would experience increased TNN, TXX, TN90P, TX90P, WSDI and decreased TN10P and TX10P. CEI, EAI, NEI and NEL would be the most impacted climatic zones as they would experience the largest increase of annual TNN (between +4 and +5°C), TXX (between +5.5 and +6°C), TN90P (between +60% and +75%), TX90P (between +50 and +55%) and WSDI (between +120 and +160 days/year). Eastern SAF climatic zones (TCO, KNC, EAI, NEI and NEL) and CEI are projected to experience decreases in TX10P (about -8%) and TN10P (between -6 and -7%). Similar to the impact of increased GHG emissions on annual temperature extremes, RCP8.5 is projected to cause hotter conditions across all climatic zones during summer (Figure 19). Eastern climatic zones (TCO, KNC, EAI, NEI, and NEL) are projected to experience the largest decrease in summer TN10P (between -6 and -8%). During winter, EAI and NEI would experience the largest increase in TNN (between +4 and +5°C), TXX (between +5 and +5.5°C), TN90P (between +70 and +80%) and TX90P (between +50 and +60%), while western SAF zones (SWS, SWN, WEI, SCO, SCI and KAI) would experience the greatest decrease in TN10P (between -6 and -8%). These results suggest that SAF's eastern zones would be the most prone to experiencing hotter temperatures and less cold nights. Overall, the entire country would become more vulnerable to extreme warm temperatures.

GLENS, Equatorial and Lower SAI are projected to decrease annual TNN, TXX, TN90P, TX90P and WSDI and increase TN10P and TX10P across all climatic zones (Figure 18). Equatorial SAI would most effectively trigger a cooling effect over most eastern climatic zones (TCO, KNC, EAI, NEI, and NEL) and CEI by simultaneously decreasing TXX (between -0.5 and -2°C), TN90P and TX90P (between -5 and -10%) and increasing TN10P (between +2 and +6%) and TX10P (between +1 and +5%). Western

climatic zones (SWS, SWN, WEI, SCO, SCI, and KAI) and TCO would be more prone to decreased TN90P and TX90P in response to all SAI experiments. Figure 19 shows that GLENS and Equatorial SAI would cause the largest projected increase in summer TN10P (about +1% for GLENS and between +1% and +2.5% for Equatorial SAI) over most climatic zones, with the largest increase occurring over KAI. TX10P would increase most largely over southern climatic zones, SCI and SCO (between +3 and +4%), and western climatic zones (SWN, SWS and WEI) in response to all SAI experiments, with Equatorial SAI causing the largest increase. These findings suggest that SAI could trigger colder summers over south-western SAF. All SAI experiments are projected to cause a decrease in TX10P decrease over north-eastern climatic zone, NEI (up to -2%) in the north-east, indicating fewer cold days. Equatorial SAI would cause the largest increase in TX10P (up to +4%), while Lower SAI would cause the largest decrease (up to -2%). GLENS and Equatorial SAI are projected to decrease summer TN90P (±3% and ±5% respectively) and TX90P (up to -4% and -8% respectively) over all climatic zones. Lower SAI would, however, cause a slight increase in TX90P (between +1 and +2%) over EAI, CEI and KAI, and decrease in TX90P (about -5%) over western climatic zones (SWS, SWN, WEI, SCO and SCI). During winter, decreases are projected for TNN (between -0.5 and -1°C), TXX (between -0.5 about -2.5°C), TN90P (between -1 and -10%), TX90P (between -2 and -15%) and increases for TN10P (between +1 and +9%) and TX10P (between +1 and +8%), across all climatic zones in response to SAI (Figure 20). These findings suggest that SAI would induce a cooling effect during winter, particularly over western SAF climatic zones (SCI, SCO, SWS, SWN and WEI) where the largest decreases in hot temperature extremes are projected under SAI. Equatorial SAI would have the largest cooling impact as it would trigger the biggest decrease for TXX (between -0.5 and -3°C), TN90P (between -5 and -10%) and TX90P (between -2 and -15%) across most climatic zones. Additionally, Equatorial SAI would trigger the greatest increase in TN10P (between +3 and +10%) and TX10P (between +3 and +7%) over eastern climatic zones (EAI, KNC, NEI and NEL) and CEI, while GLENS would cause the smallest increase in TN10P (between +1 and +7%) and TX10P (up to +7%) over these climatic zones. These results suggest that all SAI experiments are projected to induce a cooling effect over SAF's climatic zones, with Equatorial SAI being the most impactful in triggering a cooling effect.

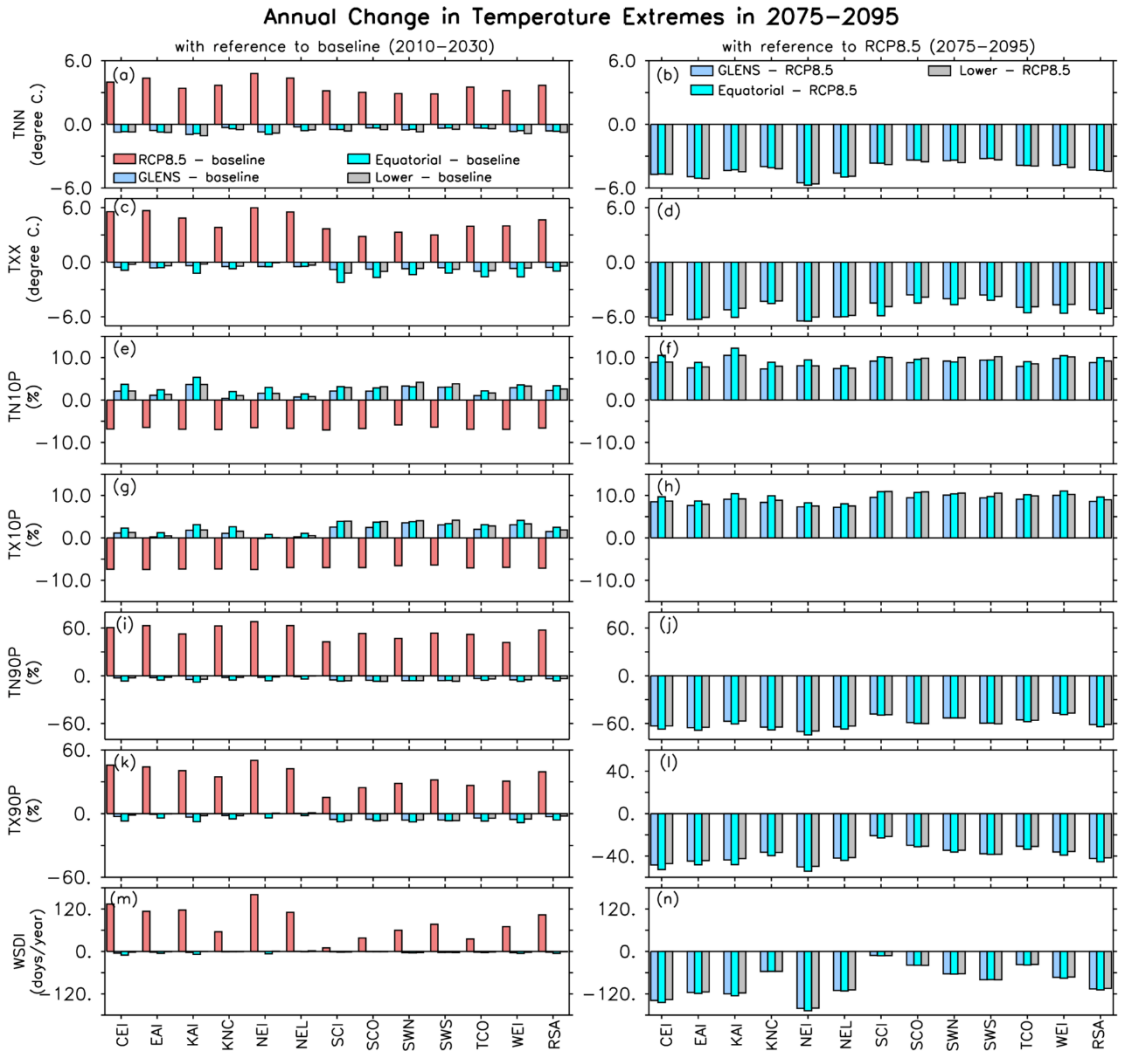

Figure 18. Bar graphs showing the mean of projected changes in annual characteristics of temperature extremes over South Africa's climatic zones) in the future (2075–2095) with and without SAI as simulated by CESM1(WACCM) in the Geoengineering Large Ensemble (GLENS) project. Three SAI experiments with different injection characteristics are used: GLENS feedback experiment or GLENS (light blue), Equatorial SAI (cyan) and Lower SAI (light grey). Graphs on the left indicate the projected changes with SAI (SAI – baseline) and without SAI (RCP8.5 – baseline) relative to the baseline (2010–2030), while the graphs on the right indicate the impact of SAI on projected temperature extremes under RCP8.5 in 2075–2095 (SAI-RCP8.5).

The right column in Figures 18, 19 and 20 shows the impact of all SAI experiments on RCP8.5 on temperature extremes over SAF's climatic zones. Figure 18 shows that all SAI experiments fully offset, to slightly varying extents, the projected annual impact of RCP8.5 on temperature extremes over all climatic zones. SAI is projected to trigger an annual nationwide cooling effect across all climatic zones between -3 and -5.5°C for TNN, between -3.5 and -5.5°C for TXX, between -50 and -

80% for TN90P, between -20 and -50% for TX90P, between -10 and -170 days/year for WSDI, between +7 and +12% for TN10P and between +9 and +11 for TX10P (Figure 18).

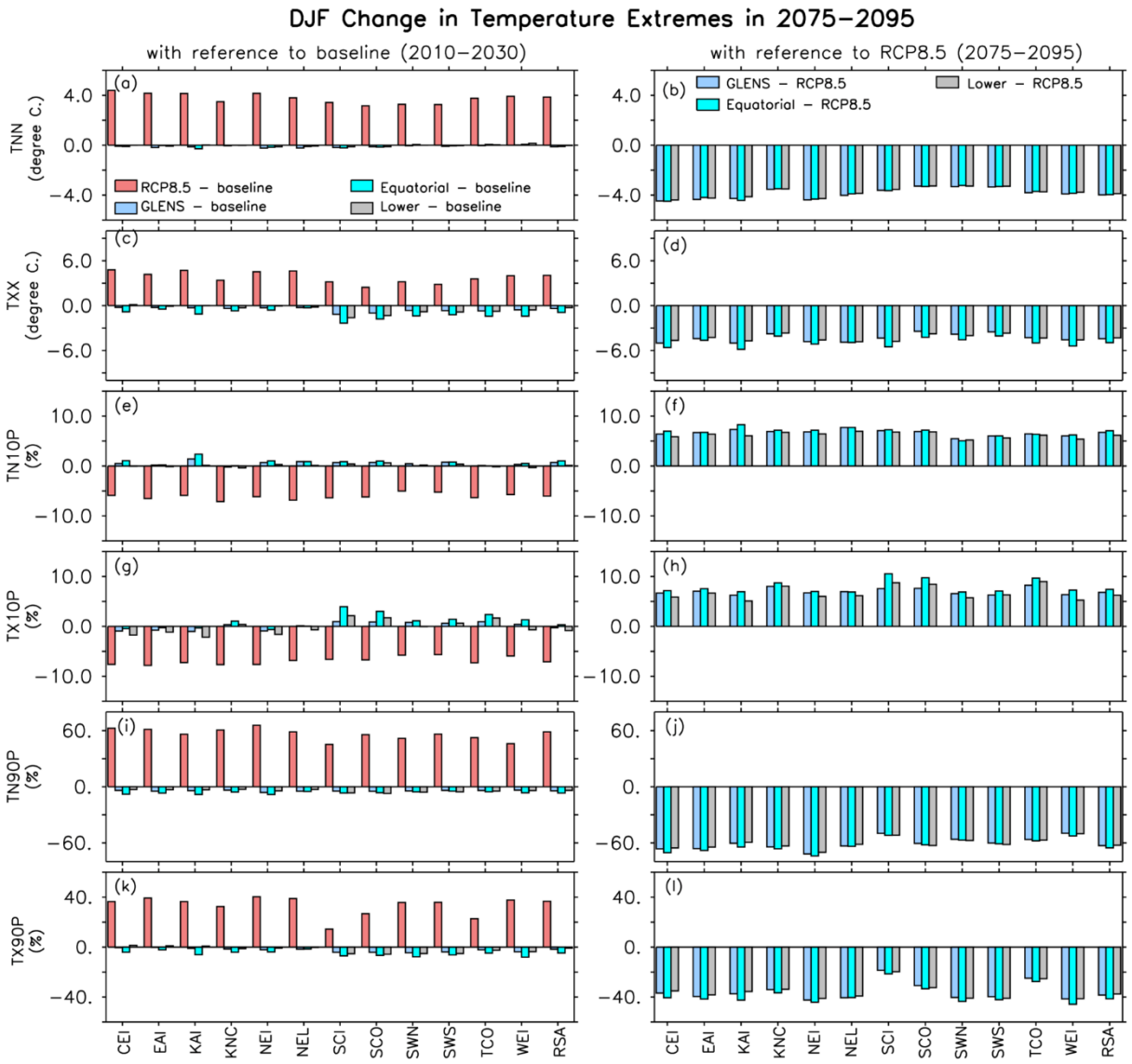

Figure 19. Bar graphs showing the mean of projected changes in characteristics of temperature extremes during summer (DJF) over South Africa's climatic zones in the future (2075-2095) with and without SAI as simulated by CESM1(WACCM) in the Geoengineering Large Ensemble (GLENS) project. Three SAI experiments with different injection characteristics are used: GLENS feedback experiment or GLENS (light blue), Equatorial SAI (cyan), and Lower SAI (light grey). Graphs on the left indicate the projected changes with SAI (SAI – baseline) and without SAI (RCP8.5 – baseline) relative to the baseline (2010-2030), while the graphs on the right indicate the impact of SAI on projected temperature extremes under RCP8.5 in 2075-2095 (SAI-RCP8.5).

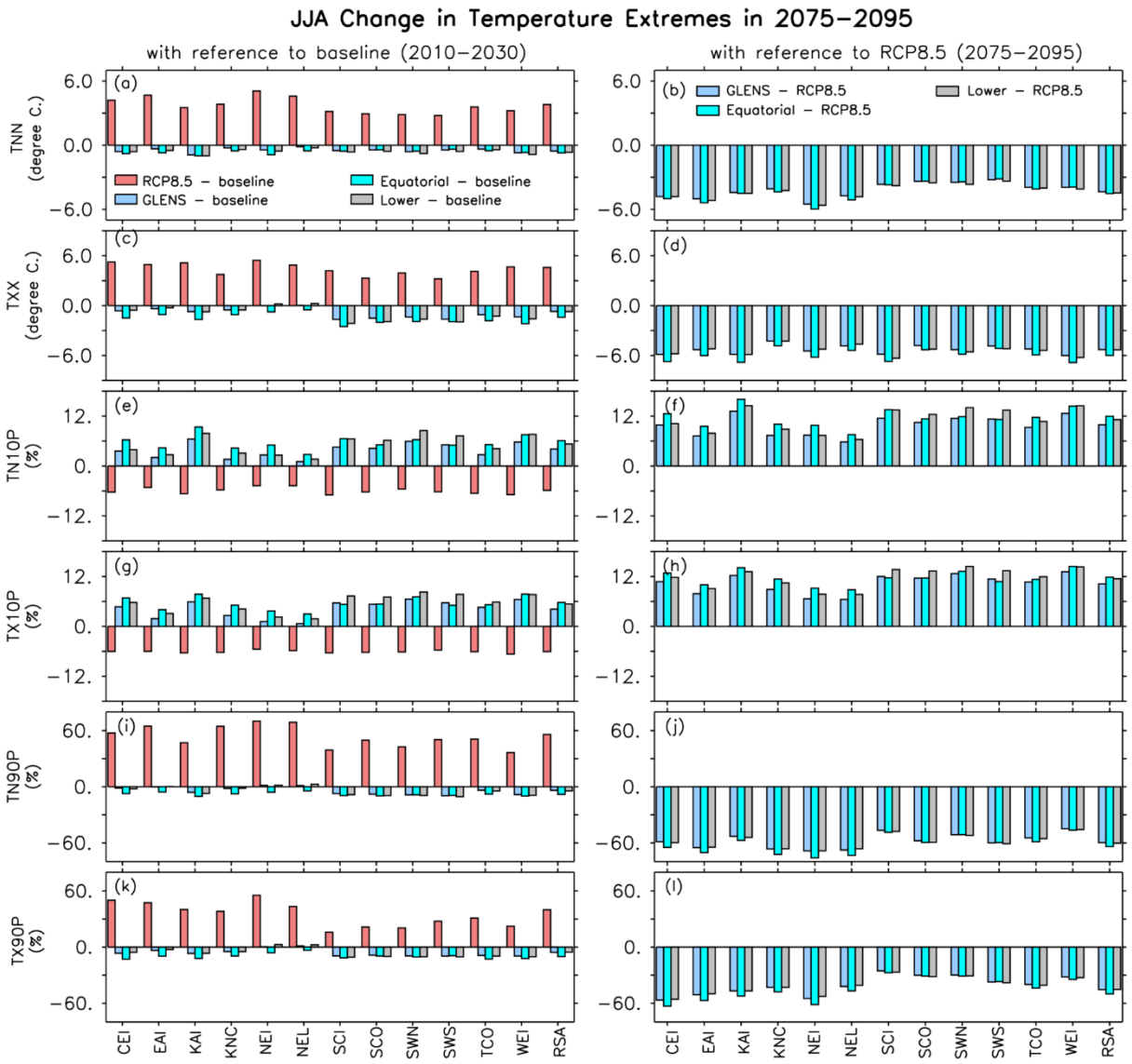

Figure 20. Bar graphs showing the mean of projected changes in characteristics of temperature extremes during winter (JJA) over South Africa's climatic zones in the future (2075–2095) with and without SAI as simulated by CESM1(WACCM) in the Geoengineering Large Ensemble (GLENS) project. Three SAI experiments with different injection characteristics are used: GLENS feedback experiment or GLENS (light blue), Equatorial SAI (cyan) and Lower SAI (light grey). Graphs on the left indicate the projected changes with SAI (SAI – baseline) and without SAI (RCP8.5 – baseline) relative to the baseline (2010–2030), while the graphs on the right indicate the impact of SAI on projected temperature extremes under RCP8.5 in 2075–2095 (SAI-RCP8.5).

Figure 19 (right-hand column) shows that all SAI experiments would offset the projected increase in hot temperature extremes during summer under RCP8.5 over all climatic zones between +3 and +4.5°C for TNN, between +3 and +5.5°C for TXX, between +50 and +90% for TN90P, and between +20 and +40% for TX90P. All experiments would simultaneously offset the projected decrease in the

frequency of cold nights and cold days across all climatic zones between +5 and +8% for TN10P and between +5 and +11% for TX10P (Figure 19). Similarly, during winter (Figure 20; right-hand column), all SAI experiments are projected to offset the projected increases in hot temperature extremes under RCP8.5 across all climatic zones between -3 and -6°C for TNN, between -4 and -7°C for TXX, between -40 and -85% for TN90P, between -20 and -60% for TX90P. Additionally, SAI would offset the projected decrease in the frequency of cold days and cold nights under RCP8.5 over all climatic zones between +8 and +17% for TN10P and between +6 and +13% for TX10P. The climatic zones where SAI would most prominently offset the RCP8.5 impact on TN10P and TX10P during both summer (Figure 19; right -hand column) and winter (Figure 20; right -hand column) are western climatic zones (SWS, SWN, WEI, SCO, SCI, and KAI). Eastern climatic zones (EAI, KAI, KNC, NEI and NEL) and CEI would also be substantially impacted by SAI which would largely offset the projected increase in TN90P and TX90P as well as TNN under RCP8.5 during summer and winter. These findings suggest that SAI deployment would relieve central and eastern SAF from the projected increases in the frequency of hot days and nights, as well as hot night-time temperatures during both summer and winter. Overall, all three SAI experiments would effectively offset, to varying degrees, the projected increase in hot temperature extremes under RCP8.5 and the projected decrease in the frequency of cold days and nights under RCP8.5, showcasing its effectiveness in cooling SAF's climatic zones in the future.

6 CHAPTER 6 – DISCUSSION

This section discusses the implications of the results from this study. Tables 4 and 5 provide a summary of the projected changes in annual precipitation and temperature extremes over SAF's climatic zones in the future under RCP8.5 emission scenario with and without SAI. This is followed by a synthesis of the projected changes in temperature and precipitation extremes in response to increased GHG emissions and under SAI deployment. The section continues and closes with a discussion of the potential implications of increased GHG emissions and SAI deployment on the country with respect to water stress, agriculture, human health, vulnerable groups and urban centres.

Table 4. Summary of projected changes in annual precipitation extremes over South Africa's climatic zones in the future (2075–2095) under RCP8.5 with and without SAI as simulated by CESM1(WACCM) in the Geoengineering Large Ensemble (GLENS). The arrow in each row represents the direction of change projected under RCP8.5 without SAI (top arrow) and with SAI deployment in response to the GLENS feedback experiment (GLENS – baseline) (bottom arrow). Orange arrows indicate dryer future conditions while blue arrows indicate wetter future conditions.

Climatic Zones	Precipitation Indices					
	CDD (days)	R10MM (days)	RX1DAY (mm)	RX5DAY (mm)	R95P (mm)	PRCPTOT (mm)
CEI	↑ ↓	↓ ↓	↓ ↓	↓ ↓	↓ ↓	↓ ↓
EAI	↑ ↓	↑ ↓	↑ ↓	↓ ↓	↓ ↓	↓ ↑
KAI	↑ ↓	↓ ↓	↓ ↓	↓ ↓	↓ ↓	↓ ↓
KNC	↓ ↓	↑ ↑	↑ ↑	↑ ↑	↑ ↓	↑ ↑
NEI	↑ ↓	↓ ↓	↓ ↓	↓ ↓	↓ ↓	↓ ↓
NEL	↑ ↑	↓ ↓	↑ ↓	↑ ↓	↓ ↓	↓ ↓
SCI	↑ ↓	↓ ↓	↓ ↓	↓ ↓	↓ ↓	↓ ↓
SCO	↑ ↓	↓ ↑	↓ ↓	↓ ↑	↓ ↑	↓ ↑
SWN	↑ ↑	↓ ↓	↓ ↓	↓ ↓	↓ ↓	↓ ↓
SWS	↑ ↓	↓ ↓	↓ ↑	↓ ↑	↓ ↑	↓ ↑
TCO	↓ ↓	↓ ↓	↑ ↓	↑ ↓	↓ ↓	↓ ↑
WEI	↑ ↓	↓ ↓	↓ ↓	↓ ↓	↓ ↓	↓ ↓

Table 5. Summary of projected changes in annual temperature extremes over South Africa's climatic zones in the future (2075–2095) under RCP8.5 with and without SAI as simulated by CESM1(WACCM) in the Geoengineering Large Ensemble (GLENS). The arrow in each row represents the direction of change projected under RCP8.5 without SAI (top arrow) and with SAI deployment in response to the GLENS feedback experiment (GLENS – baseline) (bottom arrow). Red arrows indicate hotter future conditions while blue arrows indicate cooler future conditions.

Climatic Zones	Temperature Indices						
	TNN (°C)	TXX (°C)	TN10P (%)	TX10P (%)	TN90P (%)	TX90P (%)	WSDI (days)
CEI	↑ ↓	↑ ↓	↓ ↑	↓ ↑	↑ ↓	↑ ↓	↑ ↓
EAI	↑ ↓	↑ ↓	↓ ↑	↓ ↑	↑ ↓	↑ ↓	↑ ↓
KAI	↑ ↓	↑ ↓	↓ ↑	↓ ↑	↑ ↓	↑ ↓	↑ ↓
KNC	↑ ↓	↑ ↓	↓ ↑	↓ ↑	↑ ↓	↑ ↓	↑ ↓
NEI	↑ ↓	↑ ↓	↓ ↑	↓ ↑	↑ ↓	↑ ↓	↑ ↓
NEL	↑ ↓	↑ ↓	↓ ↑	↓ ↑	↑ ↓	↑ ↓	↑ ↓
SCI	↑ ↓	↑ ↓	↓ ↑	↓ ↑	↑ ↓	↑ ↓	↑ ↓
SCO	↑ ↓	↑ ↓	↓ ↑	↓ ↑	↑ ↓	↑ ↓	↑ ↓
SWN	↑ ↓	↑ ↓	↓ ↑	↓ ↑	↑ ↓	↑ ↓	↑ ↓
SWS	↑ ↓	↑ ↓	↓ ↑	↓ ↑	↑ ↓	↑ ↓	↑ ↓
TCO	↑ ↓	↑ ↓	↓ ↑	↓ ↑	↑ ↓	↑ ↓	↑ ↓
WEI	↑ ↓	↑ ↓	↓ ↑	↓ ↑	↑ ↓	↑ ↓	↑ ↓

6.1 SYNTHESIS OF PROJECTED CHANGES IN PRECIPITATION EXTREMES

Projected changes in precipitation extremes in response to increased GHGs over the central interior moving eastward (CEI, EAI and NEI) and western and south-western climatic zones (SWS, SWN, WEI, SCO, SCI, and KAI) indicate that these regions would become less vulnerable to flood conditions due to annual and summer projected decreases in heavy precipitation indices: R10MM, RX1DAY, RX5DAY and R95P. These regions would also experience more dry spells as indicated by the projected increase in CDD. During summer SWS, SWN and WEI are projected to experience the greatest increases in CDD (between +7 and +30 days/month), suggesting that this region would be extremely vulnerable to drought conditions during summer. SWN (a winter rainfall region), would also experience increased CDD during winter by up to +3 days/month. In contrast, climatic zones along eastern-most SAF (NEL and KNC) are projected to experience increased annual and summer heavy precipitation extremes, suggesting exacerbated vulnerability to flooding conditions and overall wetter summers.

The results presented in this study suggest that all three SAI experiments (GLENS, Equatorial and Lower SAI), especially GLENS and Lower SAI, are projected to cause overall decreases in heavy precipitation extremes over most climatic zones. This finding agrees with previous studies that SAI deployment is projected to generally reduce global precipitation anomalies (Halstead, 2018). Decreases over most climatic zones in R10MM, RX1DAY, RX5DAY and R95P are projected to be larger and more widespread in a future with increased GHGs and SAI than in a future with increased GHGs and no SAI. For example, Figure 9 shows that annual R10MM would decrease over most of the country between -2 and -4 days/year without SAI, whereas R10MM would decrease between -2 and -6 days/year in response to all SAI experiments. Similarly, Figure 15 shows that annual PRCPTOT would decrease by up to -70 mm/year without SAI and by up to -110 mm/year with SAI deployment. The injection characteristics of Lower SAI would cause the largest decrease in PRCPTOT over KAI. These findings align with Pinto et al. (2020) who found that SAI would trigger significant decreases in PRCPTOT over Southern Africa. The projected results for CDD, however, show that SAI would prompt widespread decreases in CDD across most climatic zones (except NEL, SWN and WEI) by up to -8 days/year, suggesting reduced vulnerability to drought conditions. GLENS and Equatorial SAI would most largely offset CDD in western and south-western SAF (SWN and WEI) between -4

and -8 days/month during winter. This finding aligns with Odoulami et al. (2020) who found that SAI could reduce the risk severe droughts, like the *Day Zero* level drought over Cape Town (located in SWS climatic zone), by up to 90% going forward, compared to a future without SAI. These results show that SAI deployment would simultaneously decrease the country's vulnerability to extreme precipitations and flood conditions, while enhancing dryer annual conditions.

6.2 SYNTHESIS OF PROJECTED CHANGES IN TEMPERATURE EXTREMES

The findings from this study suggest that all SAF's climatic zones would grow increasingly vulnerable to extremely hot temperatures in response to increased GHGS by the period 2075–2095. A number of eastern climatic zones (EAI, NEI, and NEL) and the central interior, CEI, would experience the largest increases in the hottest day-time temperatures, in extreme high temperature days and nights and in WSDI. EAI, NEI and NEL would be the climatic zones most impacted as they would experience the largest magnitude of increased hot temperature extremes. This builds on the finding that north-east SAF has been one of the country's most vulnerable regions to harsh temperatures which has an observed rate of warming at 2°C per century (DEA, 2017). Climatic zones located along the country's coastline (KNC, TCO, SCO, SWS and SWN) are projected to experience increases in TNN and TXX both between +3 and +4°C, while climatic zones located in the interior (CEI, EAI and KAI) would experience larger increases between +3 and +5.5°C. These results align with a finding from the "South African Risk and Vulnerability Atlas" (SARVA) that overall, the country's coastal temperature increases are less than that of the interior (USAID, 2015). It is worth noting that SCI, SCO and SWN would experience the smallest increases in winter and annual TX90P, suggesting that these regions are the least vulnerable to increasing hot temperature extremes in response to increased GHG emissions.

The results presented here indicate that SAI deployment is projected to trigger an annual nationwide cooling effect. This finding agrees with previous studies that SAI deployment is projected to generally reduce global temperature anomalies, subsequently cooling the Earth (Halstead, 2018). GLENS, Equatorial SAI and Lower SAI are projected to cause a cooling effect across all climatic zones in the country on an annual time scale (Figure 18) and during summer and winter (Figures 19 and 20). This is indicated by the projected decreases in TNN, TXX, TN90P, TX90P and WSDI, and the projected increases in TN10P and TX10P in response to SAI deployment. In addition, all three

experiments, to varying degrees, would completely offset the projected increases in annual temperature extremes under RCP8.5 over all climatic zones. Overall, the findings from this study indicate that SAI deployment is projected to have a positive cooling effect over SAF's climatic zones.

6.3 IMPLICATIONS OF PROJECTED CHANGES FOR VULNERABILITY IN SOUTH AFRICA'S CLIMATIC ZONES

6.3.1 Water stress

South Africa is identified as one of the most water-stressed countries in Southern Africa, the second region in the world (following North Africa and the Middle East), most confronted by a crippling water deficit (World Wildlife Fund: WWF, 2010). As a developing country, matters of water quality and availability and extreme rainfall variability are increasingly compounded by challenges brought about by population growth and socioeconomic development (WWF, 2010; Dennis and Dennis, 2011). The SAF Department of Water Affairs (2013) has identified water as the central medium through which the effects of climate change are being experienced in the country. Figure 15 shows the concurrent projected decrease in annual PRCPTOT across all climatic zones under RCP8.5, except for KNC, and increase in CDD. This finding suggests that increasing GHG emissions will exacerbate water-stress across the country. Furthermore, the decrease in total precipitation and increased vulnerability to drought would worsen the already uneven distribution and deterioration of groundwater and freshwater resources which were recognised in South Africa's National Climate Change Adaptation Strategy (DEA, 2017). In addition, Figure 18 shows that increased GHG emissions are projected to trigger increased hot temperature extremes across SAF's climatic zones on an annual time scale; this could add increased pressure on water security over SAF. Similarly, Engelbrecht (2019) showed that the projected temperature increases in SAF during the progression of the twenty-first century could have a significant effect on water security as a consequence of increased evaporation rates.

The findings from this study show that SAI deployment would alleviate the projected effects of increased GHGs on temperature and precipitation extremes across all of SAF's climatic zones. All SAI experiments are projected to trigger a nationwide cooling effect (Figures 18, 19 and 20), suggesting reduced evaporation (Pinto et al. 2020). All SAI experiments would likewise be effective in reducing the country's vulnerability to drought, especially during winter over western climatic

zones (SWS, SWN, WEI, SCO, SCI, and KAI) (Figure 17). This finding suggests that SAI could alleviate future water stress. Decreases in total precipitation under SAI, however, could contribute to dryer conditions and subsequently exacerbate water stress. This is especially the case for the CEI, KAI and NEL climatic zones on an annual timescale (Figure 15).

6.3.2 Agriculture sector

Agricultural productivity and livestock are highly reliant on water security and rainfall variability, showcasing the extent to which SAF's agriculture sector is susceptible to the adverse impacts of climate change. A large portion of the country's land (69%) can be used for grazing, while only 12% is suitable for rain-fed crop production (World Wildlife Fund; WWF, 2010). Livestock farming is subsequently SAF's largest faction within the agricultural sector (WWF, 2010). The majority of grazing land is already overstocked which has contributed to land degradation through trampling, denudation, erosion and decreased soil fertility (WWF, 2010). The projected increases in hot temperature extremes (Figure 18) and decreases in PRCPTOT over SAF's climatic zones (Figure 15) could exacerbate the negative effects of overstocking on agriculture; and livestock could grow increasingly vulnerable to heat stress, pests and diseases (DEA, 2017). In addition, livestock mortality rates would rise in response to temperature increases (Engelbrecht, 2019). The country's grazing lands would grow vulnerable to desertification (WWF, 2010), which could have negative implications for ecosystems and biodiversity, the agriculture sector and economy, and communities dependent on agriculture for a livelihood.

Figure 15 shows that annual PRCPTOT is projected to decrease (up to -70 mm/year) over all the climatic zones (aside from KNC) in response to increased GHG emissions. This highlights the increasing vulnerability of crop growth to climate change during the climatic zone's growing season. It is worth noting that CDD is a measure of intra-seasonal dry period length, suggesting that increased CDD during an area's rainfall season could cause a drier growing season. The projected increase in CDD across most climatic zones (Figure 15) could therefore exacerbate agricultural unpredictability (WWF, 2010) and reducing crop growth during the growing season.

The projected decrease in rainfall over the Limpopo River Basin in response to reduced tropical systems brought in from the Indian Ocean because of increased GHG emissions could throw off the region's water balance, leaving the communities dependent on the river basin for agriculture

vulnerable (Malherbe et al. 2013). Agricultural communities residing around the Limpopo River Basin in SAF (parts of the NEI, NEL and EAI climatic zones, or the Limpopo, Mpumalanga, North West and Gauteng Provinces) would therefore be highly exposed to the impact of increased GHG emissions. Agriculture in the SCI, SCO and SWS climatic zones (or the Eastern Cape and Western Cape Provinces) would also become vulnerable to rainfall variability and reduced precipitation, as past droughts in the region leading up to 2010 have forced farmers to drill boreholes, truck in feed and water and sell cattle to cope with the drought (WWF, 2010). Climatic zones such as EAI, KNC and NEL, where increases are projected for R10MM, RX1DAY, RX5DAY and R95P, could experience increased flooding incidences which would exacerbate the negative impacts of overgrazing (DEA, 2017). Potential outcomes include worsened soil erosion which would have implications for the livelihoods and ecosystems that surround livestock production (DEA, 2017).

The projected increases in hot temperature extremes and decreases in the frequency of cold days and nights over all climatic zones (Figure 18) could exacerbate water unpredictability, negatively impact labour because of thermal discomfort (DEA, 2017), and leave communities dependent on rain-fed agriculture vulnerable to losing their livelihoods and food resources. Moreover, increasing temperature extremes and decreasing precipitation could increase the demand for irrigation and water, placing further strain on an already water-stressed country.

The projected annual and seasonal decreases in CDD over most climatic zones (except for SWN) in response to all three SAI experiments could assist in alleviating the strain that the intra-seasonal dry period length places on the growing season and subsequently, the agriculture sector. The projected decrease in winter CDD over south-western climatic zones (SWS, SCI, SCO and parts of WEI), characterised by winter rainfall, under SAI relative to the baseline suggests that SAI could be beneficial for the region's growing season which is the country's biggest contributor to winter cereals (canola, wheat and malting barley) (Southafrica, 2021). Additionally, the agriculture sector could benefit from the projected annual and seasonal cooling effect that all three SAI experiments would trigger over all climatic zones (Figures 18, 19 and 20). The reduced hot temperature extremes could alleviate the strain placed on crops, prevent the deterioration of food production and quality (Wright et al. 2021) and lessen heat-induced livestock mortality. More specifically, the projected decreases in TX90P, TN90P, and WSDI in response to SAI could reduce the frequency of heat waves,

thereby enhancing livestock activity and crop production. Projected decreases in heavy precipitation extremes over most of SAF's climatic zones under SAI deployment could reduce vulnerability to floods, subsequently preventing crop damage. KNC is the only climatic zone which could experience increased precipitation extremes in response to all SAI experiments, which leaves the region vulnerable to flooding and subsequent crop damage. Finally, the projected decreases in total annual precipitation over eastern climatic zones, EAI and KNC, and a number of western climatic zones (SCO, SWS and TCO) (Figure 15) in response to all three SAI experiments suggests that SAI could induce drier conditions, causing subsequent plant water stress.

6.3.3 Health sector

Climate change poses an increasingly severe threat to human health in SAF as its impacts on temperature and precipitation extremes place heavier strain on land, infrastructure, and human life (DEA, 2017). SAF is a country associated with the burden of disease: HIV/AIDS, vector-borne diseases such as malaria, food- and water-borne diseases like cholera, cardiovascular and respiratory diseases (non-communicable diseases) like asthma and bronchitis, mental health, and malnutrition (Wright et al. 2021). It is therefore essential that the health sector be considered in the face of climate change.

SAF has the largest global incidences of HIV/AIDS and tuberculosis, and projected increases in temperature extremes across the country which are associated with heat stress could affect access to medical health care and to medication, subsequently contributing to increased HIV case numbers (Wright et al. 2021). The low-lying regions in KNC, NEI and NEL (in the KwaZulu-Natal, Limpopo and Mpumalanga Provinces) are the most vulnerable to malaria during the summer rainfall season (Wright et al. 2021). The projected increases in TNN, TXX and PRCPTOT in response to increased GHGs over these climatic zones (KNC, NEI and NEL) during summer (DFJ) (Figures 16 and 19) could exacerbate incidences of malaria (Wright et al. 2021). In addition, malaria distribution is projected to spread to the Highveld (CEI and EAI), where summer TNN, TXX and PRCPTOT are expected to rise in response to increased GHG emissions (Figures 16 and 19). Projected increases in annual heavy precipitation extremes over KNC (R10MM, RX1DAY, RX5DAY, and R95P) and NEL (RX1DAY, RX5DAY and R95P) could cause increased incidences and outbreaks of water-related diseases such as cholera (Figure 15). For example, heavy rains in 1999 caused the Juksei River in Alexandria (a township in

Johannesburg) to flood, leading to a cholera outbreak so severe that the residents had to be relocated to a more sanitary area (CSIR, 2014).

Projected increases in annual and seasonal hot temperature extremes over SAF's climatic zones (Figures 18, 19 and 20) are associated with increasing heat stress in the future, which has implications for morbidity and mortality rates (Wright et al. 2021). Heat stress and exhaustion could exacerbate mental health conditions as well as non-communicable diseases, such as cardiovascular, respiratory, and renal illnesses (Wright et al. 2021). Furthermore, heat stress could decrease productivity and increase restlessness, sleeplessness, exhaustion, and sunburn (Chersich, et al. 2018). Heat stress could therefore have serious implications for parts of the population who work outdoors and underground (such as those employed by SAF's large mining industry), immunocompromised people, the elderly, children, and large portions of the population who reside in rural areas and who live in poverty. As stated by the DEA (2017), SAF is a country that is highly dependent on its strong human capital, thereby leaving the work force vulnerable to the effects of heat stress. In addition, projected increases in annual CDD (Figure 15) over most climatic zones could exacerbate vulnerability to drought conditions, which as mentioned earlier, could negatively impact agriculture and food production. Those communities already living in poverty could become even more vulnerable to malnutrition.

The deployment of SAI could play a substantial role in alleviating the effects of climate change on human health in SAF. The projected nationwide cooling effect under SAI deployment, could mitigate the harsh impacts of heat stress on mental and physical human health across all climatic zones (Figures 18, 19 and 20). The widespread decreases projected for hot temperature extremes and heavy precipitation extremes could lessen the prevalence of malaria and cholera breakouts over most climatic zones. Increased heavy precipitation indices (R10MM, RX5DAY, and R95P) in response to SAI are, however, projected for climatic zones along the country's southern and eastern coastline, KNC, SCO and TCO, suggesting intensified vulnerability to flood conditions. This could have implications for water-related diseases along the southern and eastern coastline. Lastly, the projected decreases in annual and seasonal CDD (Figures 15, 16 and 17) over most climatic zones could reduce vulnerability to drought and subsequent malnutrition.

6.3.4 Vulnerable communities

The high level of inequality, disjointed urban communities and extreme widespread poverty within SAF are outcomes of the long-term implications of spatial planning during the apartheid era (DEA, 2017). SAF, therefore, has an extensive variety of pre-existing vulnerable communities to climate change; the primary communities being populations residing in informal settlements, women, children, the elderly, fishing communities and rural subsistence farmers (Chersich et al. 2018). Informal urban settlements are extremely exposed to the impacts of climate change on temperature extremes because of, among other factors, poor infrastructure, high population density, predisposition to fires and floods, lack of funds and resources for weather-related damages and poor service delivery (DEA, 2017). Projected increases in hot temperature extremes (Figures 18, 19 and 20) over climatic zones where urban areas such as Johannesburg (EAI), Cape Town (SWS) and Durban (KNC), could negatively impact the informal settlements in these cities; in addition to heat stress, the increased hot days and temperatures could erode the already poor infrastructure. Similarly, projected increases in heavy precipitation extremes over KNC (Figure 15) in response to increased GHGs could exacerbate the vulnerability of existing infrastructures to flood conditions. HIV transmission risks in SAF are the highest in informal urban settlements (Chersich et al. 2018) which could increase if hot temperature extremes push people in rural communities to migrate to urban areas. Communities residing in rural communities are also highly, if not more, exposed to climate change, temperature and precipitation extremes and insufficient water supply. These rural communities are often dependent on climate-sensitive resources to maintain their livelihoods (Chersich et al. 2018), which could become vulnerable as decreases in PRCPTOT are projected across most climatic zones (Figure 15), while increases are projected in hot temperature extremes in response to increased GHG emissions (Figure 18).

SAI deployment could contribute to alleviating the impacts of future temperature and precipitation extremes on a number of SAF's vulnerable communities. The projected nationwide cooling effect in response to all SAI experiments could relieve strain on the elderly, children, and the South African work force. The strain of heat stress on mental wellbeing would also lessen. In addition, reduced hot temperature extremes and decreased CDD could reduce the vulnerability of rural communities dependent on climate-sensitive resources for a livelihood, such as agricultural and fishing

communities. Reduced hot temperature extremes under SAI could prevent large migrations into informal urban settlements, subsequently mitigating potential increases in the HIV transmission rates in and among these communities (Chersich et al. 2018). The combination of reduced annual and seasonal hot temperature extremes and decreased PRCPTOT across most climatic zones in response to all SAI experiments could prevent infrastructure degradation, thereby reducing the vulnerability of communities residing in informal urban settlements to climate extremes. Vulnerable communities residing in KNC would, however, become more vulnerable to flood conditions due to projected increases in heavy precipitation under SAI (Figures 15, 16 and 17).

6.3.5 Urban Centres

In SAF, over 60% of the population lives in urban centres which account for only 1.5% of the country's surface area (Department of Forestry, Fisheries, and the Environment: DFFE, 2011). The abovementioned water, agricultural and health risks play out in the urban space and SAF's growing urban population is placing increased pressure on food and water resources and infrastructure. As mentioned earlier, informal urban settlements are largely exposed to the harmful effects of climate change in response to increasing hot temperature extremes and rainfall extremes. A less discussed topic, however, is the potential effects of climate change on the day-to-day municipal services which keep cities running smoothly (South African Cities Network: SACN, 2014). In this regard, cities are especially susceptible to climate change as they adapt to environmental changes slowly and have grown deeply dependent on embedded service delivery systems (DFFE, 2011). Municipalities are responsible for food security, transportation, and water provision (SACN, 2014), all of which are susceptible to temperature and precipitation extremes. Efficient transportation (of people and resources such as food and water) into and out of and within urban centres is a vital service delivery goal which can be severely affected by climate extremes such as flooding and heat waves. Disruptions in transport mobility could also cause economic disturbances and increase loss of life (SANC, 2014). Transport into and out of the cities of Johannesburg and Pretoria (EAI), Polokwane (NEL), and Durban and Pietermaritzburg (KNC) could be affected by the projected increases in heavy precipitation extremes in response to increased GHGs (Figure 15). Additionally, the projected increases in heat extremes over Johannesburg (EAI), Cape Town (SWS), Durban and Pietermaritzburg (KNC), and Polokwane (NEL) could contribute to air and land-based transport

system delays, disturbances, damages, and breakdowns (Figure 18; SANC, 2014). Increased occurrences of hot temperature extremes in cities could also trigger pavements to soften or melt and to expand, leading to pothole formation and placing strain on bridge joints (SANC, 2014). The high risks faced by urban centres to worsening climate extremes in response to increased GHG emissions highlights the urgency for efficient urban management.

The findings in this study revealed that SAI deployment is projected to reduce the projected changes in temperature and precipitation extremes. A decrease in precipitation extremes could reduce the vulnerability of urban centres to flash floods, thereby alleviating the strain that intensified precipitation events would place on city storm water drainage systems. The projected cooling effect over SAF's climatic zones, and cities, in response to SAI deployment could prevent heat-induced disruptions to city supply chains, natural resources, and energy supplies. Lastly, the overall decrease in hot temperature extremes and heavy precipitation extremes could contribute to reducing costs spent on maintenance and repairs of infrastructure and transport systems.

7 CHAPTER 7 – CONCLUSION, LIMITATIONS AND RECOMMENDATIONS

As the climate system continues to warm in response to increased GHG emissions from human activities, researchers across the globe are looking to assess the potential of CG as a potential way to mitigate warming. The current efforts outlined by the signatories of the Paris Agreement to reduce and mitigate GHG emissions are not enough to limit warming to 1.5°C, which further supports enhanced research into CG. The effect of climate change on temperature and precipitation extremes often has the most detrimental effects on vulnerable human societies. As a developing country, vulnerable groups comprise a substantial portion of the South African population. These groups are already the most exposed to the adverse impacts of climate change and are growing increasingly vulnerable as the frequency and magnitude of climate extremes are on the rise.

This study provides an overview of the potential impact of SRM through SAI on temperature and precipitation extremes across South Africa's climatic zones in the future (2075–2095). This was done using climate simulations from the CESM1(WACCM) model from the GLENS project. The control and feedback experiments, and two additional feedback experiments (Equatorial and Lower SAI), from the GLENS project datasets were used to conduct a comparative analysis of what a future without SAI under RCP8.5 and a future with SAI deployment under RCP8.5 would look like in South Africa. The control experiment represents temperature and precipitation extremes under RCP8.5 from 2010 until the end of the century. Three SAI experiments were used to assess how temperature and precipitation extremes in SAF would respond to varying injection characteristics. The main GLENS feedback experiment continuously injects SO_2 between 20–25 km altitude at 15°N and 15°S latitude and between 18–23 km at 30°N and 30°S latitude. Equatorial SAI is a single injection location at the equator 20–25 km above ground, and Lower SAI injects SO_2 at 1 km above the tropopause at four latitudes: 15°N, 15°S, 30°N and 30°S. A selection of extreme temperature and precipitation indices were used to evaluate the response of climate extremes to the different SAI injection characteristics over SAF's climatic zones.

7.1 KEY FINDINGS

7.1.1 Under RCP8.5

The findings from this study reveal that increased GHG emissions over SAF would result in an overall annual and seasonal decrease in PRCPTOT over most climatic zones, suggesting dryer future conditions. Similarly, precipitation extremes (R10MM, RX1DAY, RX5DAY, R95P and PRCPTOT) would decrease over most climatic zones, subsequently reducing vulnerability to flood conditions. KNC, EAI and NEL are the exception as they would experience (to varying extents), increased annual and seasonal (especially summer) precipitation extremes which suggests increased vulnerability to flooding conditions. Eastern-most SAF would therefore experience wetter conditions with the potential for flooding. This could be both detrimental and beneficial for agriculture, whereas water security in the region could increase. In contrast, the remainder of SAF would become dryer and vulnerable to decreases in precipitation extremes and to exacerbated intra-seasonal dry period lengths. These changes in precipitation patterns combined with increased CDD could have negative implications for growing seasons across the country's climatic zones and subsequently, agriculture and food and water security.

Future hot annual and seasonal temperature extremes across SAF's climatic zones are consistently projected to increase, while the frequency of cool nights and cool days could decrease. SAF's eastern climatic zones would be the most prone to experiencing hotter temperatures and less cold nights. Moreover, the combination of projected increases in WSDI and TX90P across the country suggests that the frequency of heat waves would increase, especially in eastern SAF. Increased heat waves could have negative implications for the mental and physical health of SAF's population. Finally, increased evaporation rates because of more heat waves and hot temperature extremes could destabilise agricultural production and water security.

7.1.2 Under SAI

GLENS, Equatorial and Lower SAI are all projected to decrease annual precipitation extremes (R10MM, RX1DAY, RX5DAY and R95P) over most climatic zones, suggesting reduced vulnerability to flood conditions. PRCPTOT would, however, increase over SAF's coastline and eastern interior, especially during summer. Equatorial SAI could increase annual PRCPTOT over numerous climatic

zones (EAI, KNC, SCI, SCO, SWS and TCO), suggesting overall wetter conditions under Equatorial SAI. Annual CDD could decrease over most climatic zones (except for NEL, SWN and WEI), thereby reducing vulnerability to increased intra-seasonal dry period lengths, meaning fewer dry periods during the growing season.

During summer, all precipitation extremes could decrease, with Lower SAI causing the largest magnitude of decreased precipitation over western and south-western climatic zones (SCI, SCO, SWS, SWN and WEI) as well as KAI and CEI. This would have negative implications for regions dependent on summer rainfall for agricultural activities (CEI and KAI). On the other hand, summer CDD could decrease over most climatic zones, which could mitigate increased dry period lengths. KNC is the only climatic zone where SAI could increase precipitation extremes during summer. SAI (especially GLENS and Lower SAI) could trigger wetter winters and potential flooding conditions over all climatic zones (except for NEI and NEL) due to projected increases in all precipitation extremes. Heavy rainfall events could, however, provide relief by replenishing the water table and other water-stressed resources, thereby enhancing agricultural capabilities during winter. Decreased winter CDD over most climatic zones (especially in SWN and WEI), could also enhance agricultural production. The largest magnitude of increased winter precipitation extremes would occur over western SAF climatic zones (SWS, SWN, WEI, SCI, and SCO). SAI could, therefore, enhance the precipitation in SWN and SWS which are characterised by winter rainfall.

SAI deployment could reduce annual and seasonal hot temperature extremes over all climatic zones and increase the frequency of cool nights and cool days. Equatorial SAI would induce the largest decreases in hot temperature extremes. SAI could, therefore, effectively activate a cooling effect over SAF's climatic zones. Colder summer night-time temperatures and more cold nights could occur across all climatic zones under SAI, with the largest decreases occurring over western SAF climatic zones (SWS, SWN, WEI, SCI, and SCO). During summer and winter, all climatic zones could experience more cold nights and cold days. The overall annual and seasonal cooling effect triggered by all SAI experiments could have positive implications for the country's agriculture and health sectors, in addition to enhanced food and water security.

7.2 LIMITATIONS AND RECOMMENDATIONS

This research is a country-scale study, which assessed the potential impact of SAI deployment on temperature and precipitation extremes only in South Africa. The regional and or global implications of SAI deployment were not explored. The data used in this study was from a Global Circulation Model (GCM), which generally does not represent precipitation extremes accurately. This is due to the coarse resolution of GCMs which are unable to resolve the meteorological processes that affect heavy rainfall. Accurate representations of precipitation projections were therefore limited; future studies could make use of regional climate models (RCMs) to partially resolve this limitation.

The model evaluation in this study was done at a seasonal level. If more time were available, a more comprehensive evaluation could have been carried out at a daily temporal scale. Additionally, the results presented in this study are relative only to the type of SAI deployed in the GLENS project, which, as stated by Pinto et al. (2020), reflects an "extreme scenario of climate geoengineering". It is, therefore, recommended that future studies assessing the potential impacts of SAI on climate extremes make use of additional data from other SAI models such as the Geoengineering Multi-model Intercomparison Project (GeoMIP) (Kravitz et al. 2021), as the results may have been different. To further strengthen the projected climatic changes in response to SAI, it is recommended that additional research is focused on the physical and chemical processes that occur following the injection of the gaseous sulphate precursor and lead to the reflection of incoming sunlight. Lastly, this study was limited to exploring how SAI would impact climate extremes and, therefore, does not assess its potential implications for biodiversity and ecosystems, global forest fires, plant productivity, economic growth, disease distribution shifts, human health, costing and other aspects. It is recommended that the impact of SAI on these factors be investigated to attain further insight into the implications of SAI deployment.

8 REFERENCES

Abiodun, B.J., Odoulami, R.C., Sawadogo, W. Oloniyo, O.A., Abatan, A.A., New, M., Lennard, C., Izidine, P., Egbebiye, T.S. and MacMartin, D.G. 2021. Potential impacts of stratospheric aerosol injection on drought risk managements over major river basins in Africa. Climatic Change, 169(31). Available: https://doi.org/10.1007/s10584-021-03268-w

African Development Bank. 2018. National Climate Change Profile: South Africa. Available: https://www.afdb.org/sites/default/files/documents/publications/afdb_south_africa_final_2018_english.pdf

AghaKouchak, A. Chiang, F., Huning, L.S., Love, C.A., Mallakpour, I., Mazdiyasni, O., Moftakhari, H., Papalexiou, S.M., Ragno, E. and Sadegh, M. 2020. Climate Extremes and Compound Hazards in a Warming World. Annual Review of Earth and Planetary Sciences, 48: 519-48. Available: https://doi.org/10.1146/annurev-earth-071719-055228

Bauer, S. and Scholz, I. 2010. Adaptation to climate change in Southern Africa: New boundaries for Sustainable Development? Climate and Development. DOI: 10.3763/cdev.2010.0040

Cheng, W., MacMartin D. G., Dagon, K., Kravitz, B., Tilmes, S., Richter, J. H., Mills, M. J. & Simpson, I. R. 2019. Soil Moisture and Other Hydrological Changes in a Stratospheric Aerosol Geoengineering Large Ensemble. Journal of Geophysical Research: Atmospheres, 124: 12773–93. Available: https://onlinelibrary.wiley.com/doi/abs/10.1029/2018JD030237

Chersich, M.F., Wright, C.Y., Venter, F., Rees, H., Scorgie, F. and Erasmus, B. 2018. Impacts of Climate Change on Health and Wellbeing in South Africa. International Journal of Environmental Research and Public Health,15(1884). Available: https://doi.org/10.3390/ijerph15091884

Climate Data Gateway at NCAR. Dataset Geoengineering Large Ensemble (Feedback). Available:

https://www.earthsystemgrid.org/dataset/ucar.cgd.ccsm4.GLE.Feedback.html Accessed: [September 2, 2020].

Climate Data Gateway at NCAR. Dataset Geoengineering Large Ensemble (Feedback_eq). Available: https://www.earthsystemgrid.org/dataset/ucar.cgd.ccsm4.GLE.Feedback_eq.html Accessed: [September 2, 2020].

Climate Data Gateway at NCAR. Dataset Geoengineering Large Ensemble (Feedback_low). Available: https://www.earthsystemgrid.org/dataset/ucar.cgd.ccsm4.GLE.Feedback_low.html Accessed: [September 2, 2020].

Community Earth System Model (CESM). N.d. Stratospheric Aerosol Geoengineering Large Ensemble Project – GLENS. Available: https://www.cesm.ucar.edu/projects/community-projects/GLENS/ Accessed: [December 10, 2021].

Council for Scientific and Industrial Research (CSIR). 2014. Climate Information and Early Warning Systems for Supporting the Disaster Risk Reduction and Management Sector in South Africa under Future Climates. Available: https://www.sanbi.org/wp-content/uploads/2018/04/ltas22-24-jan-workshop-day-1csirclimate-information-and-ews.pdf Accessed: [July 05, 2021].

Da-Allada, C.Y., Baloïtcha, E., Alamou, E.A., Awo, F.M., Bonou, F., Pomalegni, Y., Biao, E.I., Obada, E., Zandagba, J.E., Tilmes, S. & Irvine, P.J. 2020. Changes in West African Summer Monsoon Precipitation Under Stratospheric Aerosol Geoengineering. Earth's Future, 8. Available: https://doi.org/10.1029/2020EF001595

Davis, C.L., Hoffmann, M.T., and Roberts, W. 2016. Recent trends in the climate of Namaqualand, a megadiverse arid region of South Africa. South African Journal of Science, 112(3/4): 1-9. DOI: https://doi.org/10.17159/sajs.2016/20150217

Davis-Reddy, C. & Vincent, K. 2017. Climate Risk and Vulnerability: A Handbook for Southern Africa (2nd Ed), CSIR, Pretoria, South Africa.

Dennis, I. and Dennis, R. 2011. Climate change vulnerability index for South African aquifers. Water SA, 38(3): 417-426. DOI: 10.4314/wsa.v38i3.7

Department of Environmental Affairs. 2013. Long-Term Adaptation Scenarios Flagship Research Programme (LTAS) for South Africa. Climate Trends and Scenarios for South Africa. Pretoria, South Africa.

Department of Environmental Affairs. 2017. National Climate Change Adaptation Strategy (2nd Draft). Pretoria: Department of Environmental Affairs.

Department of Environmental Affairs. 2017. South Africa's 3rd Climate Change Report. Available: https://www.dffe.gov.za/documents/research#climate_change

Department of Environment, Forestry and Fisheries. 2019. National Climate Change Adaptation Strategy. Available: https://www.environment.gov.za/mediarelease/nationalclimatechange_adaptationstrategy_ue10november19

Department of Forestry, Fisheries and the Environment. 2011. National Climate Change Response White Paper. Available: https://www.environment.gov.za/legislation/whitepapers

Department of Water Affairs, 2013. National Water Resource Strategy. Available: https://www.environment.gov.za/sites/default/files/reports/southafrica_secondnational_climatechnage_report2017.pdf Accessed: [January 29, 2021].

Driver, P. 2014. Rainfall Variability over Southern Africa. Ph.D. Thesis. University of Cape Town. ENRNS. 2018. Indian Ocean influences on Australian Climate. Available: http://elninoreadynations.com/indian-ocean-influences-on-australian-climate/

Emori, S. & Brown, S.J. 2005. Dynamic and thermodynamic changes in mean and extreme precipitation under changed climate. Geophysical Research Letters, 32. DOI: 10.1029/2005GL023272

Engelbrecht, F. 2019. Green Book – Detailed Projections of Future Climate Change over South Africa. Technical report, Pretoria: CSIR.

English, J.M., Toon, O.B. and Mills, M.J. 2012. Microphysical simulations of sulfur burdens from stratospheric sulfur geoengineering. Atmos. Chem. Phys., 12: 4775–4793. Available: https://doi.org/10.5194/acp-12-4775-2012

Firchett, J. 2021. Climate change has already hit southern Africa. The Conversation. Available: https://theconversation.com/climate-change-has-already-hit-southern-africa-heres-how-we-know-169062 Accessed: [December 07, 2021].

Funk, C., Peterson, P., Landsfeld, M., Pedreros, D., Verdin, J., Shukla, S., Husak, G., Rowland, J., Harrison, L., Hoell, A. & Michaelsen, J. 2015. The climate hazards infrared precipitation with stations - A new environmental record for monitoring extremes. Sci Data, 2(150066). Available: https://doi.org/10.1038/sdata.2015.66

Geoengineering Monitor. N.d. What is geoengineering? Available: https://www.geoengineeringmonitor.org/what-is-geoengineering/ Accessed: [December 07, 2021].

Government Communication and Information System (GCIS). 2019. South Africa Yearbook 2018/2019. Available: https://www.gcis.gov.za/south-africa-yearbook-201819 Accessed: [October 28, 2020].

Guha-Sapir, D., Hoyois, P., Wallemacq, P. and Below, R. 2016. Annual Disaster Statistical Review 2016. Université catholique de Louvain, Brussels, Belgium. Centre for Research on the Epidemiology of Disasters (CRED). Available: https://www.emdat.be/annual-disaster-statistical-review-2016

Halstead, J. 2018. Stratospheric aerosol injection research and existential risk. Futures, 102: 63-77. Available: https://doi.org/10.1016/j.futures.2018.03.004

Harris, I., Jones, P.D., Osborn, T.J., Lister, D.H. 2014. Updated high-resolution grids of monthly climatic observations - the CRU TS3.10 Dataset. Int J Climatol, 34(3): 623–642. Available: https://doi.org/10.1002/joc.3711

Harris, I.C., Jones, P.D. 2020. CRU TS4.03: Climatic Research Unit (CRU) Time-Series (TS) version 4.03 of high-resolution gridded data of month-by-month variation in climate (Jan. 1901- Dec. 2018). University of East Anglia Climatic Research Unit; Centre for

Environmental Data Analysis. Available: http://dx.doi.org/10.5285/10d3e3640f004c578403419aac167d82

Hewitson, B.C. and Crane, R.G. 2006. Consensus between GCM Climate Change Projections with Empirical Downscaling: Precipitation Downscaling over South Africa. International Journal of Climatology, 26: 1315-1337. Available: https://doi.org/10.1002/joc.1314

Hoerling, M., Hurrell, J., Eischeid, J. and Phillips, A. 2006. Detection and Attribution of Twentieth-Century Northern and Southern African Rainfall Change. Journal of Climate, 19(16): 3989-4008. DOI: https://doi.org/10.1175/JCLI3842.1

Horton, D.E., Johnson, N.C., Singh, D., Swain, D.L., Rajaratnam, B. and Diffenbaugh, N.S. 2015. Contribution of changes in atmospheric circulation patterns to extreme temperature trends. Nature, 522: 465–69

IPCC, 2012. Seneviratne, S.I., Nicholls, N., D. Easterling, Goodess C.M., Kanae, S., Kossin, J., Luo, Y., Marengo, J., McInnes, K., Rahimi, M., Reichstein, M., Sorteberg, A., Vera, C. and Zhang, X. Changes in climate extremes and their impacts on the natural physical environment. In: Managing the Risks of Extreme Events and Disasters to Advance Climate Change Adaptation [Field, C.B., V. Barros, T.F. Stocker, D. Qin, D.J. Dokken, K.L. Ebi, M.D. Mastrandrea, K.J. Mach, G.-K. Plattner, S.K. Allen, M. Tignor, and P.M. Midgley (eds.)]. A Special Report of Working Groups I and II of the Intergovernmental Panel on Climate Change (IPCC). Cambridge University Press, Cambridge, UK, and New York, NY, USA, pp. 109-230.

IPCC, 2014. Core Writing Team, R.K. Pachauri and L.A. Meyer (eds.). Climate Change 2014: Synthesis Report. Contribution of Working Groups I, II and III to the Fifth Assessment Report of the Intergovernmental Panel on Climate Change. IPCC, Geneva, Switzerland.

IPCC, 2014. Revi, A., D.E. Satterthwaite, F. Aragón-Durand, J. Corfee-Morlot, R.B.R. Kiunsi, M. Pelling, D.C. Roberts, and W. Solecki. Urban areas. In: Climate Change 2014: Impacts, Adaptation, and Vulnerability. Part A: Global and Sectoral Aspects. Contribution of Working Group II to the Fifth Assessment Report of the Intergovernmental Panel on Climate Change [Field, C.B., V.R. Barros, D.J. Dokken, K.J. Mach, M.D. Mastrandrea, T.E.

Bilir, M. Chatterjee, K.L. Ebi, Y.O. Estrada, R.C. Genova, B. Girma, E.S. Kissel, A.N. Levy, S. MacCracken, P.R. Mastrandrea, and L.L.White (eds.)]. Cambridge University Press, Cambridge, United Kingdom and New York, NY, USA, pp. 535-612.

IPCC, 2018. Masson-Delmotte, V., P. Zhai, H.-O. Pörtner, D. Roberts, J. Skea, P.R. Shukla, A. Pirani, W. Moufouma-Okia, C. Péan, R. Pidcock, S. Connors, J.B.R. Matthews, Y. Chen, X. Zhou, M.I. Gomis, E. Lonnoy, T. Maycock, M. Tignor, and T. Waterfield (eds.) Annex I: Glossary [Matthews, J.B.R. (ed.)]. In: Global Warming of 1.5°C. An IPCC Special Report on the impacts of global warming of 1.5°C above pre-industrial levels and related global greenhouse gas emission pathways, in the context of strengthening the global response to the threat of climate change, sustainable development, and efforts to eradicate poverty. In Press.

Irish Aid. 2018. Mozambique Country Climate Risk Assessment Report. Irish Aid, Resilience and Economic Inclusion Team, Policy Unit. Available: https://www.climatelearningplatform.org/sites/default/files/resources/mozambique_country_climate_risk_assessment_report_-_final.pdf

Irvine, P., Kravitz, B., Lawrence, M. & Muri, H. 2016. An overview of the Earth system science of solar geoengineering. WIREs Climate Change, 7: 815-833. Available: https://doi.org/10.1002/wcc.423

Irvine, P.J. & Keith, D.W. 2020. Halving warming with stratospheric aerosol geoengineering moderates policy-relevant climate hazards. Environmental Research Letters, 15. Available: https://doi.org/10.1088/1748-9326/ab76de

Kalaba, M. 2019. How droughts will affect South Africa's broader economy. Available: https://theconversation.com/how-droughts-will-affect-south-africas-broader-economy-111378 Accessed: [October 15, 2020].

Karami, K., Tilmes, S., Muri, H. and Mousavi, S.V. 2020. Storm Track changes in the Midle East and North Africa Under Stratospheric Aerosol Geoengineering. Geophysical Research Letters, 47. Available: https://doi.org/10.1029/2020GL086954

Kaspi, Y. and Tamarin, T. 2017. The Poleward Shift of Storm Tracks Under Climate Change: Tracking Cyclones in CMIP5. American Geophysical Union, Fall Meeting 2017. Available: https://ui.adsabs.harvard.edu/abs/2017AGUFM.A54G..04K

Knutson, T., Kossin, J.P., Mears, C., Perlwitz, J. and Wehner, M.F. 2017. Detection and Attribution of climate Change. In: Climate Science Special Report: Fourth National Climate Assessment, Volume l [Wuebbles, D.J., Fahey, K.A., Hibbard, K.A>, Dokken, D.J., Stewart, B.C. and Maycock, T.K. (eds.). U.S. Global Change Research Program, Washington, DC, USA, pp. 114-132. Available: https://science2017.globalchange.gov/chapter/3/

Kravitz, B., MacMartin, D. G., Tilmes, S., Richter, J. H., Mills, M. J., Cheng, W., et al. 2019. Comparing surface and stratospheric impacts of geoengineering with different SO2 injection strategies. Journal of Geophysical Research: Atmospheres, 124: 7900–7918. Available: https://doi.org/10.1029/2019JD030329

Kravitz, B., MacMartin, D. G., Visioni, D., Boucher, O., Cole, J. N. S., Haywood, J., Jones, A., Lurton, T., Nabat, P., Niemeier, U., Robock, A., Séférian, R., and Tilmes, S. 2021. Comparing different generations of idealized solar geoengineering simulations in the Geoengineering Model Intercomparison Project (GeoMIP). Atmos. Chem. Phys. (21): 4231–4247. Available: https://doi.org/10.5194/acp-21-4231-2021

Kruger, A.C. 2007. Trends in cloud cover from 1960–2005 over South Africa. Water SA, 33(5): 603–608.

Kruger A.C., Rautenbach, H., Mbatha, S., Ngwenya, S, and Makgoale, T.E 2019. Historical and projected trends in near-surface temperature indices for 22 locations in South Africa. South African Journal of Science, 115(5/6). Available: https://doi.org/10.17159/sajs.2019/4846

Landman, W.A., Mason, S.J., Tyson, P.D. & Tennant, W.J. 2001. Retro-active Skill of Multi-tiered Forecasts of Summer Rainfall over Southern Africa. International Journal of Climatology, 21: 1-19. Available: https://doi.org/10.1002/joc.592

Landman, W.A. & Goddard, L. 2005. Predicting southern African summer rainfall using a combination of MOS and perfect prognosis. Geophysical Research Letters, 32, L15809. Available: https://doi.org/10.1029/2005GL022910

Lawrence, M.G., Schäfer, S., Muri, H., Scott, V., Oschlies, A., Vaughan, N.E., Boucher, O., Schmidt, H, Haywood, J. and Scheffran, J. 2018. Evaluating climate geoengineering proposals in the context of the Paris Agreement temperature goals. Nature Communications, 9(3734). Available: https://doi.org/10.1038/s41467-018-05938-3

Lee, H., Ekici, A., Tjiputra, J., Muri, H., Chadburn, S.E., Lawrence, D.M., and Schwinger, J. 2019. The Response of Permafrost and High-Latitude Ecosystems Under Large-Scale Stratospheric Aerosol Injection and Its Termination. Earth's Future, 7: 605–614. Available: https://doi.org/10.1029/2018EF001146

Lenferna, G.A., Russotto, R.D., Tan, A., Gardiner, S.M. and Ackerman, T.P. 2017. Relevant climate response tests for stratospheric aerosol injection: A combined ethical and scientific analysis. Earth's Future, 5: 577–591. Available: https://doi.org/10.1002/2016EF000504

Lenton, T.M. and Vaughan, N.E. 2009. The radiative forcing potential of different climate geoengineering options. Atmospheric, Chemistry and Physics, 9: 5539–556. Available: www.atmos-chem-phys.net/9/5539/2009/

L.V. 2016. 11 Important Model Evaluation Techniques Everyone Should Know [Blog, February 20]. Available: 11 Important Model Evaluation Techniques Everyone Should Know - Data Science Central Accessed: [September 30, 2020].

Mackellar, N., New, M. and jack, C. 2014. Observed and modelled trends in rainfall and temperature for South Africa: 1960-2010. South African Journal of Science, 110(7/8). Available: https://doi.org/10.1590/sajs.2014/20130353

MacMartin, D. G., Kravitz, B., Tilmes, S., Richter, J.H., Mills, M.J., Lamarque, J-F., Tribbia, J. J. and Vitt, F. 2017. The Climate Response to Stratospheric Aerosol Geoengineering Can Be Tailored Using Multiple Injection Locations. Journal of Geophysical Research:

Atmospheres, 122(12): 12574-12590. Available: https://doi.org/10.1002/2017JD026868

Malherbe, J., Landman, W.A. and Engelbrecht, F.A. 2014. The bi-decadal rainfall cycle, Southern Annular Mode and tropical cyclones over the Limpopo River Basin, southern Africa. Climate Dynamics, 42: 3121-3138. DOI:10.1007/s00382-013- 2027-y.

Mastrandrea, M.D., Field, C.B., Stocker, T.F., Edenhofer, O., Ebi, K.L., Frame, D.J., Held, H., Kriegler, E., Mach, K.J., Matschoss, P.R., Plattner, G.-K., Yohe, G.W. and Zwiers, F.W. 2010: Guidance Note for Lead Authors of the IPCC Fifth Assessment Report on Consistent Treatment of Uncertainties. Intergovernmental Panel on Climate Change (IPCC). Available: https://www.ipcc.ch/site/assets/uploads/2017/08/AR5_Uncertainty_Guidance_Note.pdf

Matlakala, L. 2020. Is Solar Radiation Management a practical solution? Available: http://www.csag.uct.ac.za/2020/02/07/is-solar-radiation-management-a-practical-solution/ Accessed: [October 26, 2020].

Maxey, K. 2015. Geoengineering: What Is It? What Can It Do? Available: https://www.engineering.com/story/geoengineering-what-is-it-what-can-it-do Accessed: [January 12, 2021].

Mbokodo, I., Bopape, M-J., Chikoore, H., Engelbrecht, F. and Nethengwe, N. 2020. Heatwaves in the Future Warmer Climate of South Africa. Atmosphere, 11(712). Available: https://doi.org/10.3390/atmos11070712

Mills, M.J., Richter, J. H., Tilmes, S., Kravitz, B., MacMartin, D. B., Glanville, A. A.,Tribbia, J. J., Lamarque, J-F., Vitt, F., Schmidt, A., Gettelman, A., Hannay, C., Bacmeister, J. T. & Kinnison, D. E. 2017. Radiative and Chemical Response to Interactive Stratospheric Sulfate Aerosols in Fully Coupled CESM1(WACCM). Journal of Geophysical Research: Atmospheres, 122(13): 13,061–13,078. Available: https://doi.org/10.1002/2017JD02688

Moore, J.C., Yue, C., Zhao, L., Guo, X., Watanabe, S. and Ji, D. 2019. Greenland Ice Sheet Response to Stratospheric Aerosol Injection Geoengineering. Earth's Future, 7: 1451–1463. Available: https://doi.org/10.1029/

Muthige, M.S., Malherbe, J., Englebrecht, F.A., Grab, S., Beraki, A., Maisha, T.R. & Van der Merwe, J. 2018. Projected changes in tropical cyclones over the South West Indian Ocean under different extents of global warming. Environmental Research Letters, 13. Available: https://doi.org/10.1088/1748-9326/aabc60

NAS: Policy Implications of Greenhouse Warming: Mitigation, Adaptation, and the Science Base. 1992. Washington, D.C.

NASA's Goddard Institute for Space Studies (NASA/GISS). 2020. Global Temperature. Available: https://climate.nasa.gov/vital-signs/global-temperature/ Accessed: [February 01, 2021].

National Academies of Sciences, Engineering, and Medicine (NASEM). 2016. Attribution of Extreme Weather Events in the Context of Climate Change. Washington, DC: The National Academies Press. Available: 10.17226/21852 Available: https://doi.org/10.17226/21852

National Geographic. 2019. Effects of global warming. Available: https://www.nationalgeographic.com/environment/global-warming/global-warming-effects/ Accessed: [February 01, 2021].

National Weather Service. n.d. What is El Niño-Southern Oscillation (ENSO)? Available: https://www.weather.gov/mhx/ensowhat Accessed: [November 10, 2020].

NCAR CESM. Stratospheric Aerosol Geoengineering Large Ensemble Project – GLENS. Available: http://www.cesm.ucar.edu/projects/community-projects/GLENS/ Accessed: [September 2, 2020]

Nemakononi K. 2020. Implications of global warming of 1.5°C, 2.0°C, and overshooting of 2.0 Paris targets for South Africa. Master Dissertation, University of Cape Town.

Niang, I., Ruppel, O.C., Abdrabo, M.A., Essel, A., Lennard, C., Padgham, J. and Urquhart, P. 2014. Africa. In: Climate Change 2014: Impacts, Adaptation, and Vulnerability. Part B: Regional Aspects. Contribution of Working Group II to the Fifth Assessment Report of the Intergovernmental Panel on Climate Change [Barros, V.R., Field, C.B., Dokken, D.J., Mastrandrea, M.D., Mach, K.J., Bilir, T.E., Chatterjee, M., Ebi, K.L., Estrada, Y.O., Genova, R.C., Girma, B., Kissel, E.S., Levy, A.N., MacCracken, S., Mastrandrea, P.R. and White, L.L. (eds.)]. Cambridge University Press, Cambridge, United Kingdom and New York, NY, USA, pp. 1199-1265.

Notre Dame Global Adaptation Initiative (ND-GAIN). 2018. Country Index: South Africa. Available: https://gain.nd.edu/our-work/country-index/ Accessed: [January 29, 2021].

Odoulami, R.C., New, M., Wolski, P., Guillemet, G., Pinto, I., Lennard, C., Muri, H. & Tilmes, S. 2020. Stratospheric Aerosol Geoengineering could lower future risk of 'Day Zero' level droughts in Cape Town. Environmental Research Letters, 15(12). Available: https://iopscience.iop.org/article/10.1088/1748-9326/abbf13

Oggmus. 2014. Regions of South Africa. Available: https://commons.wikimedia.org/wiki/File:Regions_of_South_Africa_1.png Accessed: [November 4, 2020].

Ornes, S. 2019. Explainer: What is attribution science? Available: https://www.sciencenewsforstudents.org/article/explainer-what-attribution-science

Palmer, T.N. 2013. Climate extremes and the role of dynamics. National Academy of Sciences, 110(14): 5281-5282 Available: https://doi.org/10.1073/pnas.1303295110

Perren, B.B., Hodgson, D.A., Roberts, S.J., Sime, L., Nieuwenhuyze, W.V., Verleyen, E. & Vyverman, W. 2020. Southward migration of the Southern Hemisphere westerly winds corresponds with warming climate over centennial timescales. Communities Earth and Environment, Available: https://doi.org/10.1038/s43247-020-00059-6

Philippon, N., Rouault, M., Richard, Y. & Favre, A. 2011. The influence of ENSO on South Africa winter rainfall. International Journal of Climatology, 32(15): 2333-2347. Available: https://doi.org/10.1002/joc.3403

Pinto, I., Jack, C., Lennard, C., Tilmes, S., & Odoulami, R. C. 2020. Africa's climate response to solar radiation management with stratospheric aerosol. Geophysical Research Letters, 47, e2019GL086047. https://doi.org/10.1029/2019GL086047

Price Waterhouse Coopers (PwC). 2014. African Insurance Trends. Available: https://www.pwc.co.za/en/assets/pdf/south-african-insurance-2014.pdf

Rawat, S. 2019. Is accuracy EVERYTHING? Towards Data Science. Available: https://towardsdatascience.com/is-accuracy-everything-96da9afd540d Accessed: [December 10, 2021].

Reason, C.J.C., Rouault, M., Melice, J-L. & Jagadheesha, D. 2002. Interannual winter rainfall variability in SW South Africa and large scale ocean-atmosphere interactions. Meteorology and Atmospheric Physics, 80(1–4): 19–29. Available: https://doi.org/10.1007/s007030200011

Reason, C.J.C & Rouault, M. 2002. ENSO-like decadal patterns and South African rainfall. Geophysical Research Letters, 29(13): 13–16. Available: https://doi.org/10.1029/2002GL014663

Reason, C.J.C & Rouault, M. 2005. Links between the Antarctic Oscillation and winter rainfall over western South Africa. Geophysical Research Letters, 32, L07705. DOI: https://doi.org/10.1029/2005GL022419

Reason, C.J.C. 2017. Climate of Southern Africa. Oxford Research Encyclopedia of Climate Science. Available: https://doi.org/10.1093/acrefore/9780190228620.013.513

Shongwe, M.E., Van Oldenborgh, G.J., Van Den Hurk, B.J.J.M., De Boer, B., Coelho, C.A.S. and Van Aalst, M.K. 2009. Projected Changes in Mean and Extreme Precipitation in Africa under Global Warming. Part I Southern Africa. Journal of Climate, 22: 3819 3837.

Smith, W. 2020. The cost of stratospheric aerosol injection through 2100. Environmental Research Letters, 15(11). DOI: https://doi.org/10.1088/1748-9326/aba7e7

Southafrica. 2021. Field Crops in South Africa. Available: https://southafrica.co.za/field-crops-in-south-africa.html Accessed: [November 30, 2021].

South African Cities Network. 2014. Synthesis Report: Analysing Cities' Climate Change Resilience Food Security | Transport | Water. Available: https://www.sacities.net/climate-change-reports/

Sun, W., Wang, B., Chen, D., Gao, C., Lu, G. and Liu, J. 2020. Global monsoon response to tropical Arctic stratospheric aerosol injection. Climate Dynamics, 55: 2107–2121. Available: https://doi.org/10.1007/s00382-020-05371-7

The Royal Society. 2009. Geoengineering the Climate: Science, governance and uncertainty. RS policy document 10/09. Available: https://royalsociety.org/topics-policy/publications/2009/geoengineering-climate/

Tilmes, S., Richter, J.H., Mills, M.J., Kravitz, B., MacMartin, D.G., Vitt, F., Tribbia, J.J. and Lamarque, JF. 2017. Sensitivity of Aerosol Distribution and Climate Response to Stratospheric SO2 Injection Locations. Journal of Geophysical Research: Atmospheres, 122(23): 12,591-12,615. Available: https://doi.org/10.1002/2017JD026888

Tilmes, S., Richter, J. H., Kravitz, B., MacMartin, D. G., Mills, M. J., Simpson, I. R., Glanville, A. A., Fasullo, J. T., Phillips, A. S., & Lamarque, J-F. 2018. CESM1(WACCM) Stratospheric Aerosol Geoengineering Large Ensemble Project. Bulletin of the American Meteorological Society, 99(11): 2361–2371. Available: https://doi.org/10.1175/BAMS-D-17-0267.1

Tilmes, S., Richter, J. H., Mills, M. J., Kravitz, B., MacMartin, D. G., Garcia, R. R., Kinnison, D. E., Lamarque, J-F., Tribbia, J. and Vitt, F. 2018. Effects of different stratospheric SO2 injection altitudes on stratospheric chemistry and dynamics. Journal of Geophysical Research: Atmospheres, 123: 4654–4673. Available: https://doi.org/10.1002/2017JD028146

Tjiputra, J.F., Grini, A. and Lee, H. 2015. Impact of idealized future stratospheric aerosol injection on the large-scale ocean and land carbon cycles. Journal of Geophysical Research: Biogeosciences, 121: 2-27. DOI: https://doi.org/10.1002/2015JG003045

Trenberth, K.E. 2012. Framing the way to relate climate extremes to climate change. Climatic Change, 115: 283–290. Available: https://doi.org/10.1007/s10584-012-0441-5

United Nations Economic Commission for Africa (UNECA). 2010. “Climate Change and the Rural Economy in Southern Africa: Issues, Challenges and Opportunities”. Issues Paper. Available: https://www.uneca.org/publications/%E2%80%9Cclimate-change-and-rural-economy-southern-africa-issues-challenges-and-opportunities%E2%80%9D

United Nations Framework Convention on Climate Change (UNFCCC). The Paris Agreement. Available: https://unfccc.int/process-and-meetings/the-paris-agreement/the-paris-agreement. Accessed: [2020, August 7].

United Nations International Children’s Emergency Fund (UNICEF). 2019. Cyclone Idai and Kenneth. Available: https://www.unicef.org/mozambique/en/cyclone-idai-and-kenneth Accessed: [December 07, 2021].

United States Agency for International Development (USAID). 2015. Climate Change Information Fact Sheet: SOUTH AFRICA. Available: South Africa Climate Info Fact Sheet_FINAL.pdf (climatelinks.org) Accessed: [July 05, 2021]

Vautard, R., Yiou, P., Stott, P., Christidis, N., Oldenborgh, G.J.V. & Schaller, N. 2016. Attribution of human-induced dynamical and thermodynamical contributions in extreme weather events. Environmental Research Letters, 11 (11). DOI: 10.1088/1748-9326/11/11/114009

Wang, J., Dai, A. and Mears, C. 2016. Global Water Vapor Trend from 1988 to 2011 and Its Diurnal Asymmetry Based on GPS, Radiosonde, and Microwave Satellite Measurements. Journal of Climate, 29(14): 5205-5222. DOI: https://doi.org/10.1175/JCLI-D-15-0485.1

Wehrli, K., Luo, F., Hauser, M., Shiogama, H., Tokuda, D., Kim, H., Coumou, D., May, W., Sager, P.L., Selten, F., Martius, O., Vautard, R. & Seneviratne, S.I. 2021. The ExtremeX global climate model experiment: Investigating thermodynamic and dynamic processes contributing to weather and climate extremes. Earth System Dynamics Discussions. [preprint]. Available: https://doi.org/10.5194/esd-2021-58, in review, 2021.

World Bank Group: Climate Change Knowledge Portal. South Africa: Climate Data. Available: https://climateknowledgeportal.worldbank.org/country/south-africa/climate-data-historical Accessed: [October 28, 2020].

World Meteorological Organisation (WMO) Commission for Climatology Task Team. 2018. Guidelines on the Definition and Monitoring of Extreme Weather and Climate Events. Final Draft. Available: https://www.wmo.int/pages/prog/wcp/ccl/documents/GUIDELINESONTHEDEFINTIONANDMONITORINGOFEXTREMEWEATHERANDCLIMATEEVENTS_09032018.pdf

World Wildlife Fund (WWF). 2010. Agriculture: Facts and Trends South Africa. Available: http://awsassets.wwf.org.za/downloads/facts_brochure_mockup_04_b.pdf Accessed: [July 05, 2021].

Wright, C.Y., Garland, R.M., Norval, M. & Vogel, C. 2014. Human health impacts in a changing South African climate. South African Medical Journal, 104(8): 579-582. Available: 10.7196/samj.8603

Wright, C.Y., Kapwata, T., Preez, D.J-D., Wernecke, B., Garland, R.M., Nkosi, V., Landman, W.A., Dyson, L. and Norval, M. 2021. Major climate change-induced risks to human health in South Africa. Journal of Environmental Research, 196. Available: https://doi.org/10.1016/j.envres.2021.11097

Zamboni, J. 2018. The Advantages of a Large Sample Size. Available: https://sciencing.com/calculate-xbar-8382419.html Accessed: [February 02, 2021].

Ziervogel, G., New, M., Garderen, E.A.V., Midgley, G., Taylor, A. Hamann, R., Stuart-Hill, S., Myers, J. & Warburton, M. 2014. Climate change impacts and adaption in South Africa. WIRES Climate Change, 5: 605-620. Available: https://doi.org/10.1002/wcc.295

9 APPENDICES

9.1 PROJECTED CHANGES IN THE SPATIAL DISTRIBUTION OF PRECIPITATION EXTREMES IN RESPONSE TO EQUATORIAL SAI AND LOWER SAI

The left and middle right-hand columns in Figures A1 (annual), A2 and A3 (seasonal) show the projected impact of Equatorial SAI and Lower SAI on precipitation extremes for the period 2075–2095 relative to the baseline, respectively. Both SAI experiments could cause widespread decreases in precipitation due to overall projected decreases in R10MM, RX1DAY, RX5DAY, R95P, and PRCPTOT. CDD is projected to decrease over most of the country in response to SAI, aside from north-east and parts of the westernmost SAF where it could increase.

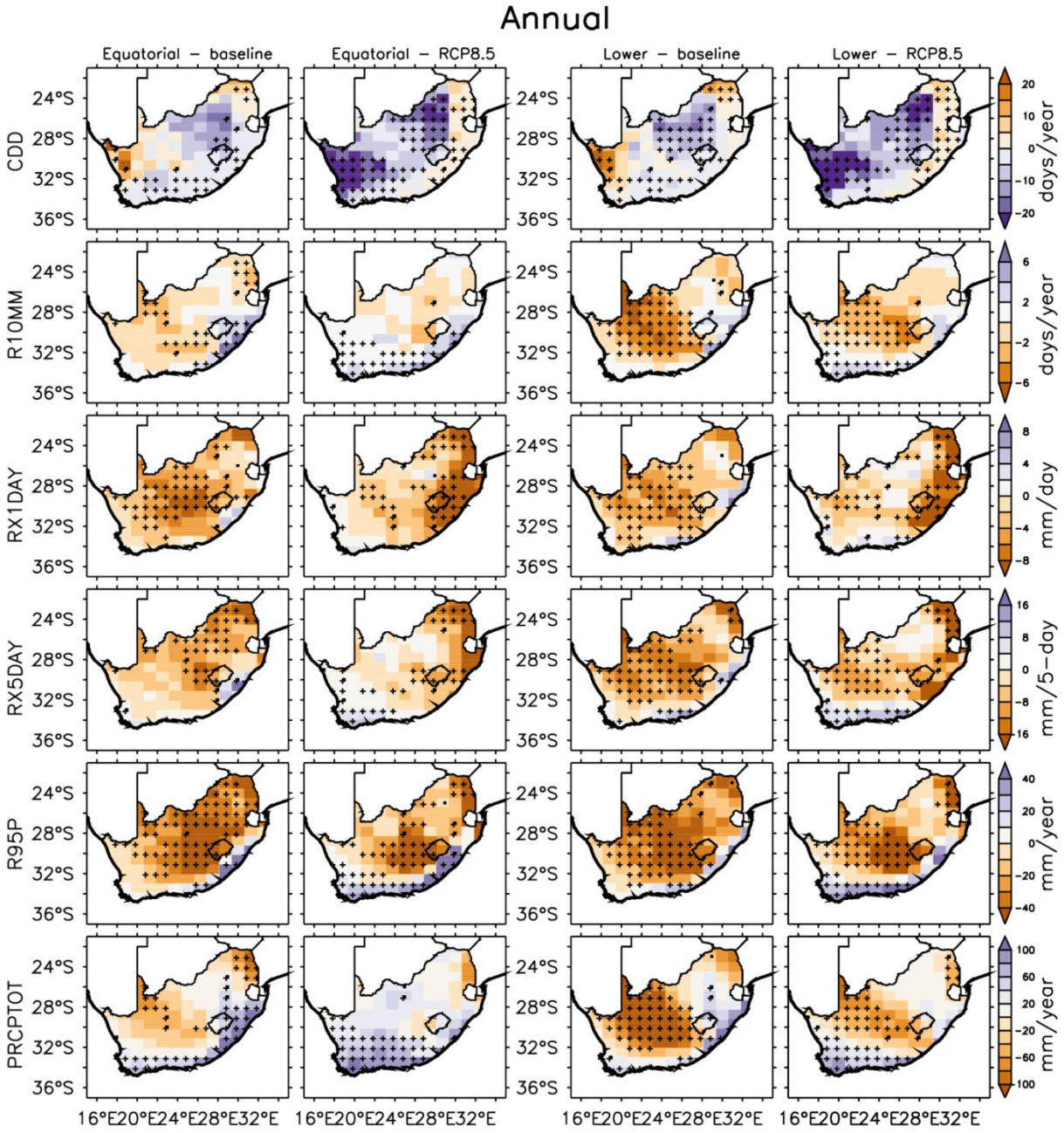

Figure A1. The ensemble mean of annual precipitation indices over South Africa for the present-day/baseline period (2010–2030; left-side column), as simulated by the CESM1 WACCM) model in the Geoengineering Large Ensemble (GLENS) project. Two SAI experiments with different injection characteristics are used: Equatorial SAI (left and middle left-hand column) and Lower SAI (right and middle right-hand column). The left column and middle right-hand column indicate the projected changes with Equatorial SAI and Lower SAI (SAI – baseline) relative to the baseline, respectively. The middle left-hand column and the right columns indicate the impact of SAI on projected precipitation extremes under RCP8.5 in 2075–2095 (SAI-RCP8.5). The '+' signs indicate areas where all ensemble members agree on the projected sign of the change.

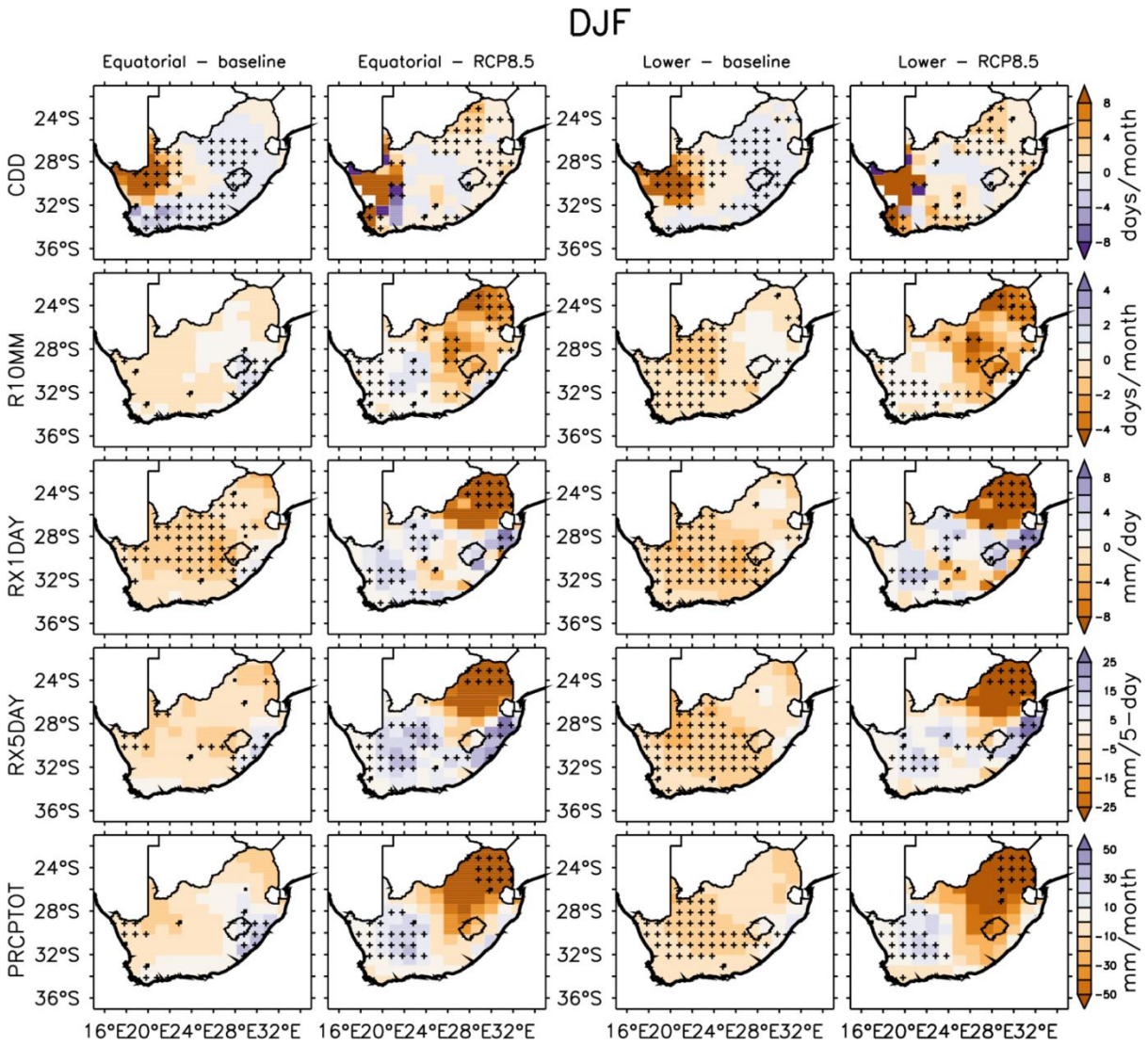

Figure 21. The ensemble mean of precipitation indices over South Africa during summer (DJF) for the present-day/baseline period (2010–2030; left-side column) as simulated by the CESM1(WACCM) model in the Geoengineering Large Ensemble (GLENS) project. Two SAI experiments with different injection characteristics are used: Equatorial SAI (left and middle left-hand column) and Lower SAI (right and middle right-hand column). The left column and middle right-hand column indicate the projected changes with Equatorial SAI and Lower SAI (SAI – baseline) relative to the baseline, respectively. The middle left-hand column and the right columns indicate the impact of SAI on projected precipitation extremes under RCP8.5 in 2075–2095 (SAI-RCP8.5). The '+' signs indicate areas where all ensemble members agree on the projected sign of the change.

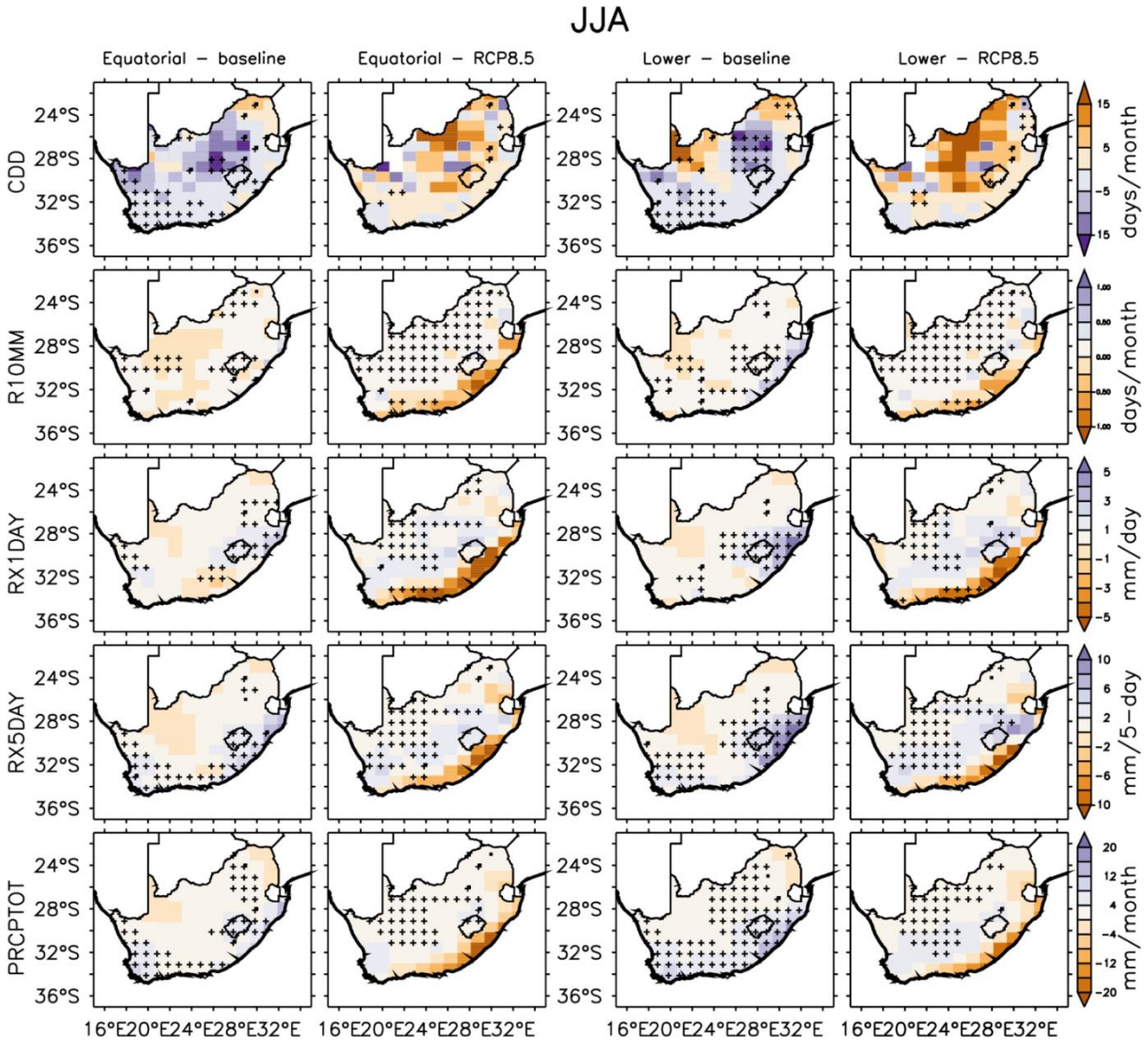

Figure 22. The ensemble mean of precipitation indices over South Africa during winter (JJA) for the present-day/baseline period (2010–2030; left-side column) as simulated by the CESM1(WACCM) model in the Geoengineering Large Ensemble (GLENS) project. Two SAI experiments with different injection characteristics are used: Equatorial SAI (left and middle left-hand column) and Lower SAI (right and middle right-hand column). The left column and middle right-hand column indicate the projected changes with Equatorial SAI and Lower SAI (SAI – baseline) relative to the baseline, respectively. The middle left-hand column and the right columns indicate the impact of SAI on projected precipitation extremes under RCP8.5 in 2075–2095 (SAI-RCP8.5). The '+' signs indicate areas where all ensemble members agree on the projected sign of the change.

The spatial distribution of changes in annual precipitation extremes under Equatorial SAI and Lower SAI are similar as widespread decreases are projected for all indices, with varying degrees of change

(Figure A1; left and middle right-hand columns). Localised areas along the eastern coastline are exempt as increases are projected for annual R10MM (between +2 and +6 days/year) and R95P (between +10 and up to over +40 mm/year), in response to both SAI experiments. Parts of the eastern and southern coastline are also projected to experience increases in RX1DAY (between +4 and +16 mm/day) and RX5DAY (between +10 and +40 mm/5-day) under Equatorial and Lower SAI. Equatorial SAI could trigger a larger increase in these precipitation extremes than Lower SAI, suggesting greater vulnerability to flooding along the eastern coastline under Equatorial SAI. Similarly, both SAI experiments could cause increased PRCPTOT (between +20 and up to over +100 mm/year) along the eastern and southern coastlines, moving into parts of the eastern interior. Equatorial SAI could, however, trigger a more widespread increase in PRCPTOT than Lower SAI. There is a high agreement among the model's ensemble members for the projected increase in PRCPTOT under Equatorial SAI.

Equatorial SAI and Lower SAI are both projected to trigger nationwide decreases in annual RX1DAY and RX5DAY with the largest decrease (up to -8 mm/day and -16 mm/5-day respectively) occurring over the central interior and north-east SAF (Figure A1; left and middle right-hand columns). Equatorial SAI could trigger a more widespread decrease in RX1DAY over the central interior, while Lower SAI could cause a more widespread decrease in RX5DAY over the central interior moving westward. North-east SAF and the central interior are also projected to experience large decreases in R95P (up to over -40 mm/year) in response to both SAI experiments. Equatorial SAI could cause a more widespread decrease in R95P over the central interior moving north-eastward, while Lower SAI could cause a more widespread decrease in R95P over the central interior moving south-westward. These findings suggest that eastern (western) SAF may become more prone to dryer conditions in response to Equatorial (Lower) SAI. Nationwide decreases are also projected for R10MM in response to both SAI experiments with the greatest decreases occurring over the central interior moving westward. Equatorial SAI could, however, only cause a decrease in R10MM by up to -4 days/year, whereas Lower SAI could cause a decrease by up to over -6 days/year. These findings suggest that both Equatorial and Lower SAI could simultaneously reduce the country's vulnerability to flooding and exacerbate vulnerability to dryer conditions, particularly over the central interior and north-east SAF. All model ensemble members agree on the projected sign of

change over areas with the largest decreases in R10MM, RX1DAY, RX5DAY, and PRCPTOT, especially the central interior.

Equatorial and Lower SAI are both projected to cause decreases in annual PRCPTOT, with the largest decreases occurring over the central interior and north-east SAF (Figure A1; left and middle right-hand columns). Equatorial SAI could, however, cause decreased PRCPTOT between -20 and -60 mm/year while Lower SAI could decrease PRCPTOT between -40 and up to over -100 mm/year. These findings suggest that Lower SAI could trigger dryer annual conditions across large parts of the country. Both SAI experiments could decrease annual CDD across most of the country (both between -5 and -20 days/year), aside from parts of westernmost and north-eastern SAF where CDD could increase (between +10 and +20 days/year). All ensemble members agree on the projected sign of the changes in CDD across most of SAF for Lower SAI and along the country's coastline for Equatorial SAI. These findings suggest that a future under both Equatorial SAI and Lower SAI could mean overall dryer conditions across the country and reduced vulnerability to flood conditions. This is most relevant over the central interior and north-east SAF. The eastern coastline and parts of the southern coastline could, on the other hand, experience wetter annual conditions and increased vulnerability to flood conditions in response to both SAI experiments. Overall, Lower SAI could be more effective in inducing dryer annual conditions across the central interior moving westward, while Equatorial SAI could be more effective in triggering wetter annual conditions along the eastern coastline.

Figure A1 (middle left-hand column and right-hand column) shows that Equatorial SAI and Lower SAI could exacerbate the projected annual decrease in all extreme precipitation indices under RCP8.5: R10MM (between -2 and -6 days/year), RX1DAY (between -4 and up to over -8 mm/day), RX5DAY (between -4 and up to over -16 mm/5-day) and R95P (between -10 and up to over -40 mm/month). The largest decreases could occur over eastern and north-east SAF and parts of the central interior, suggesting exacerbated vulnerability to dry conditions. Both SAI experiments could, however, exacerbate flood conditions along parts of the eastern and Southern coastlines and over south-western SAF where increases are projected for R10MM (between +4 and +6 days/year) and R95P (between +20 and up to over +40 mm/year). Both SAI experiments are projected to offset the projected decrease in PRCPTOT under RCP8.5 over south-west SAF where it increases between +20

and +100 mm/year, suggesting wetter annual conditions. In addition to south-west SAF, Equatorial SAI could also offset the RCP8.5 impact on PRCPTOT over most of western SAF and the eastern coastline. Lower SAI, alternatively, could aggravate the projected RCP8.5 impact on PRCPTOT over the central interior moving westward (between -20 and -80 mm/year). There is a high level of agreement among the model's ensemble members for the projected sign of change in PRCPTOT over south-west SAF in response to Equatorial SAI and Lower SAI. Lastly, both experiments are projected to offset the projected increase in CDD under RCP8.5 over most of the country between -5 and up to over -20 days/year, with the greatest decrease occurring in western SAF and parts of eastern SAF. Easternmost SAF could be the exception as both Equatorial and Lower SAI are projected to cause increased CDD (between +5 and +10 days/year). These findings suggest that Both SAI experiments could simultaneously reduce the country's vulnerability to flood conditions and enhance dry conditions.

The response of precipitation extremes to Equatorial SAI and Lower SAI during summer are very similar as both experiments are projected to induce nationwide decreases in all precipitation extremes (Figure A2; left and middle right-hand columns). The main difference is that Lower SAI is projected to cause larger decreases in R10MM (between -1 and -2 days/month), RX1DAY (between -2 and -6 mm/day), RX5DAY (between -5 and -15 mm/5-day), and PRCPTOT (between -10 and -20 mm/month), compared to Equatorial SAI which causes smaller decreases in R10MM (up to -1 day/month) and RX5DAY (between -5 and -10 mm/5-day). There is agreement among the model's ensemble members for the projected decrease in these indices in response to Lower SAI over the central interior and western SAF. The projected spatial distribution for CDD in response to both experiments is also similar as CDD could increase (between +2 and up to over +8 days/month) in western SAF and over parts of north-east SAF. On the other hand, both experiments could cause CDD to decrease (between -2 and -4 days/month) in eastern SAF and parts of Southern SAF, in addition to the eastern and southern coastline. All of the model's ensemble members agree on the projected decrease in CDD over western SAF for both experiments, and on the projected increase over the central interior moving eastward. There is also agreement among the model's ensemble members over the projected decrease in CDD over the Southern and south-western coastlines for Equatorial SAF. Overall, these results suggest that Lower SAI could reduce the country's vulnerability to flood conditions during summer and simultaneously induce dryer conditions to a greater extent

than Equatorial SAI (Figure A2; left and middle right-hand columns). Equatorial SAI and Lower SAI are projected to have a smaller impact on precipitation extremes during winter than during summer (Figure A3; left and middle right-hand columns). Both SAI experiments are projected to cause slight decreases in R10MM (up to -0.25 days/month), RX1DAY (up to -1 mm/day), RX5DAY (up to -2 mm/5-day) and PRCPTOT (up to -4 mm/month), mainly over localised areas in north-west and north-east SAF. The primary difference between the two experiments is that Lower SAI is projected to cause larger and more widely spread increases in R10MM (between +0.25 and +0.75 days/month), RX1DAY (between +1 and +5 mm/day), RX5DAY (between +4 and up to over +10 mm/5-day), and PRCPTOT (between +4 and +20 mm/month) over the eastern coastline and parts of the southern coastline. Equatorial SAI, on the other hand, could cause smaller increases in R10MM (up to +0.25 days/month), RX1DAY (between +1 and +3 mm/day), RX5DAY (between +2 and +8 mm/5-day), and PRCPTOT (between +2 and +12 mm/month). There is agreement among the model's ensemble members on the projected sign of change for these indices along the eastern coastline in response to Lower SAI. Overall, these results suggest that while both SAI experiments could enhance precipitation extremes along the eastern coastline, Lower SAI could be more impactful in triggering wetter winter conditions compared to Equatorial SAI.

During summer, Equatorial SAI and Lower SAI could exacerbate the projected increase in precipitation extremes under RCP8.5 over north-east SAF where substantial decreases are projected for R10MM (between -3 and up to over -4 days/month), RX1DAY (between -6 and up to over -8 mm/day), RX5DAY (up to over -25 mm/5-day), and PRCPTOT (up to over -50 mm/month) (Figure A2; middle left-hand column and right-hand column). There is agreement among the model's ensemble members on the projected sign of change for all of these indices over north-easternmost SAF in response to both SAI experiments. On the other hand, both SAI experiments could offset the projected decrease in precipitation extremes under RCP8.5 over western SAF and parts of the eastern coastline. From the two experiments, Equatorial SAI is projected to cause larger increases in R10MM (up to +2 days/month), RX1DAY (between +2 and +8 mm/day), RX5DAY (between +5 and up to over +25 mm/5-day), and PRCPTOT (between +10 and +30 mm/month), over these areas. All ensemble members agree on the projected sign of change for R10MM, RX1DAY, RX5DAY, and PRCPTOT over parts of western SAF in response to both SAI experiments, with a more widespread ensemble agreement for Equatorial SAI. Equatorial and Lower SAI could exacerbate the projected

increase in CDD under RCP8.5 by causing increased CDD (between +4 and up to over +8 days/month) over western SAF and over north-eastern SAF (between +2 and +4 days/month). The overall implication of these results suggests that east and north-east SAF could become more prone to dryer summers with reduced vulnerability to flood conditions in response to both SAI experiments. Equatorial SAI and Lower SAI could, however, trigger slightly wetter summers over western SAF, where Equatorial SAI could cause wetter conditions than Lower SAI.

Figure A3 (middle left-hand column and right-hand column) shows that during winter, both SAI experiments could offset the projected drying impact under RCP8.5 over the central interior moving south-eastward and south-westward by increasing RX1DAY (between +2 and +3 mm/day), RX5DAY (between +4 and +8 mm/5-day), and PRCPTOT (up to over +4 mm/month). Lower SAI could more widely offset the projected drying impact under RCP8.5 than Equatorial SAI. In contrast, both experiments could exacerbate the projected increase in winter precipitation extremes along the eastern and southern coastline by causing decreases in R10MM (between -0.25 and -1 day/month), RX1DAY (between -1 and up to over -5 mm/day), RX5DAY (between -2 and up to over -10 mm/5-day), and PRCPTOT (between -4 and up to -20 mm/month). Winter precipitation extremes over north-western areas of the country could remain unaffected by both experiments. Finally, both SAI experiments are projected to exacerbate the projected decrease in winter CDD under RCP8.5 between +5 and by up to over +15 days/month across most of the country, especially over the central interior moving northward. Lower SAI could increase CDD more than Equatorial SAI. Decreases in CDD are, however, projected over south-west SAF (up to -5 days/month) and areas in western and north-eastern SAF (up to -15 days/month) in response to both SAI experiments. There is high level of agreement among the model's ensemble members for both SAI experiments on the projected sign of change for RX1DAY, RX5DAY, and PRCPTOT over parts of the central interior moving westward. These findings suggest that Equatorial and Lower SAI could simultaneously reduce vulnerability to flood conditions along the eastern coastline and exacerbate future drying conditions during winter and could consistently offset the projected decrease in precipitation extremes under RCP8.5 in south-west SAF.

9.2 PROJECTED CHANGES IN THE SPATIAL DISTRIBUTION OF TEMPERATURE EXTREMES IN RESPONSE TO EQUATORIAL SAI AND LOWER SAI

The left and middle-right-hand columns in Figures A4 (annual), A5, and A6 (seasonal), show the projected impact of Equatorial SAI and Lower SAI respectively, on temperature extremes for the period 2075–2095 relative to the baseline period (2010-2030). Both SAI experiments are projected to induce a cooling effect due to widespread decreases in most extreme temperature indices, with Equatorial SAI being more impactful in triggering a cooling impact than Lower SAI. There are high levels of agreement among the model's ensemble members for the cooling effect projected for temperature extremes across most parts of the country in response to Equatorial SAI and Lower SAI. There is generally more widespread agreement among the model's ensemble members in response to Equatorial SAI.

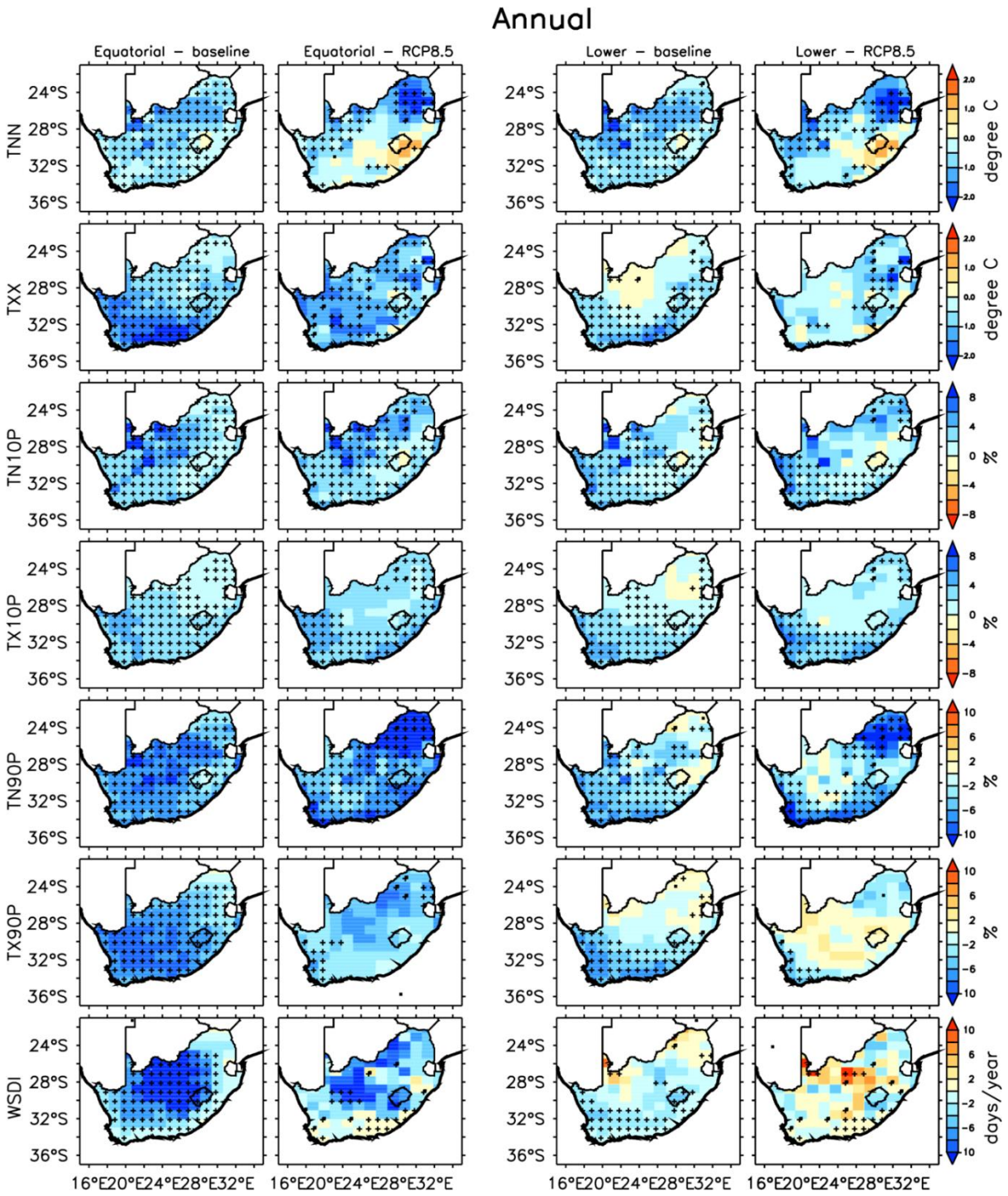

Figure 23. The ensemble mean of annual temperature indices over South Africa for the present-day/baseline period (2010–2030; left-side column) as simulated by the CESM1(WACCM) model in the Geoengineering Large Ensemble (GLENS) project. Two SAI experiments with different injection characteristics are used: Equatorial SAI (left and middle left-hand column) and Lower SAI (right and middle right-hand column). The left column and middle right-hand column indicate the projected changes with Equatorial SAI and Lower SAI (SAI – baseline) relative to the baseline, respectively. The middle left-hand column and the right

columns indicate the impact of SAI on projected temperature extremes under RCP8.5 in 2075–2095 (SAI-RCP8.5). The '+' signs indicate areas where all ensemble members agree on the projected sign of the change.

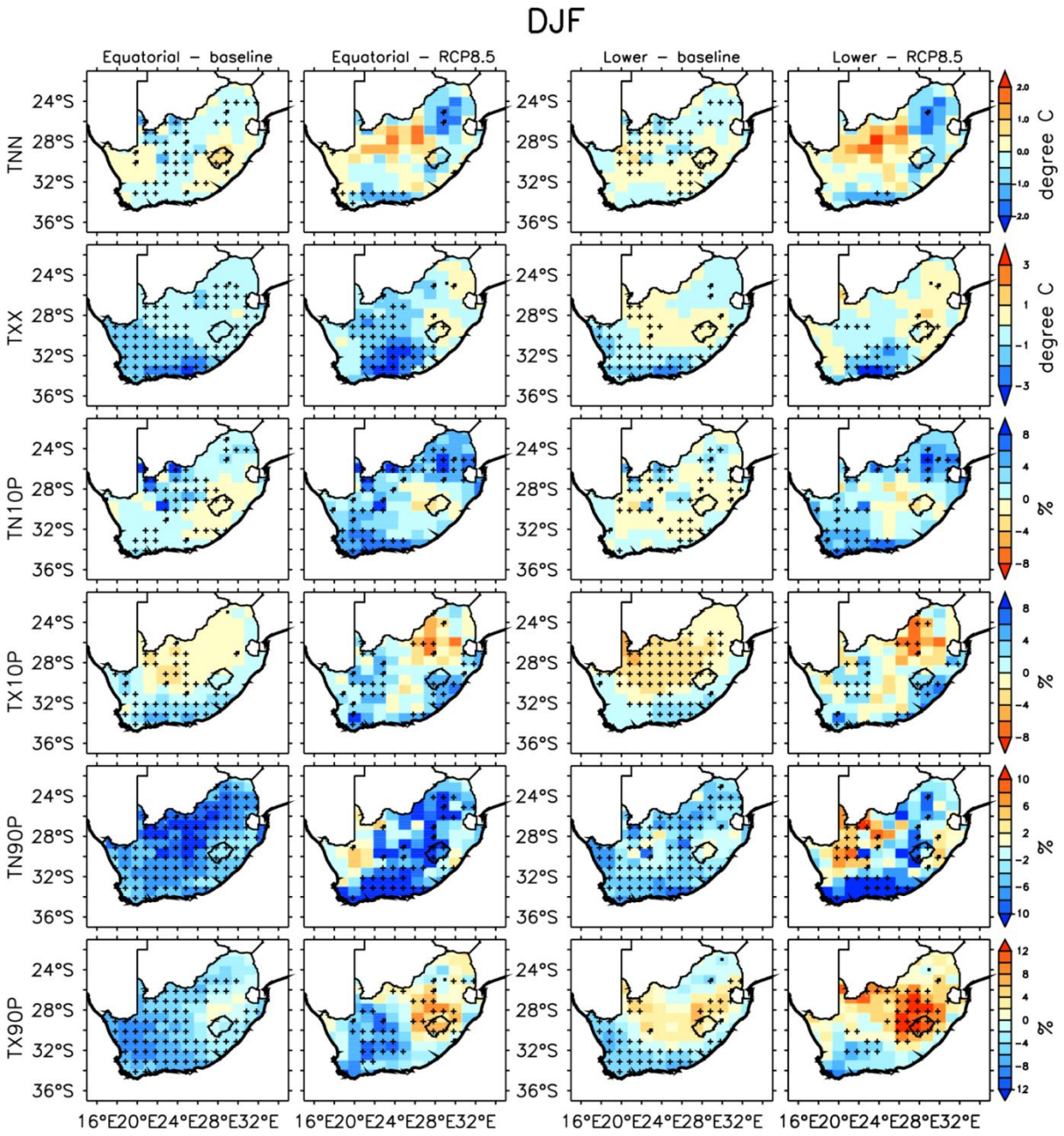

Figure A24. The ensemble mean of temperature indices over South Africa during summer (DJF) for the present-day/baseline period (2010–2030; left-side column) as simulated by the CESM1(WACCM) model in the Geoengineering Large Ensemble (GLENS) project. Two SAI experiments with different injection characteristics are used: Equatorial SAI (left and middle left-hand column) and Lower SAI (right and middle right-hand column). The left column and middle right-hand column indicate the projected changes with Equatorial SAI and Lower SAI (SAI – baseline) relative to the baseline, respectively. The middle left-hand column and the right columns indicate the impact of SAI on projected temperature extremes under RCP8.5 in 2075–2095 (SAI-RCP8.5). The '+' signs indicate areas where all ensemble members agree on the projected sign of the change.

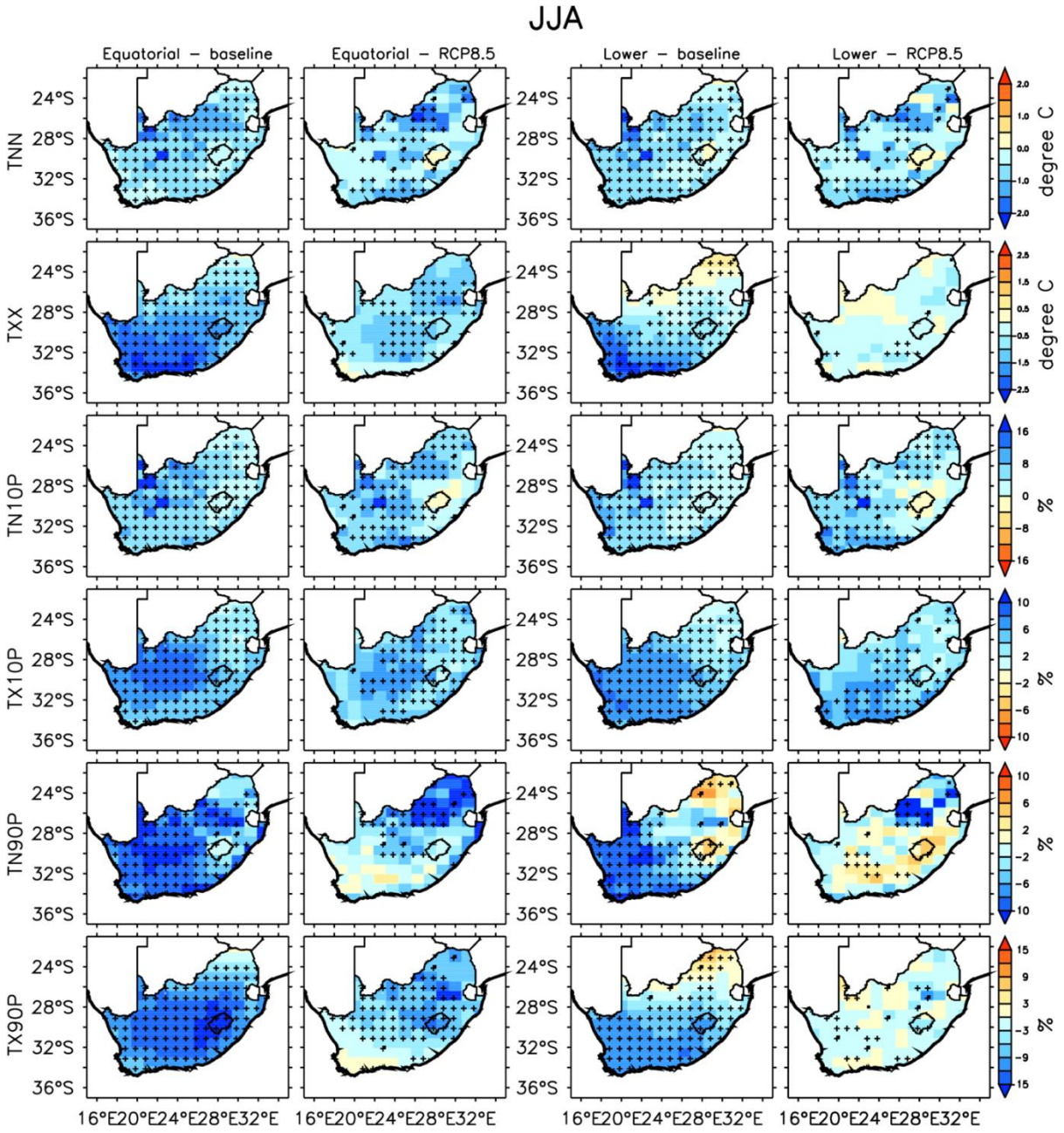

Figure 25. The ensemble mean of temperature indices over South Africa during winter (JJA) for the present-day/baseline period (2010–2030; left-side column) as simulated by the CESM1(WACCM) model in the Geoengineering Large Ensemble (GLENS). Two SAI experiments with different injection characteristics are used: Equatorial SAI (left and middle left-hand column) and Lower SAI (right and middle right-hand column). The left column and middle right-hand column indicate the projected changes with Equatorial SAI and Lower SAI (SAI – baseline) relative to the baseline, respectively. The middle left-hand column and the right columns indicate the impact of SAI on projected temperature extremes under RCP8.5 in 2075–2095 (SAI-RCP8.5). The '+' signs indicate areas where all ensemble members agree on the projected sign of the change.

Figure A4 (left-hand column) shows that Equatorial SAI is projected to trigger a nationwide annual cooling effect as it could cause decreases in annual TNN and TXX (between -0.5 and by up to over -2°C), TN90P and TX90P (between -2 and -10%), and WSDI (between -2 and up to over -10 days/year) and increases in TN10P (between +2 and up to over +8%) and TX10P (between +2 and +6%). There is agreement among the model's ensemble members on the projected sign of change for all temperature extremes in response to Equatorial SAI across most of the country. Lower SAI is also projected to trigger an annual widespread cooling effect, but to a lesser extent and magnitude than that of Equatorial SAI (Figure A4; middle right-hand column). This is especially the case for TNN (between -0.5 and up to over -2°C), TN90P and TX90P (both between -2 and -8%), and WSDI (between -2 and -6%). All model ensemble members agree on the projected nationwide decrease in TNN in response to Lower SAI. On the other hand, Lower SAI is projected to increase TXX (up to +0.5°C), TN90P and TX90P (up to +2%), WSDI (between +2 and +8 days/year) and decrease TX10P (up to -2%), over parts of east and north-east SAF and north-west SAF. There is a high level of agreement among the model's ensemble members on the projected sign of change in all extreme temperature indices over south-west SAF in response to Lower SAI. These results suggest that Equatorial SAI could be more effective in causing a nationwide cooling impact than Lower SAI.

The middle left-hand column and right-hand columns in Figure A4 shows the projected annual impact of Equatorial SAI and Lower SAI on RCP8.5. The projected impact of SAI is prominent over north-east SAF where both SAI experiments could offset the projected increase in the following annual hot temperature extremes under RCP8.5: TNN (between -0.5 and up to over -2°C), TXX (between -0.5 and up to over -1.5°C on average), TN90P (between -6 and up to over -10%), and TX90P (between -2 and -8%). Equatorial and Lower SAI are also projected to offset the projected decrease in TN10P (between +2 and +6%) and TX10P (between +2 and +4%) over north-east SAF. All ensemble members agree on the projected sign of change in TNN, TXX, TN10P, TX10P, TN90P, and TX90P over north-east SAF in response to Equatorial SAI. In south-west SAF, all ensemble members agree on the projected sign of change for TN10P, TX10P, and TN90P in response to both SAI experiments. TNN responds differently as Equatorial and Lower SAI could both exacerbate the projected increase TNN under RCP8.5 along parts of the eastern and southern coastline between +0.5 and +1.5°C. Lower SAI could also exacerbate the projected increase in TX90P under RCP8.5 over the central interior moving north-westward and southward, where it increases between +2 and

+4%. These results suggest that Equatorial SAI could be more effective in offsetting extreme warm temperatures over most of the country than Lower SAI. Lastly, Equatorial SAI is projected to offset the projected increase in WSDI under RCP8.5 over most of the country, particularly the central interior and parts of north-east SAF, between -2 and up to over -10 days/year. Parts of the southern coastline could, however, experience exacerbated WSDI (between +2 and +4 days/year) under Equatorial SAI. Lower SAI could exacerbate the projected increase in WSDI under RCP8.5 across most of the country, especially the central interior and north-west SAF, between +2 and up to over +10 days/year. The westernmost and easternmost areas of the country are exempt as Lower SAI could offset the projected increase in WSDI between -2 and -6 days/year.

During summer, Equatorial SAI is projected to cause nationwide decreases in TXX (between -1 and up to over -3°C), TN90P (between -2 and up to over -10%) and TX90P (between -2 and -10%), while Lower SAI could cause a nationwide decrease in TN90P (between -2 and -10%) (Figure A5; left and middle right-hand columns). These results suggest that both experiments could induce fewer warm nights across the country during summer. On the other hand, Lower SAI is projected to cause an increase in TXX in the central interior moving north-westward and eastward by up to +1°C, while it decreases across the remainder of the country between -1 and -3°C. All ensemble members agree on the projected decrease in TXX over south-west and Southern SAF in response to Lower SAI. TNN is projected to decrease over parts of north-east, south-west and the central interior (where all ensemble members agree on the projected sign of change) in response to Equatorial SAI (between -0.5 and -1.5°C) and Lower SAI (between -0.5 and -1°C). TNN could increase over the remainder of the country by up to +1°C in response to both SAI experiments. TX10P is projected to decrease over the central interior and parts of north-east SAF in response to bot Equatorial SAI (between -2 and -4%) and Lower SAI (between -2 and -6%), with Lower SAI causing a larger magnitude of decreased TX10P over a larger area. There is agreement among the model's ensemble members on the projected sign of change for TX10P over the central interior and southern coastline in response to Lower SAI. On the other hand, the country's coastline could experience increased TX10P in response to both Equatorial (between +2 and +6%) and Lower (between +2 and +4%) SAI. This finding suggests that while both experiments could increase the frequency of cool summer nights along SAF's coastline, Equatorial SAI could cause more cool nights.

The response of TN10P to both SAI experiments varies as Equatorial SAI is projected to cause a decrease in TN10P over south-east SAF (up to -2%) and an increase over the rest of the country (between -2 and up to over +10%) (Figure A5; left column). In contrast, Lower SAI could cause increases in TN10P along parts of the country's coastline and over areas in the central interior, north-east SAF and north-west SAF (between +2 and +6%) and to decrease over the rest of the country (between -2 and -4%). Lastly, Lower SAI is projected to increase TX90P over the central interior moving north-westward and eastward between +2 and +8% and to decrease in south-west and north-east SAF between -2 and -8%. All ensemble members agree on the projected sign of change for TX90P over south-west SAF in response to Lower SAI. These findings suggest that Lower SAI could enhance hotter day-time temperature extremes over parts of the central interior and eastern SAF, while Equatorial SAI could have a more substantial cooling effect during summer.

During summer, Equatorial SAI and Lower SAI could both exacerbate the projected increase in TNN under RCP8.5 over the central interior moving south-westward, and parts of the eastern coastline, between +0.5 and up to over +2°C (Figure A5; middle left-hand column and right-hand column). The remainder of the country (especially north-east SAF and the southern coastline), on the other hand, could benefit from both experiments which could offset the projected increase in TNN by- -0.5 to -2°C. Both SAI experiments could exacerbate the projected increase in TXX under RCP8.5 over parts of eastern SAF and north-eastern SAF by up to +1°C. In addition, Lower SAI could also exacerbate the RCP8.5 impact on TXX by up to +1°C, over areas in western and north-western SAF and localised areas in the central interior. The remainder of the country could benefit (especially the southern coastline) from both experiments as they could offset the projected increase in TXX between -1 and up to over -3°C. All ensemble members agree on the projected sign of change in TXX over most of western and southern SAF in response to Equatorial SAI, while there is agreement among the ensemble members only in Southern SAF for Lower SAI. These findings suggest that Equatorial SAI could be more effective in offsetting the hottest day and hottest night during summer. Equatorial and Lower SAI could both offset the projected decrease in TN10P under RCP8.5 over most of the country between +2 and up to over +8% (Figure A5; middle left-hand column and right-hand column). Both experiments could, however, exacerbate the projected decrease in TN10P under RCP8.5 over parts of the central interior between -2 and -4%. All model ensemble members agree on the projected sign of change for TN10P over parts of north-eastern and south-western SAF in

response to both SAI experiments. Equatorial and Lower SAI could both offset the projected decrease in TX10P under RCP8.5 over most of south-western SAF and along the country's coastline between +2 and +8%. In the northern and north-east SAF, both SAI experiments could exacerbate the projected increase in TX10P under RCP8.5 between -2 and -8%. These findings suggest that, while both experiments could offset the RCP8.5 impact on TN10P and TX10P, Equatorial SAI could be more effective and over more parts of SAF. Lastly, Equatorial and Lower SAI could both add to the projected RCP8.5 impact on TN90P over parts of western and north-western SAF and the eastern coastline between +2 and +6%, and between +2 and up to over +10%, respectively. Equatorial SAI could offset (exacerbate) the projected increase in TX90P over western (eastern) SAF between -2 and -10% (+2 and +10%). The pattern of change for TX90P in response to Lower SAI is similar, however, the magnitude and extent to which Lower SAI could exacerbate the projected increase in TX90P under RCP8.5 is larger (between +2 and up to over +12%) and extends to parts of western and north-western SAF. All ensemble members agree on the projected sign of change in TX90P over parts of central SAF (where the largest magnitude of change is projected to occur) in response to both SAI experiments. These findings suggest that Equatorial SAI could be more effective in inducing a cooling effect over SAF during summer than Lower SAI.

The response of temperature extremes to Equatorial SAI and Lower SAI during winter is relatively consistent as widespread decreases are projected for most indices (Figure A6; left and middle right-hand columns). Equatorial SAI is projected to cause a nationwide cooling effect by decreasing TNN (between -0.5 and up to over -2°C), TXX (between -0.5 and up to over -2.5°C), TN90P (between -2 and up to over -10%), TX90P (between -3 and up to over -15%) and increasing TN10P (between +4 and up to over +16%) and TX10P (between +2 and +10%). There is a high level of agreement among all of the model's ensemble members on the projected sign of change across the country in response to Equatorial SAI. These results suggest that Equatorial SAI could be effective in reducing hot temperature extremes during winter and increasing the frequency of cool extremes. Lower SAI is projected to trigger nationwide decreases in TNN (between -0.5 and up to over -2°C) and increases in TN10P (between +4 and up to over +16%) and TX10P (between +2 and +10%). The response for warm nights and warm days to Lower SAI varies as TN90P is projected to increase in north-east SAF (between +2 and +8%) and to decrease over the remainder of the country (between -2 and by up over -10%). Similarly, north-easternmost SAF is projected to experience increases in TX90P

(between +3 and +9%) and TXX (between +0.5 and +1°C), while the rest of the country could experience decreases in TX90P (between -3 and -12%) and TXX (between -0.5 and up to over -2.5°C). Similarly to Equatorial SAI, all of the model's ensemble members agree on the projected sign of change for temperature extremes across most of the country in response to Lower SAI. The overall implications of these findings are that Equatorial SAI could have a more substantial cooling effect across SAF during winter compared to Lower SAI.

During winter, Equatorial SAI could effectively offset the projected increases in hot temperature extremes and decreases in cool temperature extremes across most of the country (Figure A6; middle left-hand column and right-hand column). Although Lower SAI could effectively offset the projected RCP8.5 impact on temperature extremes, the results vary more than that of Equatorial SAI. Both SAI experiments could offset the projected RCP8.5 impact on extreme temperature indices over most parts of the country: TNN (between -0.5 and -2°C), TN10P (between +4 and +16%) and TX10P (between +2% and +10%). These findings suggest that both SAI experiments could effectively induce cooler winter night-time temperatures and increase the frequency of cool days and nights. Equatorial SAI could offset the projected increase in TXX (between -0.5 and -1.5°C), TN90P (between -2 and up to over -10%) and TX90P (between -3 and up to over -15%) under RCP8.5 across most of SAF. There are, however, localised areas in western and south-western SAF where Equatorial SAI could exacerbate the projected increase in TN90P (between +2 and +4%) and TX90P (by up to +3%). There is high model agreement on the projected sign of change for all extreme indices in response to Equatorial SAI over the central interior and parts of north-east and western SAF. The overall implication of these findings is that Equatorial SAI could effectively induce cooler winters across SAF. The results for Lower SAI are more varied as it could offset (exacerbate) the projected increase in TXX under RCP8.5 over most of the country (parts of north-west, north-east, and southern SAF) between -0.5 and -1°C (up to +0.5°C). Lower SAI could exacerbate the projected increase in TN90P under RCP8.5 over most of the country's interior moving south-westward and south-eastward between +2 and +6% and offset it between -2 and up to over -12% across the country's borderline regions. Lastly, Lower SAI could offset the projected increase in TX90P under RCP8.5 across most of SAF between -3 and -9%, while exacerbating the RCP8.5 impact on TX90P in localised areas in southern SAF, and the central interior moving northward by up to +3%. These findings suggest that Lower SAI could alleviate the projected heating under RCP8.5 over most of SAF, aside from localised

areas in the central interior, north-west, and southern SAF. Overall, both experiments could be effective in triggering a cooling effect during winter across SAF, with Equatorial SAI being more effective.